

**CHARACTERIZATION AND PERFORMANCE OF  
INJECTION-LOCKED QUANTUM-DASH LASER IN  
OPTICAL COMMUNICATION**

BY  
**MUHAMMAD TALAL ALI KHAN**

A Thesis Presented to the  
DEANSHIP OF GRADUATE STUDIES

**KING FAHD UNIVERSITY OF PETROLEUM & MINERALS**

DHAHRAN, SAUDI ARABIA

In Partial Fulfillment of the  
Requirements for the Degree of

**MASTER OF SCIENCE**

In

**ELECTRICAL ENGINEERING**

**January 2017**

KING FAHD UNIVERSITY OF PETROLEUM & MINERALS

DHAHRAN- 31261, SAUDI ARABIA

DEANSHIP OF GRADUATE STUDIES

This thesis, written by **Muhammad Talal Ali Khan** under the direction his thesis advisor and approved by his thesis committee, has been presented and accepted by the Dean of Graduate Studies, in partial fulfillment of the requirements for the degree of **MASTER OF SCIENCE IN ELECTRICAL ENGINEERING**.



Dr Ali Ahmad Al-Shaikhi  
Department Chairman



Dr. Salam A. Zummo  
Dean of Graduate Studies

19/1/17

Date:



Dr. Mohammed Zahed M. Khan.  
(Advisor)



Dr. Khurram Karim Qureshi  
(Member)



Dr. Samir Al-ghadhban  
(Member)

© Muhammad Talal Ali Khan

2017

*Dedicated to*  
*my beloved Parents, Muhammad Ishaq Kamran and Tabassam Naz*  
*my elder sisters and little brothers.*

## ACKNOWLEDGMENTS

All praise is due to ALLAH and peace be upon the last Prophet Muhammad ﷺ and his family, his companions and his followers.

With respect, I would like to extend my deepest gratitude to my family because without their prayers, love, positive reception, I would not have been able to achieve my desired goals in life. I will always be thankful to them for their continuous moral and emotional support and ever-needed prayers.

It has been my honor to be able to work with my adviser, Dr. Mohammed Zahed M. Khan, you have been a tremendous mentor for me. I would like to admire his supervision, suggestions and guidance right from the beginning till the end of this research. His constant motivation and patience helps me to produce quality work. Your advices have been priceless in both research as well as on my career.

I would like to thank my committee members: Dr. Samir Alghadhban and Dr. Khurram K. Qureshi for their useful response, advice and the time they spent reviewing this thesis.

I would like to extend my gratitude to Dr. Khurram K. Qureshi for allowing us to utilize his fiber optics laboratory. I also thanks to our main collaborators, Prof. Habib Fathallah and Dr. Amr Ragheb for their constant support, ideas and determination. Our sincere gratitude to all our collaborators for helping us in conducting system level experiments in communication & networking lab (CNL), a part of Prince Sultan Advanced Tech Research Institute (PSATRI), and KACST-TIC on Radio Frequency and Photonics for the e-Society (RFTONICS), at King Saud University.

I am very obliged to King Fahd University of Petroleum & Minerals for providing me with an opportunity to pursue my graduate degree.

# TABLE OF CONTENTS

ACKNOWLEDGMENTS .....	v
TABLE OF CONTENTS .....	vii
LIST OF TABLES.....	xi
LIST OF FIGURES .....	xii
LIST OF ABBREVIATIONS .....	xvi
ABSTRACT .....	xix
<b>CHAPTER 1 INTRODUCTION.....</b>	<b>1</b>
<b>1.1 Optical Fiber Communication.....</b>	<b>1</b>
<b>1.1.1 The General System.....</b>	<b>3</b>
<b>1.1.2 Capacity Increasing Demand.....</b>	<b>5</b>
<b>1.1.3 Optical Communication Networks.....</b>	<b>6</b>
<b>1.1.4 Optical Access Networks .....</b>	<b>9</b>
<b>1.1.5 Passive Optical Networks .....</b>	<b>10</b>
<b>1.1.6 WDM-PONs .....</b>	<b>13</b>
<b>1.1.7 WDM-PON Architecture .....</b>	<b>14</b>
<b>1.1.8 WDM-PON Challenges.....</b>	<b>15</b>
<b>1.1.9 Colorless WDM-PON Literature Review.....</b>	<b>16</b>
<b>1.1.10 Challenges in Optical Communication.....</b>	<b>19</b>
<b>1.2 Optical Wireless Communication.....</b>	<b>21</b>
<b>1.2.1 Introduction .....</b>	<b>21</b>
<b>1.2.2 History.....</b>	<b>22</b>
<b>1.2.3 Features and Applications .....</b>	<b>23</b>
<b>1.2.4 Challenges .....</b>	<b>24</b>
<b>1.2.5 Literature review .....</b>	<b>25</b>

1.3	Light Emitters.....	29
1.4	Research Motivation.....	31
1.5	Thesis Research Contribution .....	34
1.6	Thesis Structure.....	34
<b>CHAPTER 2.....</b>		<b>37</b>
<b>QUANTUM DASH LASER CHARACTERIZATION .....</b>		<b>37</b>
2.1	Semiconductor Laser Introduction .....	37
2.2	Quantum Dash Device Structure.....	44
2.3	Bare Semiconductor Laser Diode Characterization Setup .....	45
2.4	Semiconductor Laser Diode Performance Parameters .....	48
2.4.1	I-V Characteristics.....	48
2.4.2	L-I Characteristics .....	49
2.4.3	External Differential Quantum Efficiency .....	51
2.4.4	Internal Quantum Efficiency .....	53
2.4.5	Internal Loss.....	54
2.4.6	Transparency Current Density .....	54
2.4.7	Emission Spectrum .....	55
2.5	Comparison of Fixed and Chirped barrier QDash Laser .....	56
<b>CHAPTER 3 INJECTION-LOCKING CHARACTERIZATION.....</b>		<b>61</b>
3.1	Introduction.....	61
3.2	Injection-Locking Operation .....	63
3.3	Applications of Injection-Locking .....	66
3.4	Injection-Locking in Semiconductor Laser .....	67
3.5	Experimental Optical Injection Setup.....	71



3.5.1	Tunable Master laser.....	72
3.5.2	Slave (QDash) Laser .....	73
3.5.3	Injection-Locked Mode .....	75
3.6	Characterization of Injection-Locked Modes .....	76
3.6.1	Tunability .....	76
3.6.2	Short-Term Stability .....	78
3.6.3	Injection-Locked Hysteresis .....	79
 <b>CHAPTER 4 INJECTION-LOCKED QUANTUM DASH LASER IN OPTICAL FIBER COMMUNICATION .....</b>		<b>81</b>
4.1	Introduction.....	81
4.2	CW Characteristics of Chirped QDash Laser Diode .....	83
4.3	Injection-locked Optical Communication .....	86
4.3.1	Optical Fiber Transmission Setup .....	87
4.3.2	Transmission Experiments.....	93
4.3.3	32/64 Gb/s DP-QPSK WDM-PON Transmission.....	94
4.3.4	100 Gb/s DP-QPSK WDM-PON Transmission .....	97
4.4	Proposed Transmitter for NG WDM-PON.....	99
4.4.1	Proposed WDM-PON Power Budget.....	100
 <b>CHAPTER 5 INJECTION-LOCKED QUANTUM DASH LASER IN OPTICAL WIRELESS COMMUNICATION .....</b>		<b>103</b>
5.1	Introduction.....	103
5.2	Injection-locked Indoor Communication .....	106
5.2.1	Optical Wireless Transmission Setup .....	107
5.2.2	Eye Safety Standards .....	111
5.2.3	4 m DP-QPSK Indoor FSO Communication .....	113

5.2.4	2 m DP-QPSK Indoor FSO Communication .....	115
5.2.5	2 m & 4 m FSO BER curves Comparison .....	117
5.2.6	Laser Beam Misalignment .....	118
5.3	Comparison of IL QD-LD and TLS Carrier.....	120
<b>CHAPTER 6 CONCLUSION AND FUTURE WORK .....</b>		<b>122</b>
6.1	Thesis Conclusion .....	122
6.2	Future Work .....	125
REFERENCES .....		127
Appendix.....		143
VITAE .....		146

## LIST OF TABLES

1.1: Major spectral windows of optical fiber [6]. .....	5
2.1: Resistance values and turn on voltages of different cavity length lasers.....	49
2.2: Threshold current density and efficiency slope of different cavity length fixed barrier QDash laser devices. ....	52
2.3: Internal quantum efficiency and Internal loss of fixed barrier QDash laser.....	53
2.4: Comparison between fixed barrier and chirped $4 \times 700 \mu\text{m}^2$ ridge QDash laser diode in terms of efficiency parameters. ....	60
2.5: Comparison between fixed barrier and chirped $4 \times 800 \mu\text{m}^2$ ridge QDash laser diode in terms of efficiency parameters. ....	60
4.1: The maximum received powers and their corresponding Q-factors over 10 km fiber. ....	99
4.2: Proposed NG-PON power budget employing a 20 dB far L-band amplifier at CO (Downstream) and RN (Upstream). ....	101
4.3: Estimated power budget of 100 Gb/s transmission without including any amplifier.	101
5.1: Classification of Laser safety and permissible emission ranges for 850 nm and 1550 nm wavelengths [27]. ....	111
5.2: Maximum permissible exposure (MPE) for 850 nm and 1550 nm wavelengths [173]. ....	113

## LIST OF FIGURES

1.1:	Working principle of fiber optics communication. ....	3
1.2:	Optical losses in full spectrum silica-based fiber (b) optical communication bands, [5]. ....	4
1.3:	Cisco forecasts IP traffic 194.4 EB per month in 2020 [7]. ....	6
1.4:	Communication network topology [8]. ....	7
1.5:	(a) point-to-point (P2P) (b) point-to-multipoint (P2MP). ....	10
1.6:	A simplified PON architecture. ....	11
1.7:	PON technology evolution [15]. ....	13
1.8:	Typical WDM-PON configuration. ....	15
1.9:	Bidirectional WDM-PON architecture based on MWLS injection-locking [20]. ....	16
1.10:	Colorless WDM-PON transmission based on multi-wavelength source [22]. ....	17
1.11	WDM-PON configuration based on wavelength reuse scheme [24]. ....	19
1.12	Optical fiber communications transmission limit [25]. ....	20
1.13	Block diagram of OWC communication. ....	21
1.14	Integration of local area networks (LAN) to wide area networks (WAN) [30]. ....	24
1.15	Transmission distance versus free-space link length for wireless technologies [32].	25
1.16	Transmission distance vs. data rate for different technologies [58]. ....	29
1.17	A typical WDM optical communication system. ....	33
1.18	WDM optical communication system employ in a single broadband laser. ....	33
2.1	(a) homo-structure junction (b) double hetero-structure junction [72]. ....	38
2.2	(a) Semiconductor material quaternary configurations, showing the materials employed to attain 1300 nm and 1550 nm emissions [76-78], (b) self-assembled epitaxial grown method. ....	41
2.3	AFM images of InAs grown (a) QDots and (b) QDashes on InP substrate [87]. ....	42

2.4	(a) band diagram of the InAs/InAlGaAs QDash laser (b) plane-view atomic force microscopy (AFM) of the surface QDash [97].	44
2.5	a) A single laser bar containing several fixed cavity-length devices. (b) a microscopic image of a single laser bar.	45
2.6	Laser characterization laboratory setup.	46
2.7	a) Photodetector for collection of photons (b) Laser light coupling into a lensed single mode fiber.	47
2.8	Demonstration of laser characterization setup at device level before coupling power into SMF.	47
2.9	I-V characteristics of different cavity length fixed barrier QDash laser diodes.	48
2.10	L-I characteristics of different cavity length fixed barrier QDash laser diodes.	50
2.11	$1/\eta_i$ vs different cavity lengths of fixed barrier QDash laser.	51
2.12	Threshold current density $J_{th}$ vs. the inverse of different cavity length values.	55
2.13	Emission spectra of the 4 $\mu\text{m}$ ridge devices of cavity lengths 600, 800 and 1500 $\mu\text{m}$ fixed barrier QDash lasers.	56
2.14	QDash Laser diode device structure (a) fixed barrier (b) chirped.	57
2.15	Light output injected current measured voltage (L I V) characteristics of (a) fixed barrier QDash 4 $\times$ 700 $\mu\text{m}^2$ laser, (b) chirped barrier QDash 4 $\times$ 700 $\mu\text{m}^2$ laser, (c) fixed barrier QDash 4 $\times$ 800 $\mu\text{m}^2$ laser, (d) chirped barrier QDash 4 $\times$ 800 $\mu\text{m}^2$ laser. The corresponding insets show the lasing emission at 3 $I_{th}$ injection current.	59
3.1	Typical schematics for injection-locking system (a) transmission style, (b) reflection-style [105].	64
3.2	Frequency detuning vs. injection power for different stability conditions [105].	66
3.3	(a) Optical spectrum of the SMLL at free running (dashed-line/blue) and locked (solid-line/red) (b) Optical spectrum of the SAML. (c), (d) RF spectrum corresponding to (a) and (b) [143].	70
3.4	Experimental setup for the injection-locking of QDash laser diode.	71
3.5	Single mode TLS carrier at 1621 nm.	72
3.6	Free running QDash laser spectrum centered at 1625 nm.	73
3.7	Emission center wavelength and average integrated power as functions of times.....	74
3.8	QDash laser characteristics under free running mode and injection locked mode....	75

3.9	Tuning range (1611–1634 nm) of injection-locked modes of a QDash laser at different wavelengths, and at a fixed CW external injection of ~5 dBm. ....	77
3.10	Output power and SMSR versus different lasing wavelength with tuning steps of ~1 nm. ....	78
3.11	Short term stability test of the 1619.68 nm IL mode (a) in terms of wavelength and output power variations, (b) in terms of output power and SMSR variations. ....	79
3.12	Injection powers vs. output powers of the injection-locked QD-LD. The IL mode is fixed at 1621.01 nm. ....	80
4.1	Demonstration of laser characterization setup at device level. ....	84
4.2	The facet end L-I-V characteristics (a) pulsed operation and, (b) CW operation. ....	85
4.3	L-I -V characteristic of free running QDash laser, measured at the SMF end. The inset shows the bare QDash FP-LD power coupled to a lensed SMF. ....	86
4.4	Experimental setup of DP-QPSK WDM transmission via injection locked QDash FP-LD. The signal transmission is characterized first in a back-to-back (BtB) configuration and then over a 10 km single mode fiber (SMF). ....	87
4.5	Agilent optical spectrum analyzer for characterization of an injection-locking. ....	88
4.6	Free-running lasing spectra of the bare $4 \times 800 \mu\text{m}^2$ QDash laser. The inset shows an injection-locked single FP mode of the broadband QDash laser at ~ 1621 nm. ...	89
4.7	Optical isolator (b) 3-port optical circulator (OC), and (c) polarization controller (PC).	89
4.8	The optical modulation circuit utilized during communication experiments. ....	90
4.9	Variable optical attenuator (VOA). ....	91
4.10	Keysight optical modulation analyzer (OMA). ....	92
4.11	A complete illustration of an experimental optical communication setup via injection-locking technique showing all the system and device level components. ..	92
4.12	BER versus received optical power at 32 and 64 Gbit/s under BtB and after 10 km SMF transmission. ....	94
4.13	Eye diagrams and QPSK constellations of 32 Gb/s data rate (a) BtB and, (b) 10 km SMF transmission, at FEC threshold. ....	96
4.14	Eye diagrams and QPSK constellations of 64 Gbit/s data rate for (a) BtB and, (b) over 10 km transmission. ....	96
4.15	Bit error rate as a function of received optical power for 100 Gbit/s after 10 km SMF transmission. ....	98

4.16	Eye diagrams and QPSK constellations for 100 Gbit/s transmission (a) BtB and, (b) over 10 km SMF. ....	98
4.17	Proposed colorless NG-PON based on QD-MLL as seeding source and QD-LDs and QD-PDs transceivers at ONU/IF-OLT with 100 Gb/s data traffic capacity. The inset shows the broadband lasing spectrum of QD-LD and QD-MLL with half of the spectrum for downstream (DS) and half for upstream (US) transmission (symmetric bandwidth case). ....	100
5.1	The optical spectra of QD-LD with/without injection locking. The master TLS laser linewidth is visible. ....	106
5.2	Injection-locked mode (1621.42 nm) of the QD-LD. ....	107
5.3	Experimental setup of DP-QPSK transmission employing externally modulated IL QD-LD. ....	108
5.4	2 m indoor laboratory FSO setup. ....	109
5.5	4 m indoor laboratory FSO setup. ....	109
5.6	(a) Optical power meter (b) 1550 nm tunable narrow linewidth laser110 .....	110
5.7	(a) Constellation diagram and, (b) eye diagram, for 4-m/100 Gb/s transmission rate.	114
5.8	(a) Constellation diagram and, (b) eye diagram, for 4-m/64 Gb/s transmission rate..	114
5.9	Measured BER curves of the IL QD-LD-based FSO link over 4 m channel length, and at transmission rate of 64 and 100 Gb/s. ....	115
5.10	(a) Constellation diagram and, (b) eye diagram, for 2-m/64 Gb/s transmission rate..	116
5.11	(a) Constellation diagram and, (b) eye diagram, for 2-m/100 Gb/s transmission rate.	116
5.12	Bit error rate as a function of received optical power of IL QD-LD-based FSO link over 2 m channel length, and at transmission rate of 64 and 100 Gb/s. ....	117
5.13	Comparison of the measured BER curves of the IL QD-LD-based FSO link over 2 m and 4 m long free space channels, and at 100 Gb/s transmission. ....	118
5.14	BER values of 4 m/64 Gb/s IL QD-LD FSO link under different laser beam misalignment conditions. ....	119
5.15	Setup of two-dimensional translation stage into the reception collimator SMF for different beam misalignments. ....	120
5.16	(a) 1621.42 nm IL QD-LD and 1620.90 nm TLS carrier, (b) measured BER comparison of IL QD-LD and TLS, for 4 m/100 Gb/s transmission system. ....	121

## **LIST OF ABBREVIATIONS**

<b>AFM</b>	<b>Atomic Force Microscopy</b>
<b>ASE</b>	<b>Amplified Spontaneous Emission</b>
<b>BLS</b>	<b>Broadband Laser Source</b>
<b>AWG</b>	<b>Array Waveguide Grating</b>
<b>BER</b>	<b>Bit Error Rate</b>
<b>BTB</b>	<b>Back-to-Back</b>
<b>CW</b>	<b>Continuous Wave</b>
<b>DOS</b>	<b>Density of States</b>
<b>DPQPSK</b>	<b>Dual-Polarization quadrature Phase-Shift</b>
<b>Keying</b>	
<b>EDFA</b>	<b>Erbium Doped Fiber Amplifier</b>
<b>FP</b>	<b>Fabry Perot</b>
<b>FSO</b>	<b>Free Space Optics</b>
<b>MBE</b>	<b>Molecular Beam Epitaxy</b>
<b>OOK</b>	<b>On-Off Keying</b>
<b>VLC</b>	<b>Visible Light Communication</b>



<b>OWC</b>	<b>Optical Wireless Communication</b>
<b>DFB</b>	<b>Distributed Feedback Laser</b>
<b>DBR</b>	<b>Distributed Bragg Reflector Laser</b>
<b>VCSEL</b>	<b>Vertical Cavity Surface Emitting Laser</b>
<b>OSA</b>	<b>Optical Spectrum Analyzer</b>
<b>OMA</b>	<b>Optical Modulation Analyzer</b>
<b>PON</b>	<b>Passive Optical Network</b>
<b>WDM</b>	<b>Wavelength Division Multiplexing</b>
<b>AON</b>	<b>Active Optical Network</b>
<b>ONU</b>	<b>Optical Network Unit</b>
<b>OLT</b>	<b>Optical Line Terminal</b>
<b>RN</b>	<b>Remote Node</b>
<b>ONT</b>	<b>Optical Network Termination</b>
<b>SMF</b>	<b>Single Mode Fiber</b>
<b>OFDM</b>	<b>Orthogonal Frequency Division Multiplexing</b>
<b>TDM</b>	<b>Time Division Multiplexing</b>
<b>RSOA</b>	<b>Reflective Semiconductor Amplifier</b>

<b>QDMLL</b>	<b>Quantum-Dash Mode Locked Laser</b>
<b>NRZ</b>	<b>Non-Return-to Zero</b>
<b>TLS</b>	<b>Tunable Laser Source</b>
<b>WRC</b>	<b>Weak Resonant cavity</b>
<b>FEC</b>	<b>Forward Error Correction</b>
<b>PRBS</b>	<b>Pseudo Random Binary Sequence</b>
<b>DAC</b>	<b>Digital to Analogue Converter</b>
<b>EVM</b>	<b>Error Vector Magnitude</b>
<b>SMSR</b>	<b>Side Mode Suppression Ratio</b>

|

## **ABSTRACT**

Full Name : Muhammad Talal Ali khan  
Thesis Title : Characterization and Performance of an injection-locked Quantum-Dash laser in Optical Communication.  
Major Field : Electrical Engineering  
Date of Degree : January 2017

The massive surge in the demand for bandwidth and ultra-large capacity transmission has prompted extraordinary growth in the internet traffic in the recent years. To enable faster growth in network capacity of future optical communications, different light emitters have been considered, especially quantum confined active region based devices. In particular, a recent new class of quantum dash laser has shown some niche characteristics which has been exploited in optical communication system, particularly the broadband nature, which enables wide wavelength tunability. Ultra-broadband lasing emission quantum dash laser devices appear to be promising contender for next-generation passive optical networks by employing these broadband light emitter as sources.

In this work, characterization and performance of quantum dash laser is evaluated at both device and system level. To improve the laser performance, optical external injection locking technique is introduced. The performance of injection-locked QDash laser is characterized which shows a wide wavelength tuning range, to which QDash laser diode could be injection-locked. We thoroughly performed both optical fiber and wireless communication using a single injection-locked Fabry-Perot mode of a QDash laser. Specifically, the system performance is evaluated and compared by utilizing Quadrature

Phase Shift Keying modulation format. The found results demonstrated the potential of QDash laser diode as a light source for future high speed broadband communication, capable of providing 100 Gb/s transmission rate in the far L-band wavelengths in both fiber and wireless communication.

## ملخص الرسالة

الاسم الكامل: محمد طلال علي خان.

عنوان الرسالة: أداء وتشخيص الليزر الخط الكمي المحكم حقنياً في الاتصالات الضوئية.

التخصص: الهندسة الكهربائية.

تاريخ الدرجة العلمية: يناير 2017.

أدت موجة الاحتياج الهائلة لنقل البيانات فائق السعة ذي نطاق العرض الترددي الواسع إلى زيادة النمو في حركات المرور على الإنترنت بشكل استثنائي في السنوات الماضية. من أجل تمكين عملية التطور والنمو في سعة شبكات الاتصالات، فإنه يتم دراسة مختلف من المصادر الضوئية وخاصة تلك التي تتميز بوسائط فعالة حبيسة كمومياً. بالتحديد، أظهرت فئة من ليزرات الخطوط الكمية خصائص مركزة التي تم اتسغلالها في أنظمة الاتصالات الضوئية وخصوصاً تلك ذات النطاق الترددي الواسع مما يؤدي إلى إمكانية الضبط الواسعة. ليزرات الخطوط الكمية ذات نطاق الإشعاع الترددي فائق العرض مؤهلة كأحد الأجهزة الواعدة في شبكات اتصالات الجيل الجديد الضوئية عن طريق توظيف هذه الأجهزة فائقة العرض الترددي كمصادر ضوئية.

في هذه الدراسة يتم تقييم وتشخيص أداء ليزر الخطوط الكمية على مستوى الجهاز ومستوى النظام. من أجل تحسين أداء الليزر فإنه تم تقديم تقنية الإحكام الحقي الضوئي خارجياً. أداء الليزر المحكم حقناً أبقى مجالاً واسعاً في الأطوال الموجية التي يمكن أن يحكم فيها ليزر الخطوط الكمية حقناً. بعد ذلك قمنا بشكل كامل بعملية الاتصال لاسلكياً وعن طريق الألياف البصرية من خلال طول فابري-بيرو (Fabry-Perot) موجي واحد عن طريق إحكام ليزر خطي كمي حقناً. بالتحديد، تم تقييم أداء النظام ومقارنته باستخدام تضمين الطور الرباعي (QPSK). تبرهن النتائج المتحصل عليها على جدوى ديودات ليزر الخطوط الكمية الكامنة كمصادر ضوئية في الاتصالات السريعة ذات النطاقات الترددية الواسعة قابلة لتزويد معدلات نقل بيانات تصل إلى 100 جيجابت في الثانية في نطاق الأطوال الموجية (L-band) سواء خلال الألياف البصرية أو لاسلكياً.

# **Chapter 1**

## **INTRODUCTION**

A brief introduction about optical fiber communications is explained in Section 1.1 highlighting the requirements of wavelength multiplexed network and colorless passive optical networks for next generation high speed communications. Later, the basic of optical wireless communication and its rapid developments in both indoor and outdoor free space optical communications, is discussed in Section 1.2. An overview about light emitting sources utilized in passive optical network is discussed in section 1.3. In Last, research motivation, thesis contribution and thesis organization are mentioned in section 1.4, section 1.5 and section 1.6.

### **1.1 Optical Fiber Communication**

The historical backdrop of communication is humankind's quest for approaches to enhance yelling. Communication starts with dialect, a particular capacity which has made conceivable the development of human culture. With dialect any message, regardless of how perplexing, can be passed on between individuals over a long and short distances. In old ages, pigeons and fire were used to convey the signal for long distances. As time passes

electric telegraph was invented by Sir Charles Wheatstone in 1837 [1]. In 1849, the voice over a line electrical transmission device was invented. However, user has to setup a receiver near to his mouth in order to listen [2]. For many years use of light has been a valuable resource in communication. Using light beam, Alexander Graham bell was able to transmit speech in 1880. However due to limited light sources, restricted atmosphere and low capacity, the use of photophone after the discovery of telephone was limited.

In order to overcome this problem electromagnetic waves helped in transferring information especially at longer wavelengths but the bandwidth limitation was a challenge at that time. The advancement to increase the capacity to higher frequency was accomplished by Radio telecommunication. In 1841, Jean-Daniel Colladon trapped the light using total internal reflection inside a dielectric [3] But for long haul distance, Charles Kao used optical fiber to guide a light for the first time in telecommunication. However, losses were too high until Corning were able to reduce the loss up to 20 dB/km [4]. The invention of laser in 1960 was the major breakthrough in optical communication due to its coherency, modulation at high frequency and low beam divergence provided a more possibility of communication via free space beside optical fiber channel. The use of efficient light source was needed at that time and then there was a revolution in telecommunication when Robert Hall introduced the first laser diode in 1962 with emission wavelength of 850 nm in the near infra-red [5–6]. There was a need for a better solution as compared to the exhausted copper-wired transmission lines as communication system evolved. At that time, light-wave communication systems showed a great potential in



achieving significantly higher transmission rates and higher channel capacities with low attenuation in long-haul communication.

### 1.1.1 The General System

The general schematic of optical fiber communication consist of three basic elements, a compact light source, low loss optical fiber and photodetector. The fiber transmission includes transmission of signals as light which is completely different from transmission via copper wire wherein electrical signals going through the link. The block diagram of fiber optic communication comprise of transmitter, receiver, a light source and detector, as shown in Figure 1.1. At the point when the information, as electrical signals, is given to the transmitter hardware, it changes over them into light signal. The amplitude, frequency and phases of the source which could be of LED or Laser diode (LD) must stay steady and fluctuation free to have effective transmission.

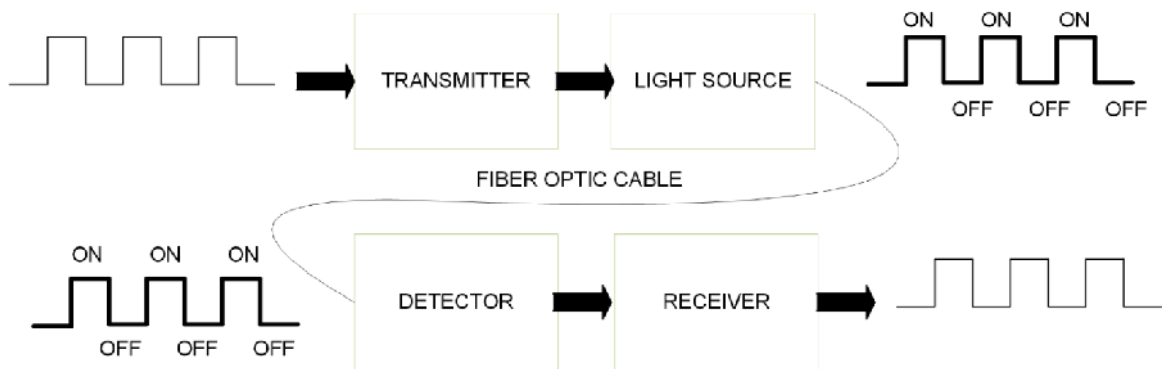


Figure 1.1 Working principle of fiber optics communication.

The receiver circuit comprises of a photodetector in order to detect the light. Initially attenuation of an optical fiber was too high in addition to fiber joint problems. To obtain better performance and maintain low loss, for long distance; thanks to silica fibers which have solved these problems. Figure 1.2 (a) depicts the used range of wavelengths in optical communications which are divided into three main windows at near infra-red region, also tabulated in Table 1.1. Initially semiconductor optical devices were fabricated using Aluminum Gallium Arsenide (AlGaAs) at near infrared region between  $0.8 \mu m$  to  $0.9 \mu m$ . Afterwards using other compound semiconductors (i.e InGaAsP) the emission wavelengths were successfully extended to multiple communication bands, as shown in Figure 1.2 (b).

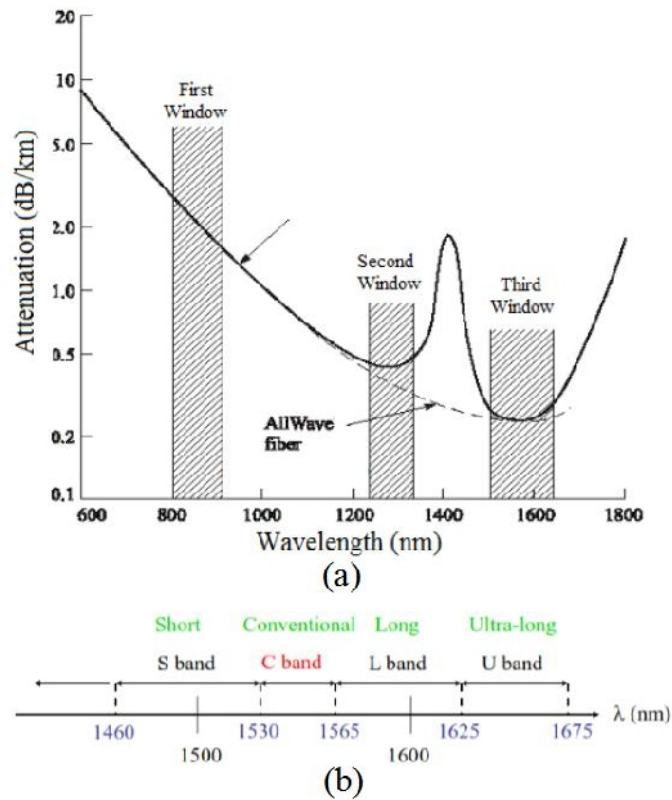


Figure 1.2 (a) Optical losses in full spectrum silica-based fiber (b) optical communication bands, [5].

**Table 1.1: Major spectral windows of optical fiber [6]**

Spectral windows	Wavelength (nm)	Attenuation (dB/km)	Material
1 <sup>st</sup> window	850	2	GaAs
2 <sup>nd</sup> window	1300	0.5	InGaAsP
3 <sup>rd</sup> window	1550	0.2	InGaAs

### **1.1.2 Capacity Increasing Demand**

Fiber optics communication has changed the modern society. It has brought sensational changes to the worldwide communication system and to a great extent affected our day by day life. Broadband communication technology has been progressing very rapidly in recent years and so is the developments through cutting edge research. The massive surge in the demand for bandwidth and ultra-large capacity transmission, to accommodate the ever-increasing demands of individual users, has prompted extraordinary growth in the internet traffic demand in the recent decade, with no sign of stopping. According to the Cisco forecast presented in June 2016, the internet data traffic in 2016 has already reached 88.7 Exabyte (1 Exabyte =  $10^{18}$  bytes) per month and is expected to increase to 194 Exabyte per month by 2020 [7]. Applications such as video on demand (VoD), audio streaming, file sharing, high definition television (HDTV), voice over internet protocol (VoIP), online gaming, have shown a rapid growth trend in network traffic than the available system capacity. Moreover, the system requires portability and interoperability in deployment of next generation mobile networks for upgradation. In the following decades, there will be

significant challenges in terms of technology and ever-increasing traffic demands for telecommunication industry and is of crucial importance to develop optical solutions in order to solve such challenges. As depicted in Figure 1.3, it has been forecasted by Cisco that global traffic will pass the 1.1 Zettabyte annually at the end of 2016 (1 Zettabyte =  $10^{21}$  bytes) and will hit 2.3 Zettabyte per year in 2020.

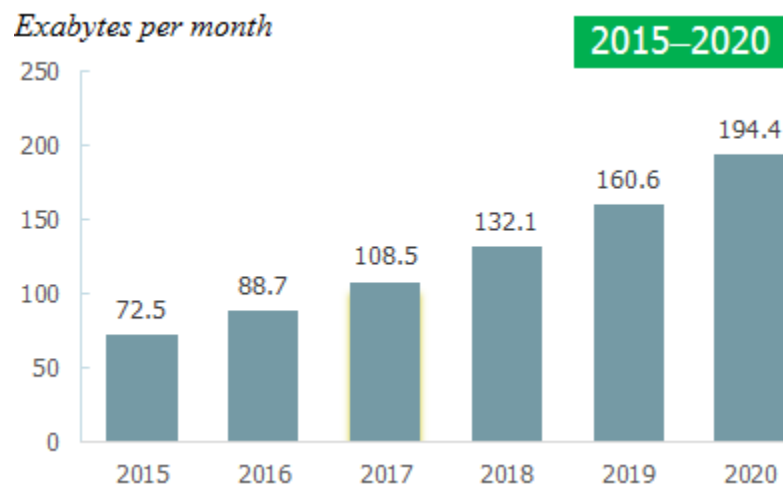


Figure 1.3 Cisco forecasts IP traffic 194.4 EB per month in 2020 [7].

### 1.1.3 Optical Communication Networks

A typical communication network architecture consists of three parts long-haul, metropolitan area and access networks, as illustrated in Figure 1.4. A *long-haul core* network, also known as backbone network of the communication system, connect all

countries in different continents. The links are made up of terrestrial and submarine and usually span thousands of kilometers. The ultra-long distance and high speed transmission is supported by optical fiber media. The reliable communication has been made possible through the use of coherent detection, optical amplification, and various advanced modulation schemes with forward error correction [8-9]. To provide robust communication links, a mesh topology is usually utilized between exchange nodes in network design.

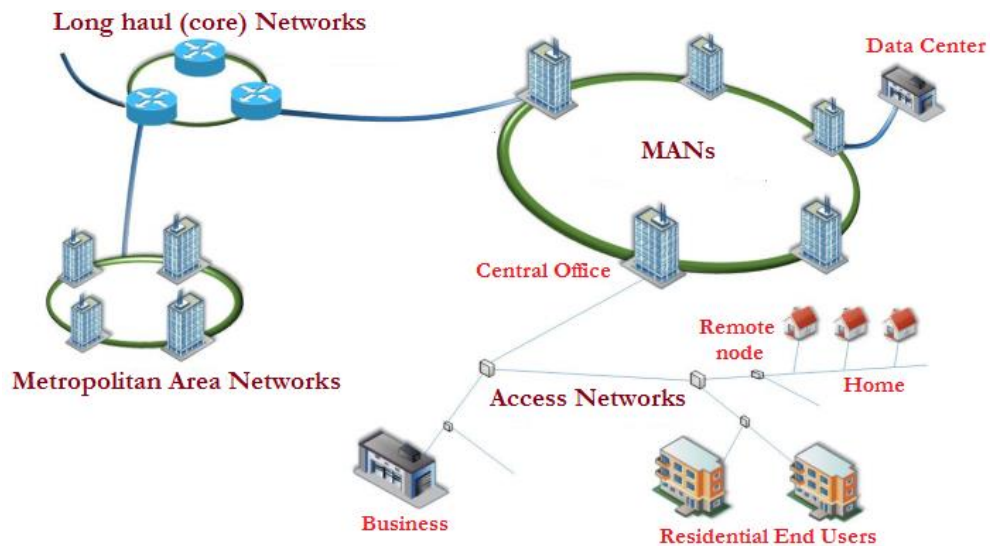


Figure 1.4 Communication network topology [8].

The *metropolitan* area networks provide interconnectivity between core networks and access networks within cities. A coverage span usually covers a range from tens to

hundreds of kilometers. These networks adopt a ring topology representing traffic exchange nodes to connect central offices, as shown in Figure 1.4. It is necessary for metro networks to balance with current core network standard while concurrently meeting skyrocket traffic requirements.

The *access* networks are referred as last/first mile of the networks depending upon the direction of communication, and provide the connection between the end users and the rest of the network. The covering range of access networks extends out to a few hundred meters or tens of kilometers (i.e. about 20 km) and connect the central office (CO) to the network user which can be either residential or business. Access networks employ complicated distribution architectures to deliver user applications and data to the massive number of subscribers. Remote node (RN) access networks, which is connected to the CO via optical fiber, is commonly known as hybrid fiber-coaxial (HFC) network, where the optical signal is converted into electrical signal to provide broadband connectivity. Alternatively, deployment of fiber-to-the-X (FTTx) transmission system has caught recent attention at RN owing to its capability of full-duplex transmission at high rates with the end user compared to the conventional HFC network. FTTx refers to fiber-to-the-home (FTTH), fiber-to-the-node (FTTN), fiber-to-the-cabinet (FTTC), fiber-to-the-premise (FTTP) and fiber-to-the-building (FTTB), and utilizes different network topologies like tree, bus, star and ring for bi-directional transmission.

Traditional access networks such as radio frequency (RF), millimeter wave and microwave technologies [10] are limited in terms of the physical media constraints, available bandwidth, and maximum reach. Likewise, the wireless alternatives are also limited for long distances and unreliability of free-space channel to provide flexible access network

solutions. In this regard, optical fiber is one of the promising candidate for future broadband services as compared to the limited bandwidth and bit-rate-distance techniques. Optical access networks have the potential to meet the rapidly increasing bandwidth demand and in fact, has been commercially deployed with FTTx technology [11].

#### **1.1.4 Optical Access Networks**

To connect a central node to the user end nodes at the optical distribution networks, different architectures are available in the optical fiber networks. Point-to-point (P2P) and point-to-multipoint (P2MP) are the two common topologies which can realized as optical access networks. In point-to-point connection, single fiber is connected from each user node end to central node for the dedication of huge bandwidth to each customer (see Figure 1.5 (a)). The main disadvantage of this access network is to deploy a separate fiber for each optical network unit (ONU) from the CO, ultimately requires a large number of ports in the CO, hence require large capital budget. On the other hand, when a single optical fiber is deployed from the optical line terminal (OLT), situated in the CO, to the active or passive remote node (RN) nearest to the user end, this is known as point-to-multipoint access networks (see Figure 1.5 (b)) [12]. Active optical network (AON) and passive optical network (PON) are the two major categories of optical access networks. AON uses active electronic components (i.e. amplifier) at the RN, thus require electrical power supplies and hence increases the cost for operational and maintenance of active devices, whilst PON employs passive components (i.e. array waveguide (AWG), optical splitters, couplers) at the RN for a transmission between OLT and optical network unit (ONU).

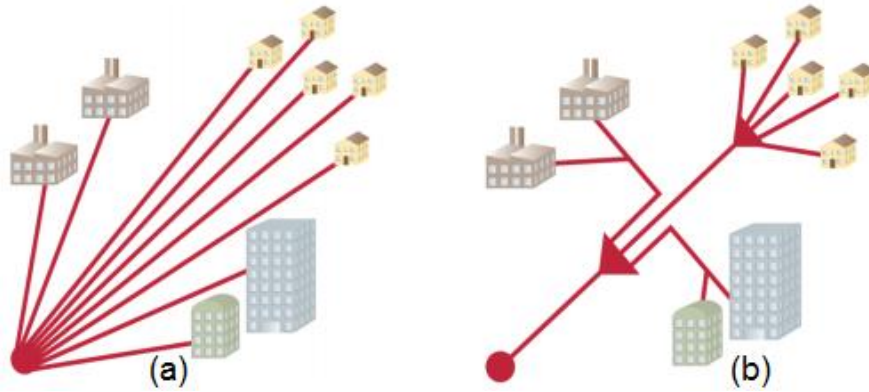


Figure 1.5 (a) point-to-point (P2P) (b) point-to-multipoint (P2MP).

### 1.1.5 Passive Optical Networks

Figure 1.6 shows the most simplified PON infrastructure for FTTx technology. The optical transmission path in PON does not contain any active elements like AON. OLT provides the communication link between access network and remote nodes where active elements are being deployed with an optical transceiver device in the CO. Optical network units (ONUs) or optical network terminations (ONT) are placed near or inside the subscriber home for the delivery of broadband services. Only passive connection exists between OLT and ONU in passive optical networks. RN is located near the user premises to link the OLT and ONUs by passive devices like optical splitter. All the passive devices in RN along with single mode fiber (SMF) and distribution fiber are called optical distribution network (ODN) [10].



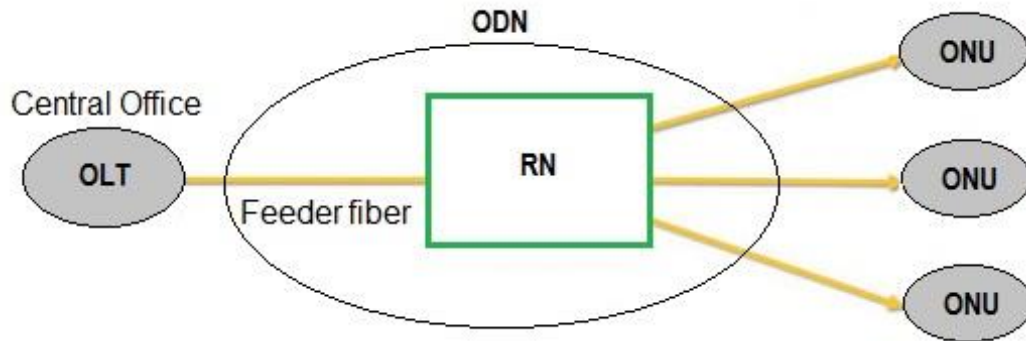


Figure 1.6 A simplified PON architecture.

Through optical fiber access, PON provides a variety of broadband applications to user and can meet the ever increasing bandwidth demand as an efficient technology since the conversion of optical signal coming from the CO is converted to electrical signal at ONU. Some of the advantages like high bandwidth, use of passive components and cost effective infrastructure urge the researchers to investigate PON extensively. Massive components can be installed using PON technology with less technical difficulties and maintenance constraints. PON has several benefits over AON in optical fiber access networks, for instance, PON utilizes infrastructure efficiently by sharing feeder fiber as compared to large number of fibers and additional transceivers required in the AON network, and non-requirement of electrical switching devices for power supply [13]. However, to prevent the data traffic of different ONU, a number of mechanisms are required to be employed in PON to avoid collision as no routing is performed to direct the traffic.

Different PON technologies in terms of Gigabit PON (GPON) and Ethernet PON (EPON) has been standardized and deployed in America & Europe and Korea & Japan, respectively.

These conventional PON architectures are being forced to evolve in ten Gigabit PON (XG-PON) and next-generation (NG-PON) for up to 10 Gb/s and 40 Gb/s - 100 Gb/s access networks, respectively, due to rise of hungry bandwidth applications and faster internet services [14]. The main objectives of NG-PON involve massive users, lower maintenance cost and ultra-high transmission rate which can be achieved by higher modulation formats and various architectures such as wavelength division multiplexing (WDM), time division multiplexing (TDM), orthogonal frequency division multiplexing (OFDM), orthogonal code division multiplexing (OCDM), hybrid TDM/WDM, available in literature. Figure 1.7 shows the evolution of PON technology in terms of data speed. From these candidates, most of the research and development is dedicated to TDM- and WDM- PON systems for FTTx solutions. TDM has been widely studied in PON network such as ATM-PON (APON), Broadband-PON (BPON) and Gigabit-PON (GPON). In TDM-PON scheme, the end subscriber can share the bandwidth according to the time slots used at the OLT, in the time domain. However, for NG-PON where high data rates are targeted, TDM technique is becoming more challenging due to the requirement for the burst mode receiver where security can be compromised. Also, the transmission capacity will be limited when several ONU share the bandwidth of a PON [15]. So, WDM-PONs have been identified as potential scheme for NG-PONs and is currently being developed to provide higher bandwidth in terms of better privacy and scalability.

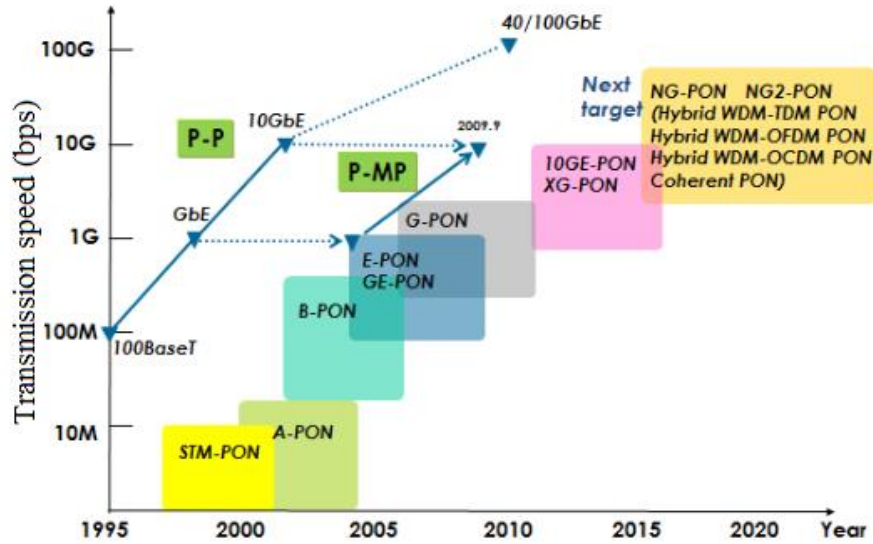


Figure 1.7 PON technology evolution [15].

### 1.1.6 WDM-PONs

WDM-PON can provide long term solutions for NG-PON system in competition with TDM. The use of WDM technology in optical networks were accessed in the late 1980 [15]. In a WDM-PON, each ONU is assigned a different wavelength to make a connection with the OLT, rather than sharing a single wavelength in time domain. The respective upstream and downstream can be performed through array waveguide (AWG) or multiplexer/ de-multiplexer (MUX/DEMUX). The shortcoming like limited bandwidth per user and network upgradation difficulty in TDM can be addressed by WDM scheme [16]. The dedicated wavelength for upstream and downstream transmission in WDM-PON provides a point-to-point connection by creating a virtual channel between each ONU and the OLT. However, the main challenge for practical WDM-PON system is complexity and the high cost of WDM components to initialize the setup [17]. Many devices such as Fabry-

Perot laser diode (FP-LD), semiconductor optical amplifier (SOA) and AWG have been formulated and developed in WDM-PONs for commercial purpose [18]. For future broadband optical access networks, WDM-PON has gained much research interest in recent years as a promising solution.

### **1.1.7 WDM-PON Architecture**

A typical WDM-PON architecture is shown in Figure 1.8 which consists of OLTs, AWGs, feeder fiber, distribution fibers, and ONUs. The OLT at central office has many transmitters and receivers instead of single transmitter and receiver in the case of TDM-PON. Each Tx/Rx connects to one ONU using single wavelength carrier that means 'N' ONUs would require 'N' different wavelengths. The first MUX/DEMUX located at CO is utilized to multiplex and de-multiplex the downstream and the upstream wavelengths. The second MUX/DEMUX located at RN receives the multiplexed downstream wavelengths through the feeder fiber and then sends to the ONU for. Hence, MUX/DEMUX are the key components in WDM-PON that replaces the power splitter in TDM-PON. WDM-PON schemes provide many peer-to-peer connections because the communication between OLT and ONU is realized with different wavelengths.

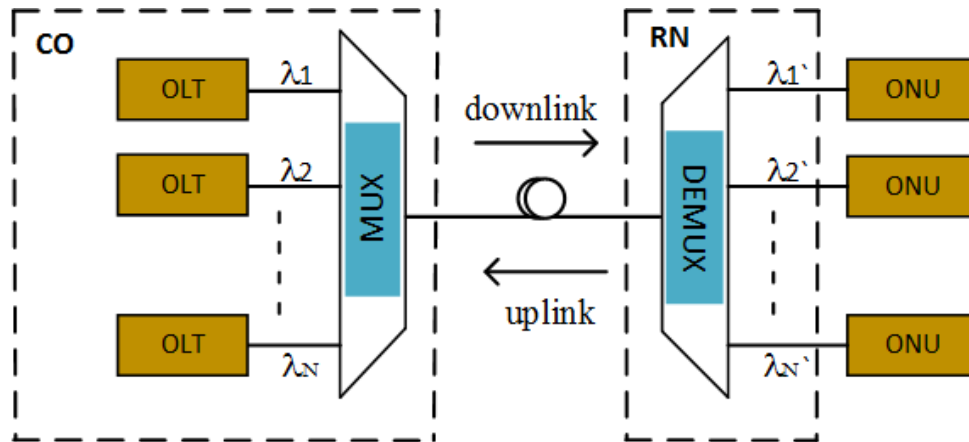


Figure 1.8 Typical WDM-PON configuration.

### 1.1.8 WDM-PON Challenges

WDM-PON has still challenging issues which needs to be addressed apart from its features like easy upgradation, network security and privacy, easy network management and large capacity. Two operations, colored (wavelength color) and colorless, are associated with WDM-PON. The light sources should be fixed wavelength sources in the ONU, so ultimately different wavelengths need to be assigned to ONUs by the WDM-PON system. Therefore, colorless operation is more flexible and adopted. The colorless operation makes each ONU unselective in wavelengths and makes convenient in maintenance. However, the most important challenge is to use a cost effective ONU by employing colorless operation to have an independent wavelength in WDM-PON [19]. Another challenge is that P2MP architecture in WDM-PON which has limited protection feature, where large amount of data can be lost if any component fails.

### 1.1.9 Colorless WDM-PON Literature Review

To achieve high channel capacity, various WDM-PON architecture have been studied so far. It is desired to have a low cost ONU for initial deployment. To realize colorless ONU, optical source such as amplified spontaneous emission (ASE), broadband light source (BLS), and reflective semiconductor optical amplifier (RSOA) and typical FP-LD have been deployed. A bidirectional WDM-PON is demonstrated using multi-wavelength source (MWLS) for colorless transmitter [20] as shown in Figure 1.9.

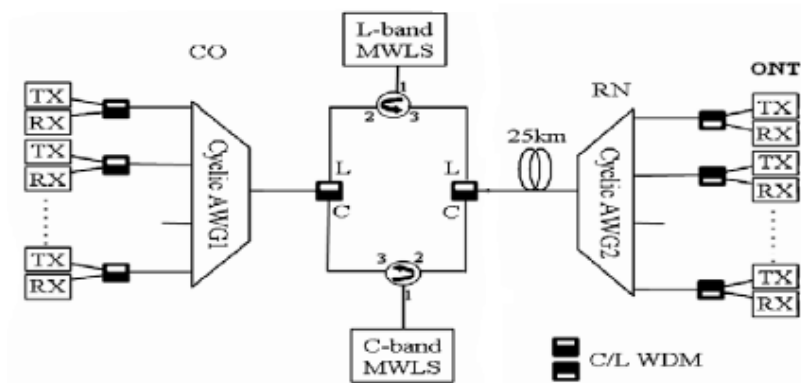


Figure 1.9 Bidirectional WDM-PON architecture based on MWLS injection-locking [20].

In the proposed scheme, C- and L-band wavelengths of MWLS, located at CO, are injection- locked for upstreaming and down streaming, respectively. To enhance the modulation bandwidth in low cost colorless WDM-PONs, injection-locking technique is adopted and has shown significant improvement in achieving high data rates [20]. A FP-LD is utilized with a central wavelength of 1548 nm having a 10 dB bandwidth of ~10 nm.

The proposed injection locked MWLS showed that half of the pump power could be saved and can perform better than conventional BLS. Moreover, a demonstration using multi-wavelength seeding source based on injection locked-FP-LD for colorless WDM-PON bidirectional transmission is explained in [21] where Quantum-dash mode locked laser (QD-MLL) serve as a seeding source for both upstream and downstream transmission. The proposed architecture in which dual fiber is placed between CO and RN for seeding and upstreaming to weaken the Raleigh backscattering effect, is one of the limitation in WDM-PON. Error free transmission is achieved over 25 km SMF at 2.5 Gb/s transmission rate for eight channels.

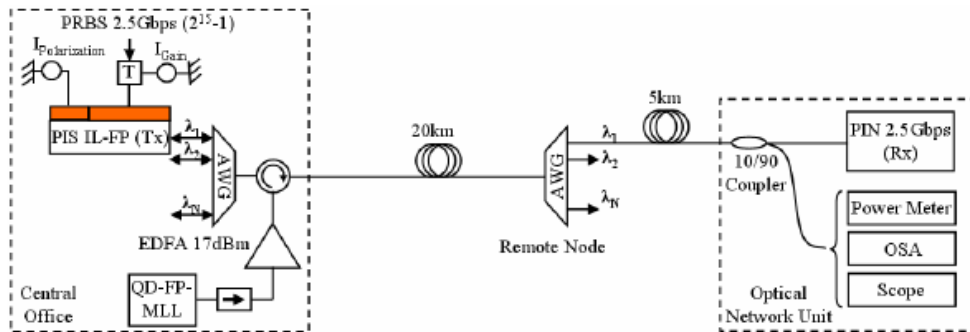


Figure 1.10 Colorless WDM-PON transmission based on multi-wavelength source [22].

Likewise, a colorless WDM-PON architecture is proposed and demonstrated by the same authors where single QD-MLL is located at CO serving as a multi-wavelength source, for injection-locked 16 channels at 2.5 Gb/s over 25 km SMF [22]. Due to high intensity noise

of spectrum slicing, transmission rate is limited in these types of WDM-PON transmitter (see Figure 1.10).

In [23], another type of colorless source, where two sets of continuous wave (CW) seed lights from CO is fed into ONU to injection-locked FP-LD. Both the CW laser source are located at CO and can be shared with multiple WDM-PON for low deployment cost, one optical light source being used for downstream seed source and another as upstream seed source. It is reported that 10 Gb/s transmission can be achieved over 10 and 15 km fiber up to 16 IL- FP longitudinal modes. In this scheme, upstream transmission rate and length can be limited due to fiber dispersion and the used colorless source direct modulation bandwidth (dependent on carrier lifetime).

Other schemes like wavelength reuse where wavelength specific light source (seeding source) is eliminated at the ONUs is proposed in [24]. The injection-locked WDM PON configuration based on wavelength reuse scheme is illustrated in Figure 1.11. This schemes demonstrates that downstream data is over-modulated/re-modulated with upstream data. When downstream carrier wavelengths are injection-locked at ONU then modulation is performed on the selected wavelengths and transmitted to the OLT for upstreaming. The master FP-LD placed at ONU used for injection-locking and injection-locked signal transmitted back to the OLT by directly modulated non-return-to-zero (NRZ) signals. As the passive splitter is used to split each channel at RN, TDM can be utilized to serve more users in this proposed architecture. A wavelength reuse is a cost-effective configuration as compared to the costly tunable laser source (TLS) or distributed feedback lasers (DFB) and RSOA. However, the interference can decrease upstream transmission at the CO since



downstream wavelengths were used for upstreaming. Error-free transmission is achieved by direct modulation at 1.25 Gb/s over 100 SMF in On-off keying (OOK) versus NRZ.

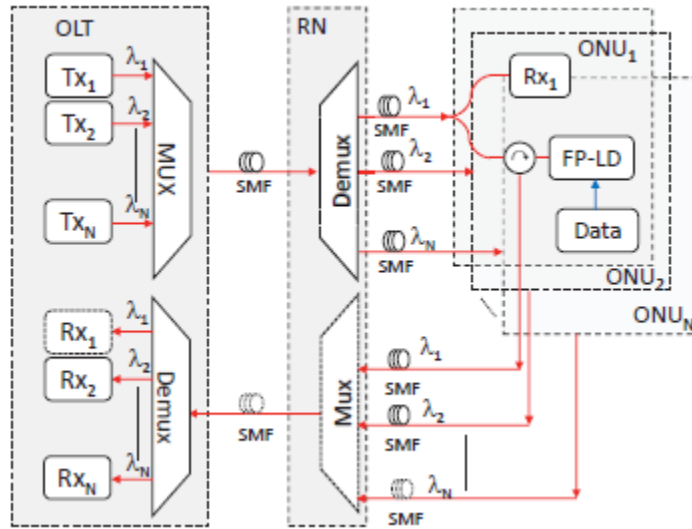


Figure 1.11 WDM-PON configuration based on wavelength reuse scheme [24].

### 1.1.10 Challenges in Optical Communication

Over the past few decades, optical fiber communications have been continuously developing with improved quality of service and new applications. Moreover, network traffic had grown exponentially due to large number of emerging applications and technology. In this regard, it is necessary to have a smooth operation of system by the telecommunication operators as the data traffic is consistently increasing. The type of transmission signal and the communication channel are subject to the capacity of optical communication. It is expected that the capacity of an optical channel via a single fiber will make no progress by year 2020 and will reach its physical limit known as “fiber wall” [25].

Figure 1.12 shows the low signal-to-noise ratio as one limit, at low optical powers, while on the other hand, high nonlinearity is observed at high power, at longer fiber transmission distances. Another challenges include system reconfiguration, limitations in local area network and economic evolution which requires a major change in existing hardware networks and systems. Moreover, the installation of fiber is problematic in some areas within the access networks. It could be difficult to get an access and digging across the sensitive infrastructures. So, a potential candidate is needed to find a new solution for optical backbone networks to get a mobility for both indoor and outdoor users.

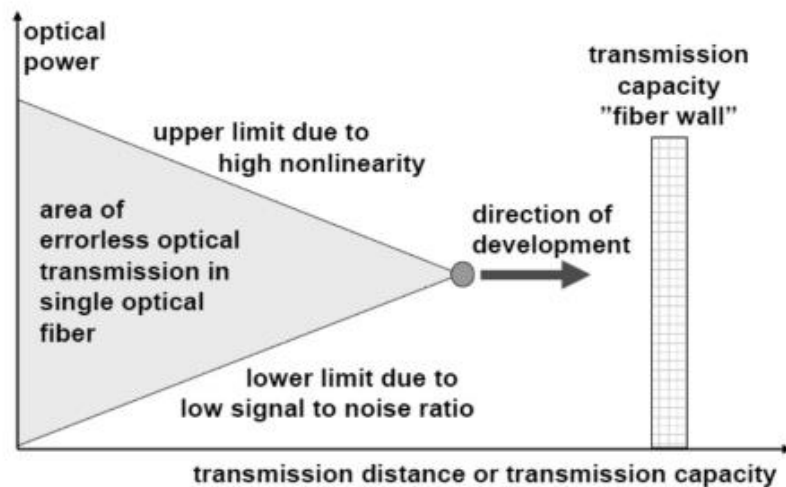


Figure 1.12 Optical fiber communications transmission limit [25].

## 1.2 Optical Wireless Communication

Optical wireless (OWC) communication is being considered as an alternative optical access technology for future networks. OWC is expected to provide a broadband communication, after successfully deployment, to the existing homes where optical fiber could not be installed. It is a viable candidate as a ‘last mile bottleneck’ to address the problems of huge bandwidth [26]. It can be deployed as an emergency backup link in optical access networks without or with fiber system [13]. Figure 1.13 illustrates a typical OWC system comprised of transmitter, channel and receiver where collimators or lenses are used for collimating the optical beam for transmission and reception

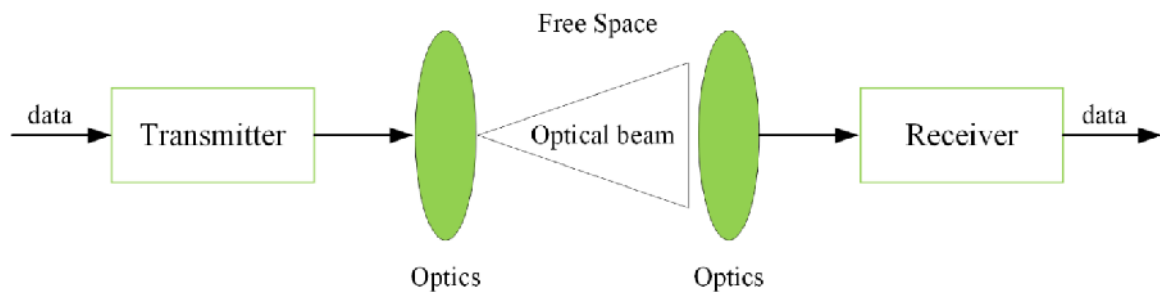


Figure 1.13 Block diagram of OWC communication.

### 1.2.1 Introduction

OWC is a technology where an optical carrier is used to transfer information through free-space channel. OWC can be classified into two major classes, namely indoor and outdoor

optical wireless communication. While the indoor links are mostly based on visible light sources (visible light communication (VLC) besides infra-red (IR) sources, the outdoor communication is dominant by IR sources, and commonly referred as free space optical (FSO) communication. Today, it is capable of transmitting 2.5 Gb/s data traffic (10 Gb/s using WDM in future) through free space medium. OWC does not require an optical fiber cable or spectrum license for an optical connection. Light travels faster through air as compared to the glass so OWC is a strong source of transmission at the speed of light. This technology is quite simple and based on the optical transceivers which consist of transmitter and receiver for bi-directional transmission. An optical source of high power is injected into lens for collimation, which transmit the light through air to another lens at receiving side. Laser is a commonly used source in OWC systems. and is based on line of sight (LOS) communication, operating at 750-820 nm and 1520-1600 nm transmission windows, providing low attenuation and adhering to the eye-safety standards [27].

### **1.2.2 History**

Alexander Graham bell invented the first free space optics system prototype ‘Photophone’ in 1880 [28]. Using sunlight as a carrier, photophone transfer signal to the receiving end. This idea could not be commercialized due to lack of enough light sources. The development of free space communication systems was boosted by the invention of laser in 1960s. A lot of experiments were performed for deep space communication and aerospace application by military and national aeronautics and space administration (NASA) for more than 30 years [29]. However, it suffered a setback since 1970 when all research was focused on optical fiber communication due to the invention of low-loss fiber.

Recently, OWC system has started gaining attention owing to its potential to provide similar bandwidth transmission abilities as fiber optics, and hence is an emerging technology.

### **1.2.3 Features and Applications**

OWC technology has a several advantages in terms of transmission capacity (GHz) as compared to the radio and microwaves (MHz). Some of its features are following:

- requires no license for spectrum,
- low mass requirement,
- easy and quick upgradation,
- high transmission rates (i.e. commercially available wireless system 100 Mb/s to 10 Gb/s [30])
- high security with less interception due to the transmission of narrow beam pulses,
- cost-effective, consume less power, reduced interference (Green communication technology).

IR light based OWC finds application in inter-satellite communication, terrestrial communication (building-to-building), deep space communication, disaster recovery (back-haul for wireless communication), unmanned aerial vehicles (UAV) and indoor communication (for data centers and high performance computing). Alternatively, visible light based OWC are potential candidates for light fidelity (Li-Fi) technology, etc.

## 1.2.4 Challenges

In reference [31], it is estimated that OWC communication market is already a worth of \$ 116.7 million and is expected to reach \$ 940.2 million by 2020. This is a direct indication of its potential in addressing future data transmission capacity requirement. However, there are still several challenges in OWC that requires extensive research. For instance:

- weather attenuation (fog, rain, dust, snow, smoke, haze) due to unguided medium which leads to the degradation of communication system. Atmospheric absorption, scattering and optical scintillation can affect optical signal propagation.
- geometric loss (narrow unguided beam divergence through free space as FSO require clear LOS).
- misalignment error by earthquake, building vibration, strong winds.
- atmospheric turbulence.

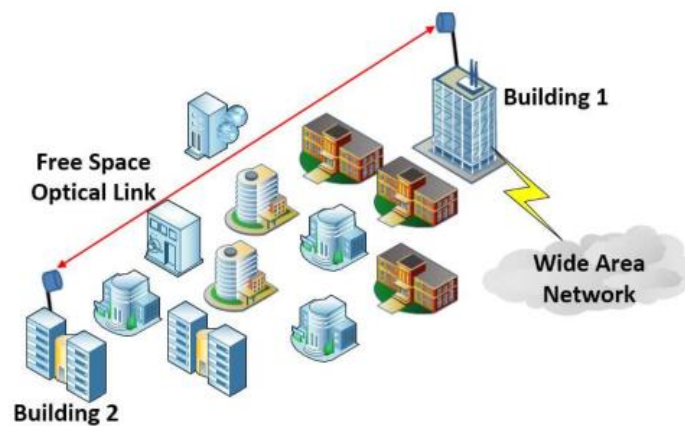


Figure 1.14 Integration of local area networks (LAN) to wide area networks (WAN) [30].

Figure 1.14 shows the FSO technology based solution by integration of LAN to WAN using FSO communication as a last mile access, where building 1 is directly connected to WAN via optical fiber and building 2 has an indirect connection to WAN via free-space link between both buildings. Many system parameters depend upon the FSO system performance and is critical to understand these parameters in FSO design. Some of these parameters includes high transmission rates, channel lengths, misalignment effect, eye-safety for the performance of indoor OWC, etc.

### 1.2.5 Literature review

OWC has been considered as a promising candidate because of its rapid development and capability to meet the higher data rate demand. Figure 1.15 depicts the data rate in term of link range (transmission distance) for different wireless technologies [32].

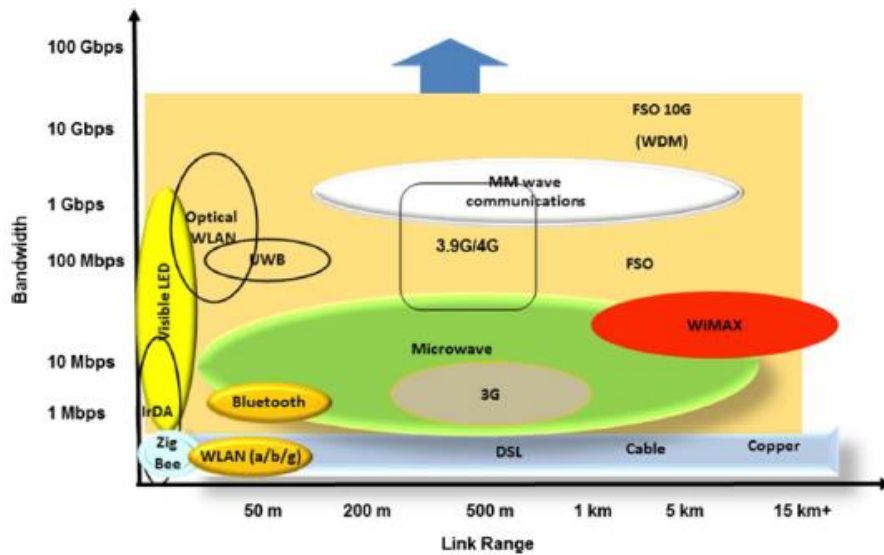


Figure 1.15 Transmission distance versus free-space link length for wireless technologies [32].

Different types of sources at different wavelengths have been employed to realize the OWC in visible and IR region. OWC has been applied to address various types of communication channels such as an outdoor building-to-building FSO communication, an indoor free space optical data centers for rack-to-rack communication and radio over FSO (RoFSO) technology [33–35].

Indoor VLC is a developing technology which offers a number of functionalities. It is proposed as an alternative for indoor IR technologies and offers short range applications [36]. Both IR and visible links can be used for the uplink in VLC systems. Pang *et al.* used the concept of fast switching LEDs and modulated visible light, for the first time in 1999 [37]. In 1999, a user controlled technology called RONJA (Reasonable Optical Near Joint Access) transmitted 10 Mb/s data using visible light beams over 1.4 km [38]. This optoelectronics device (RONJA) could be mounted on the roof and able to connect the servers with different networks. This device got quite reliable and uninterrupted operation without any interference except dense fog environment. In early 2000, Tanaka *et al.* proposed OWC with white- LED (WLED) for consumer communication networks [39]. Both illumination and communication functionality shows the emergence of WLED as one optical source and expected >100 Mb/s data rate using pulse-amplitude modulation (PAM) and discrete multitone transmission (DMT) [40]. Wireless personal area networks (WPANs) group (IEE 902.15) published the first IEEE standard for 802.15.7 VLC, which supports up to 96 Mb/s in 2011 [41-42]. Several papers have been published in the literature regarding VLC system. Due to high energy efficiency and wide bandwidth, VLC is considered as a potential candidate for 5G wireless communication in a recent survey by Wu *et al.* [43]. VLC has a potential in addressing indoor light-based wireless



communication (LiFi) which addresses many key advantages and solution. Tsonev *et al.* conducted comprehensive research on light fidelity systems especially for wireless networks utilizing OFDM [44]. Recently, VLC system has been introduced with laser diodes (LD-VLC) as a source of communication, to achieve higher data rates. Hussein *et al.* proposed LD-VLC system, capable of providing 5 Gb/s using OOK with minimum receiver sensitivity of  $10^{-6}$  [45]. Off-the-shelf LEDs such as organic and white phosphor LED (WPLED) have a limited bandwidth of 400 KHz to <10 MHz, respectively. VLC system can achieve more than 200 Mbps data rate using commercial LEDs [32]. System bandwidth can be increased by utilizing DMT and OFDM modulation schemes in VLC [46]. In this regard, VLC has been experimentally demonstrated using RGB LED and authors reported highest data rate of 1.5 Gb/s/channel using DMT technique [47]. Similarly, Vucic *et al.* reported 230 Mb/s data rate via OOK format by using avalanche photodiode (APD) [48] in the VLC system. For visible light link, some of the challenges like high bandwidth, inter-symbol interference (ISI) and high path losses need to be address to integrate VLC fully in current wireless topologies.

On the other hand, outdoor OWC has been considered as a promising solution in mobile-wireless backhaul, disaster recovery, metro ring extensions etc. operating at all three transmission window of optical communication band [49]. FSO has witnessed its market in many applications due to rapid development of optoelectronic devices. Recently, the radio over FSO (RoFSO) is viewed as a new innovation technology to enable the optical fiber and FSO communication, hence broadband connectivity would be beneficial to remote areas [50]. Another alternative approach has been proposed as a WLAN and FSO for internet access method as a data uplink and downlink for digital video broadcasting

[51]. Several outdoor experiments have been evaluated and tested during different times of the day. In [52], Juaraz *et al.* demonstrated the 10 Gb/s bi-directional FSO transmission over 147 km span communication link between two islands in U.S for 14 days. These type of investment flourished and increased the FSO development in commercialization. While the FSO for urban area applications are normally short-range link lengths (i.e. 500 m). It is an alternative approach to the RF links for providing broadband connectivity to the business and residential areas with high bandwidth. Full duplex FSO systems can operate up to 3.5 km length at 1.25 Gb/s transmission in all weather conditions reliably [53]. Numerous high speed FSO transmission have been reported in literature including 212 m FSO link of 1.28 Tb/s ( $32 \times 40$  Gb/s) [54], 320 Gb/s ( $8 \times 40$  Gb/s) transmission based on WDM [55], 160 Gb/s ( $16 \times 10$  Gb/s) terrestrial FSO transmission over 2.16 km free-space channel length [56] and 1.6 Tb/s ( $8 \times 40$  Gb/s) transmission over a ( $2 \times 210$  m) free space optical link [57].

Figure 1.16 illustrates the capacity of both optical fiber and optical wireless communications in terms of longer distances and high data rates [58]. In 5G technology, it is expected that the network speed for each user will reach 10 Gb/s [59]. Optical communications have the capacity to reach such requirements with certain constraints and limitations of each technology.

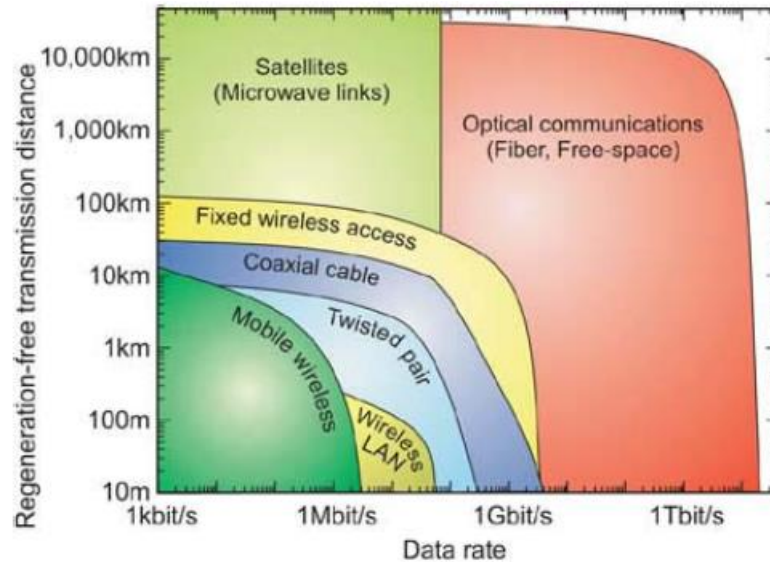


Figure 1.16 Transmission distance vs. data rate for different technologies [58].

### 1.3 Light Emitters

To deliver HD video and high quality audio data, high speed optical transmission is needed in near future. Modern optical communication exploits light emitting diodes (LEDs) or laser diodes (LDs) for modulating light sources. Semiconductor lasers have been much focused due to its coherent light transmission within a narrow cone, thus beam coupling efficiency is much higher into fiber. Injection-locking has been utilized for many years to increase the modulation bandwidth of communication system. This approach was applied in many colorless transmitters for WDM-PON applications through optical sources such as ASE, BLS, RSOA and FP-LDs [60–62]. The more details about proposed PON literature is explained in subsection 1.1.9. These transmitters have low-cost but their transmission performance is limited. Moreover, the master sources such as BLS may suffer from high

intensity noise those includes ASE sources [63]. Similarly, the spectrum sliced ASE also showed high intensity noise and limited wavelength tunability when injection-locked with typical FP-LD [64]. Likewise, the directly modulated RSOAs WDM-PONs are often used in remodulation process where modulated downstream signal reuses as an injection light source but are found to be limited by transmission capacity [65]. Also, the conventional FP-LDs are typically narrow band and limits on the number of subscribers in PONs and hinders bulk production of transceivers in ONUs. However, they have appeared to be promising candidates compared to costly externally tunable lasers (TLs) and typical contenders like DFB, distributed Bragg reflector (DBR) lasers and vertical cavity surface emitting laser [66].

Alternatively, broadband lasing emission laser devices based on Quantum dashes are also shown to promising candidates in optical communications. [63], particularly, WDM systems. In general, QDash based active region have wide gain profile due to inhomogeneous optical transitions, and hence translated into ultra-broadband lasing devices with tunable spectral range. Such devices are highly attractive in next generation optical fiber and optical wireless communication. Broadband nature of these devices have great advantage in high speed wavelength-division multiplexed (WDM) system as a single multi-wavelength source, as depicted in Figure 1.17 and Figure 1.18.

The quickly expanding interest for rapid information transfers and higher information transmission rates is becoming an integral part of our day by day life necessities. we can achieve maximum forecast data rate only through optical communication. A typical WDM

system is shown in Figure 1.17 which uses N-lasers for N-channels. A single shared medium could be used to transmit multiple channels simultaneously by WDM, coarse WDM and Dense WDM.

On the other hand, a broadband emitter can supply these sub-carriers as shown in Figure 1.18, possesses the potential to cut down the required N number of laser diodes in the WDM system significantly. However, broadband emitters in the form of light emitting diodes (LEDs) suffered from small power-bandwidth product which limits their usage in communications. Recently, novel broadband semiconductor laser with large power-bandwidth product have been reported which has the potential to be used as a source in WDM system. In order to have a green communication (energy efficient), a broadband laser which utilizes Quantum dashes in the active region, (QDash) is a potential candidate for optical WDM systems, given that its emission is wide enough.

## **1.4 Research Motivation**

Colorless sources should be a capable of wide wavelength tuning range via optical injection to encompass maximum sub-carriers. Most of the existing lasers available in literature are limited in wavelength tunability [67–71]. For instance, very recent 20 Gb/s upstream transmission using directly modulated weak resonant cavity (WRC) FP-LD is demonstrated, which is capable of ~26 nm (~13 nm) C-band (L-band) wavelength tunability (i.e. ~25–30 sub-carriers) via low power optical injection [ 67,68]. A directly

modulated 2.5 Gb/s ONU transmitter based on antireflection coated Fabry-Perot laser amplifier (AR-FPLA) is reported with a wavelength tunability of 30 nm in C-band encompassing 25 channels [69]. Likewise, a polarization insensitive FP-LDs with ~35 nm C-band tunability (i.e. ~17 sub-carriers) and 2.5 Gb/s OOK direct modulation is reported by injection-locking scheme [70]. In this work, we have utilized broadband and wide tunable injection-locked QDash laser source in next generation WDM-PON performance. This L- and U- band QDash FP-LD transmitter, which is capable of wide wavelength tuning from ~1611 to ~1634 nm (~23 nm) via optical injection, is shown to be capable of 100 Gb/s transmission capacity, encompassing ~50 longitudinal modes or sub-carriers.

On the other hand, OWC is being considered as an alternative optical access technology to the existing wireless RF solutions, especially for future WDM-based PON networks. For future access networks, several WDM FSO transmissions links have been demonstrated with different laser sources and transmission rates such as a 212 m FSO link based on wavelength division multiplexed 32 DFB-LDs in C-band (1535.7–1560.5 nm) has been demonstrated in [54] at 40 Gb/s/channel data rate. Likewise, 100 Gb/s transmission capacity per carrier, using 1550 nm LDs, has been reported in [57] on 80 m FSO links based on WDM. In this regard, we addressed a single channel 100 Gb/s 4 m indoor free space transmission system using QDash FP-LD and explored the feasibility of employing same tunable IL broadband QDash laser diode as a potential source also in outdoor FSO link for future high speed free space optical information and communication technology.

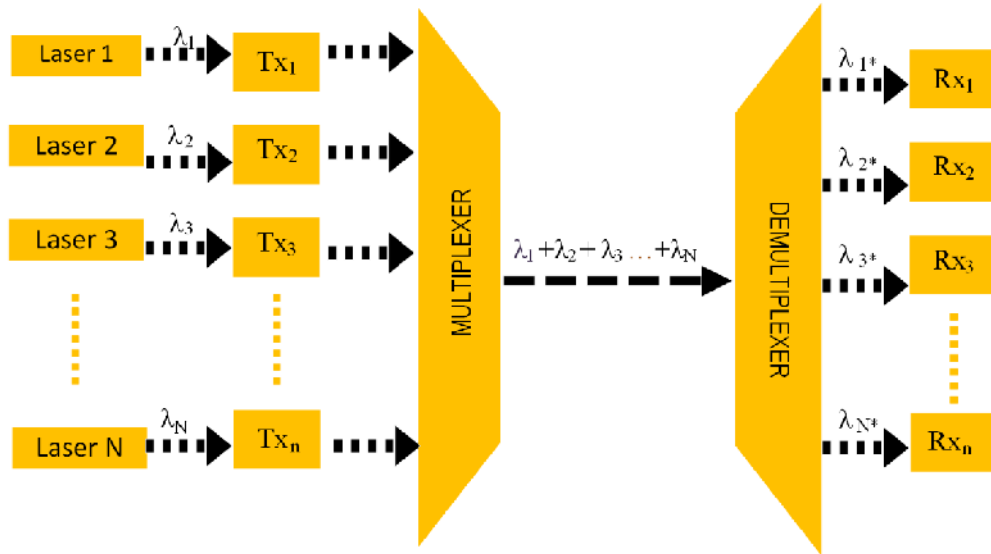


Figure 1.17 A typical WDM optical communication system.

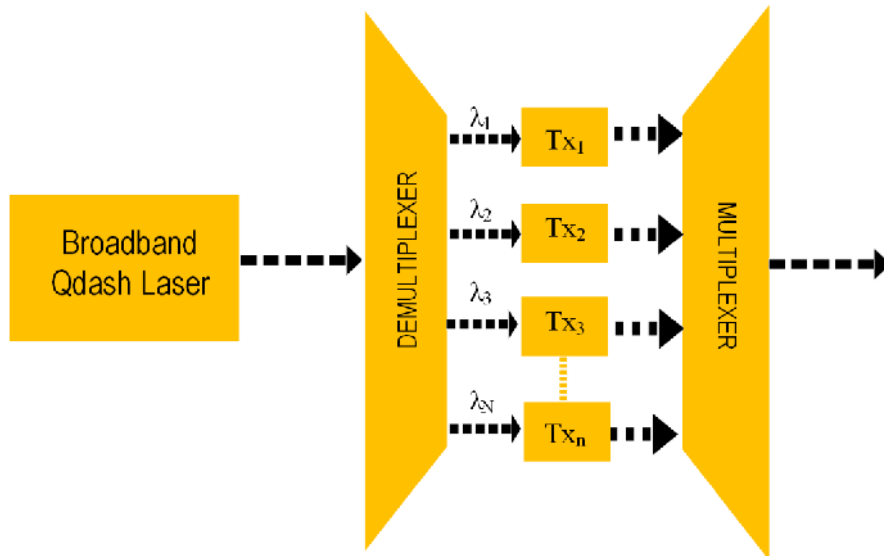


Figure 1.18 WDM optical communication system employ in a single broadband laser.

## 1.5 Thesis Research Contribution

The following are the thesis contributions:

- We evaluated the performance of InAs/InP quantum dash laser with different device structures in terms of internal quantum efficiency, internal loss, transparency current density, etc.
- We proposed and demonstrated the feasibility of employing L- and U-band QDash laser as light transmitters in both down transmission and up transmission for next generation 100Gbit-PONs. This will enable mass production and deployment of proposed QDash laser and photodiode based transceivers, thus significantly reducing the cost.
- Another contribution is QDash laser diode as a promising candidate in optical wireless communication. Specifically, we demonstrate the viability of engaging QDash broadband laser diode as a source in indoor free space optical communication for high-speed broadband wireless access applications.

## 1.6 Thesis Structure

The organization of thesis is follow as:

Chapter one contains the brief introduction about optical fiber communications. Then, the basic of optical wireless communication and its rapid developments is discussed in both indoor and outdoor free space optical communications.



Chapter two discusses the various light sources for optical communication and the literature survey on different quantum confined structures. The quantitative study is performed through experimental characterization of Quantum dash laser. In addition, the chapter also includes the comparison of fixed barrier with chirped QDash device.

Chapter three investigate the experimental characterization of injection-locked QDash laser diode. Injection-locking technique and its applications is briefly reviewed. Moreover, the chapter explores the different characteristics and parameters for their implementation in optical communication system.

In chapter four, the experimental transmission of an externally modulated far L-band injection-locked QDash laser diode is demonstrated. The chapter starts by discussing need for a unified WDM-PON transmitter for next generation. Following, the device level laser characterization setup is demonstrated. Later, a single channel high-speed dual-polarization quadrature phase shift keying transmission using broadband injection-locked QDash laser is explained via single mode fiber. Finally, the chapter presents the proposed WDM-PON upstream and downstream transmitter for next-generation passive optical networks.

In chapter five, the potential of optical wireless communication as an indoor and outdoor free space communication is discussed. Then, the single channel free space optical transmission and indoor laboratory setup using injection-locked QDash laser over 4 m and 2 m free space channel, is explained. Chapter five ends with the comparison between injection-locked slave QDash laser and tunable master laser, as an independently carrier.

Chapter six concludes the thesis work and summarizes some future potential work to extend this novel work.

## Chapter 2

### QUANTUM DASH LASER CHARACTERIZATION

The literature survey on broadband Quantum dash laser and device growth process is demonstrated in section 2.1. In section 2.2 and 2.3, the experimental characterization of Quantum dash laser is investigated device structure and characterization setup is discussed, respectively. To extract fundamental laser parameters, the quantitative study is performed in section 2.4. Finally, the chapter includes the comparison of fixed barrier with chirped QDash device in section 2.5.

#### 2.1 Semiconductor Laser Introduction

After the invention of first laser diode at 850 nm which was a regular GaAs p-n homojunction (Figure 2.1 (a)) where p-type and n type regions are of same materials, a novel concept of heterojunction structures was introduced by H. Kroemer [72]. Very soon, the first double hetero-structured (DH) laser was demonstrated with a layer of GaAs sandwiched between two layers of AlGaAs using liquid phase epitaxy (LPE) whose

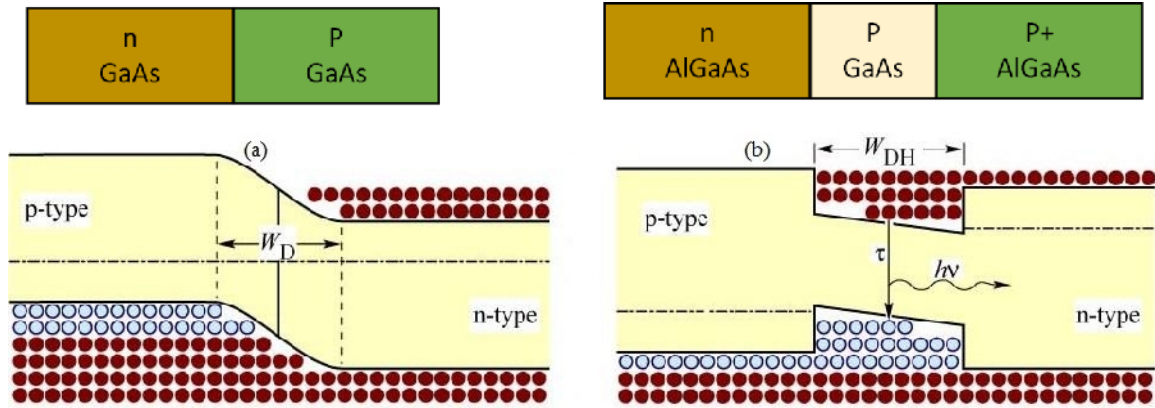


Figure 2.1 (a) homo-structure junction (b) double hetero-structure junction [72].

bandgap is larger than that of GaAs resulting in a relatively more confined active region as compared to regular p-n homojunctions [73], as shown in Figure 2.1 (b). The energy band diagram in the DH lasers are more confined inside the active region rather than homostructure junctions, thus improving the radiative recombination of electron-hole pairs occurring within the active region. Moreover, the variation in the refractive indices of the active region and the p and n regions, of the heterojunction forms an optical waveguiding mechanism that enables confinement of photons within the transverse modes of the optical waveguide, as suggested by Charles B. Henry with respect to GaAs/AlGaAs wave guides [74].

In the early 1970s, the idea of utilizing quantum effects in a laser diode was reported. However, at that time, the generally employed LPE technique for growing LEDs and bulk laser, were capable of producing thickness greater than 200 nm which created difficulty for the realization of quantum well lasers. In 1976, quantum-well lasers were grown with the help of molecular beam epitaxy (MBE) and demonstrated in [75]. The superiority of

quantum well laser as compare to the DH lasers in terms of reliability was further confirmed by R.Dingle [74]. Quantum well technology has several advantages in term of growth where we can control the depth, range and arrangement of quantum potential wells. Also by using Quantum wells there was a dramatic increase in the population inversion phenomenon in the active region. However, the produced optical power of these lasers were small compared with bulk lasers because of the faster gain saturation as a result of the restricted size of the active medium. In [76], the proposal and demonstration of a multiple quantum-well laser solved this issue by growing many single quantum-well layers one over the other, providing high power but with an expense of higher threshold current. Different configuration have been introduced since then, to control the thickness of quantum well; in order to lase in ultra-violet to visible to infra-red regions [77].

For proper telecommunication applications,  $In_{1-x}Ga_xAs_yP_{1-y}$  had been commonly used till now which can emit at  $1.3 \mu\text{m}$  and  $1.55 \mu\text{m}$  spectral windows. To grow quantum well laser diode at these wavelength windows, metal-organic chemical vapor deposition (MOCVD) epitaxial technique was introduced. Figure 2.2 shows the different possible compositions alongside the resulting effective energy bandgap. The corners of the polygon show the binary compounds, namely, GaP, GaAs, InP, and InAs. On the other hand, solid lines of the polygon show the ternary compounds, i.e. InGaAs, InAsP, GaAsP, and, InGaP and the points inside the polygon represent the quaternary  $In_{1-x}Ga_xAs_yP_{1-y}$  material. The composition of the grown materials must be in such a way that their bandgap energy is  $0.9537 \text{ eV}$  and  $0.7999 \text{ eV}$  in order to lase at  $1.3 \mu\text{m}$  and  $1.55 \mu\text{m}$  according to [78 –81]; as depicted in Figure 2.2 (a). Moreover, each layer should be lattice matched to the

subsequent layers in layer-by-layer fashion during the growth as shown Figure 2.2 (b). The vertical line in Figure 2.2 (a) indicates material composition of identical lattice constants. This type of growth i.e. the subsequent layers is used, lattice matched to the substrate is essential to have a minimum strain mismatch in order to reduce defects formation which drastically degrades the device performance [82].

To get three dimensional highly confined quantum dots (QDots), Stranski–Krastanov or self-assembled growth technique is used. A deliberately lattice mismatch is introduced in the epitaxial growth, in this technique, where the first layer will be a two-dimensional layer (barrier layer). Afterwards because of lattice mismatch, three-dimensional shape become to appear when enough different material is deposited in two dimensional fashion. Also a wetting layer underneath them of about 1-2 nm thickness is formed. Various studies employed InAs/GaAs and InGaAs/GaAs QDots active material to demonstrate 1.3  $\mu\text{m}$  laser at room temperature, and discuss about the threshold current, gain and characteristics temperature  $T$  values (reported in the range of 50-100 K) [83-85].

When the lattice mismatch strain is not identical in all directions in QDots formation, quantum dashes (QDashes) is shown to appear, which are highly inhomogeneous in nature. Figure 2.3 (a) and (b) show atomic force microscopic images (AFM) of InAs QDots and QDashes grown on InP material system, respectively [86]. It is observed that QDashes, when grown on InP substrate are a mixture of QDots and quantum wire-like structures and follows a quasi-zero dimensional density of states (DOS) (like that of a quantum wire). In order to explore more on C-U bands (1.5  $\mu\text{m}$  -2.0  $\mu\text{m}$ ) applications, InAs/InP QDots/QDashes based quantum confined structures have been focused more rather than

GaAs based QDots which are unable to cover these bands [87]. Using existing techniques, and InGaAlAs material over InP substrates, a QDot laser was reported in [88] emitting at  $1.63 \mu\text{m}$  having an internal loss of  $3.6/\text{cm}$ . In [82], Akahane *et al.* showed a lasing emission of  $1.58 \mu\text{m}$  out of a multi-stack of InAs/InGaAlAs Qdot lasers with a threshold current density of  $2.7 \text{ kA}/\text{cm}^2$ . A lower threshold current density value of  $1.72 \text{ kA}/\text{cm}^2$  was reported later in [89] which is the lowest reported value for any InAs/InP grown QDot laser.

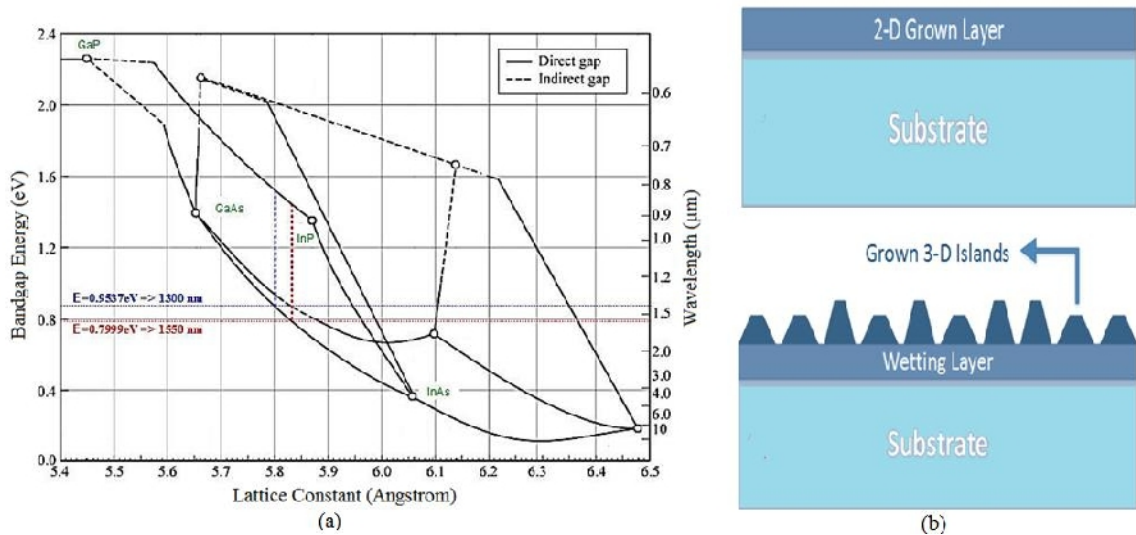


Figure 2.2 (a) Semiconductor material quaternary configurations, showing the materials employed to attain 1300 nm and 1550 nm emissions [76-78], (b) self-assembled epitaxial grown method.

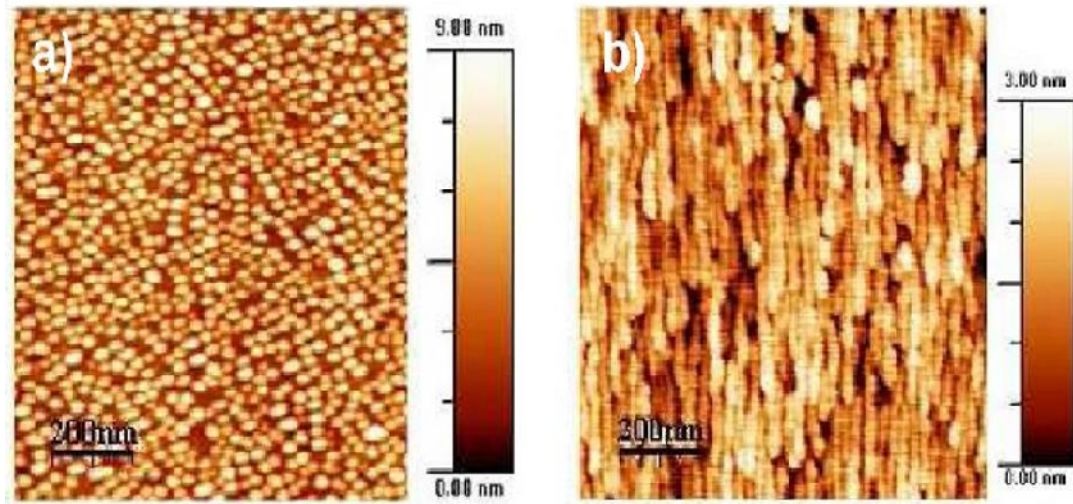


Figure 2.3 AFM images of InAs grown (a) QDots and (b) QDashes on InP substrate [87].

For QDash laser, the first report of InAs QDash laser over a substrate of InP emitted at  $1.60 \mu\text{m}$  [90]. The reported threshold current density was  $410 \text{ A/cm}^2$  while the internal loss and internal quantum efficiency were  $\sim 10/\text{cm}$  and  $60\%$  respectively. The better performance of results also depends upon the quality of growth process. Afterwards, Schwertberger *et al.* reported a great tunability range of their QDash laser based on the same materials whose emission peak ranged from  $1.54$  to  $1.78 \mu\text{m}$  by the virtue of changing the thickness of the deposited InAs layers while keeping the threshold current at the low value of  $900 \text{ kA/cm}^2$  [91].

Better results were reported as the quality of the growth process improved. In [92], longest emission wavelength of  $2.03 \mu\text{m}$  was achieved using a stack of 5 layers of InAs QDashes embedded in an InGaAs quantum well by Rotter *et al.* In both QDashes and Qdots material system, varying the barrier thickness, composition and thickness of monolayer grown



material to form Qdots/QDashes (called as chirping thus creating addition inhomogeneity of active region) as well as the fixed barrier structure (unchirped or typically grown structures) are reported. Chirped active region device structure provide broad gain, attractive for semiconductor optical amplifier and broadband laser applications. Different research works have followed the chirped active region technique such as [93] and [94] with internal loss values of  $4.6 \text{ cm}^{-1}$  and  $11 \text{ cm}^{-1}$ , respectively, and internal quantum efficiencies of 60% and 85%, respectively, while lasing at  $1.53 \text{ }\mu\text{m}$  and  $1.62 \text{ }\mu\text{m}$ , respectively.

In general, broadband nature of QDots and QDashes, are undesirable since it degrades the laser performance, however exploiting the broadband nature of these laser, they can confined potential applications in energy efficient optical telecommunication. Moreover, broadband lasers can produce extremely short light pulses in the order of picoseconds and femtoseconds through phase-locked mode locking inside the laser cavity. In [95], broadband QDash laser emitting at  $1.55 \text{ }\mu\text{m}$  are utilized with 8 channels (Fabry Perot modes from the lasing emission were used as a sub-carrier) in WDM system of 100 GHz spacing. A data transmission of 10 Gb/s was reported using OOK. Later, they were able to achieve 1.562 Tb/s over a 75 Km long single mode fiber transmission using WDM and higher modulation schemes [96]. All these demonstrations show the potential of broadband QDash laser as a potential source in optical communications.

## 2.2 Quantum Dash Device Structure

The semiconductor laser source used in this work for device characterization is a fixed barrier InAs/InAlGaAs/InP QDash laser. The device structure was grown by molecular beam epitaxy over InP substrate. The laser is a *p-i-n* structure with active region consisting of four-sheet of InAs QDashes, and each dash layer is embedded in an asymmetric InAlGaAs quantum well. The wells are then sandwiched between two sets of separately confined heterostructures (SCHs). The QDash-in-well structure consists of a 1.3 nm thick compressively strained  $In_{0.64}Ga_{0.16}As_{0.2}As$  layer, a five monolayer thick *InAs* dash layer and a 6.3 nm thick compressively strained  $In_{0.64}Ga_{0.16}As_{0.2}As$  layer. Each dash-in-well stack is separated by a 15 nm thick tensile strained barrier layer of  $In_{0.50}Ga_{0.32}As_{0.18}As$ . The lower and upper cladding consist of a 200 nm thick  $In_{0.52}As_{0.48}As$  layer with doping Si at  $1 \times 10^{18} \text{ cm}^{-3}$  and a 160 nm thick  $In_{0.52}As_{0.48}As$ , a 150 nm thick  $In_{0.53}Ga_{0.47}As$  with Be doping Si at  $2 \times 10^{18} \text{ cm}^{-3}$ , respectively [97]. Figure 2.4 (a) shows the band diagram of the InAs/InAlGaAs QDash laser while Figure 2.4 (b) show a plane-view AFM of the surface QDash.

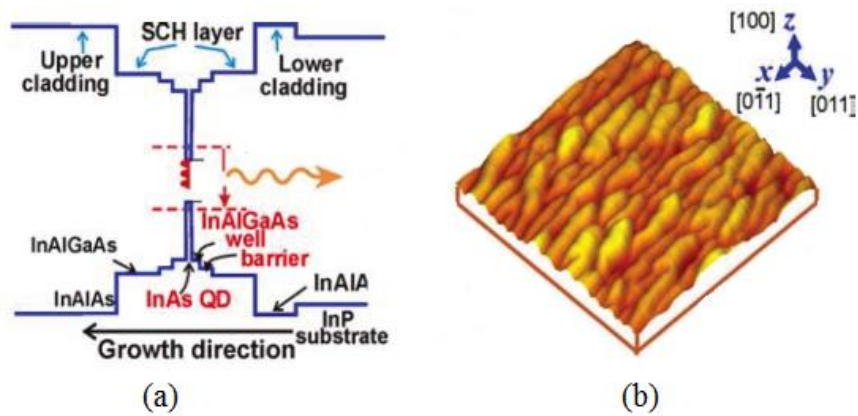


Figure 2.4 (a) band diagram of the InAs/InAlGaAs QDash laser (b) plane-view atomic force microscopy (AFM) of the surface QDash [97].

The device structure is then fabricated using conventional laser fabrication technique and then cleaved in to laser bars of several cavity lengths. Figure 2.5 (a) shows such a single laser bar containing several fixed cavity-length devices. Each bar contains laser devices with different ridge width values, namely  $2\ \mu\text{m}$ ,  $3\ \mu\text{m}$ , and  $4\ \mu\text{m}$ . Figure 2.5 (b) shows a microscopic image of a partial laser bar displaying two laser diode devices.

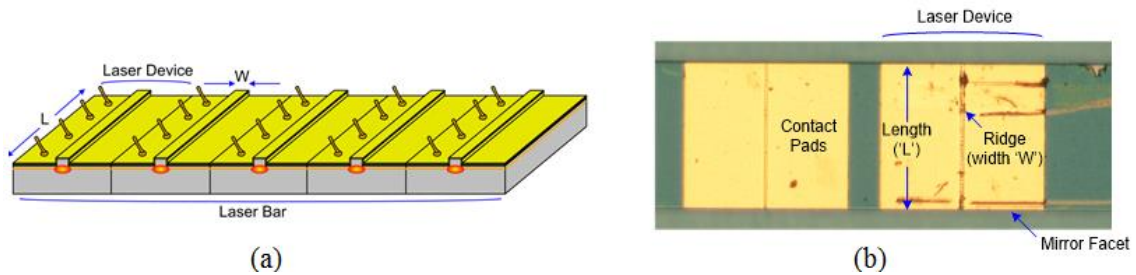
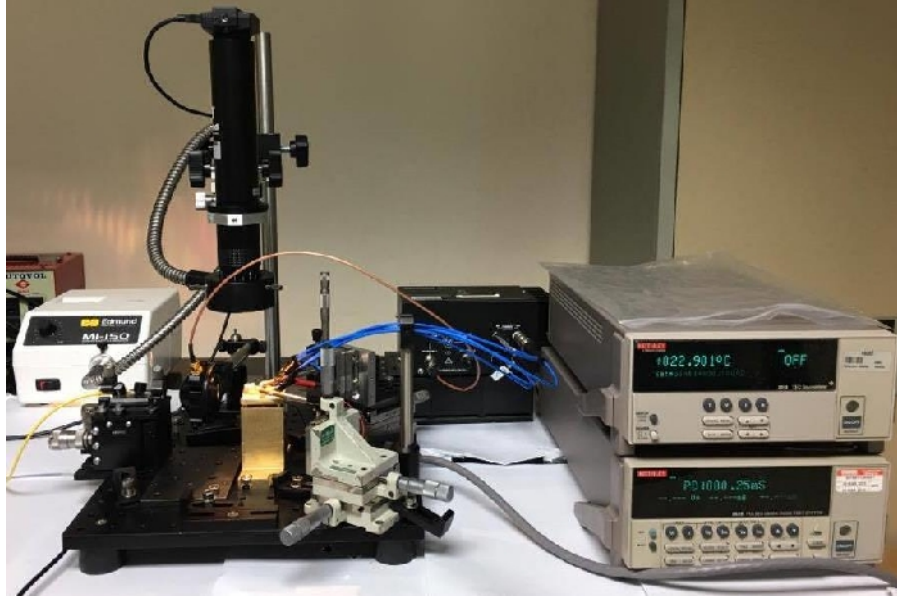


Figure 2.5 a) A single laser bar containing several fixed cavity-length devices. (b) a microscopic image of a single laser bar.

### 2.3 Bare Semiconductor Laser Diode Characterization Setup

To characterize different laser devices of different cavity lengths, laser diode characterization setup was used, as shown in Figure 2.6. As mentioned earlier, each laser bar contains different laser devices with different ridge width values of  $2\ \mu\text{m}$ ,  $3\ \mu\text{m}$ , and  $4\ \mu\text{m}$ . We used  $4\ \mu\text{m}$  ridge width device of eight cavity lengths for testing. Each laser device was probe-injected with a pulsed 0.2 % duty-cycled current between 0.001 A to 1.5 A in a 0.003 A step size. To get current- voltage (I-V) characteristics, voltage drop across each

device was measured at each current step. Subsequently, in order to find output light power vs injection current (L-I) characteristics of each laser, we collected the emitted photons from one of the facet using photodetector (see Figure 2.7 (a)) and obtain its equivalent photo-current which was related to an optical power once the lasing wavelength is known, by its responsivity value. Afterwards, in order to couple the optical power into single mode fiber, the best laser device, in terms of threshold current, efficiency slopes (extracted from L-I characteristics) is selected. One end of the fiber is connected to optical spectrum analyzer (OSA) Yokogawa AQ6370D while other end of optical fiber facet is placed on the three axis translation stage in front of laser device facet for proper alignment, as shown in Figure 2.7 (b).



**Figure 2.6 Laser characterization laboratory setup.**

The wavelength range was swept from 1635 to 1700 nm centered at 1675 nm with a resolution of 0.02 nm. Next, emission spectrum of each device were measured at different

injected current values to find their emission profiles and -3 dB bandwidth. All the measurements were performed at room temperature. The complete illustration of device level characterization setup before coupling the power into SMF is shown in Figure 2.8

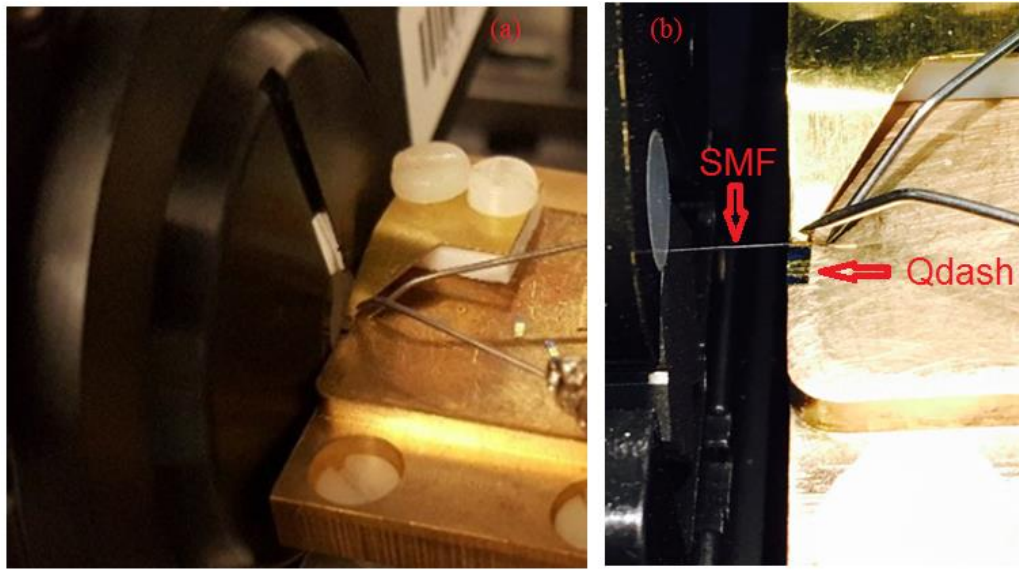


Figure 2.7 a) Photodetector for collection of photons (b) Laser light coupling into a lensed single mode fiber.

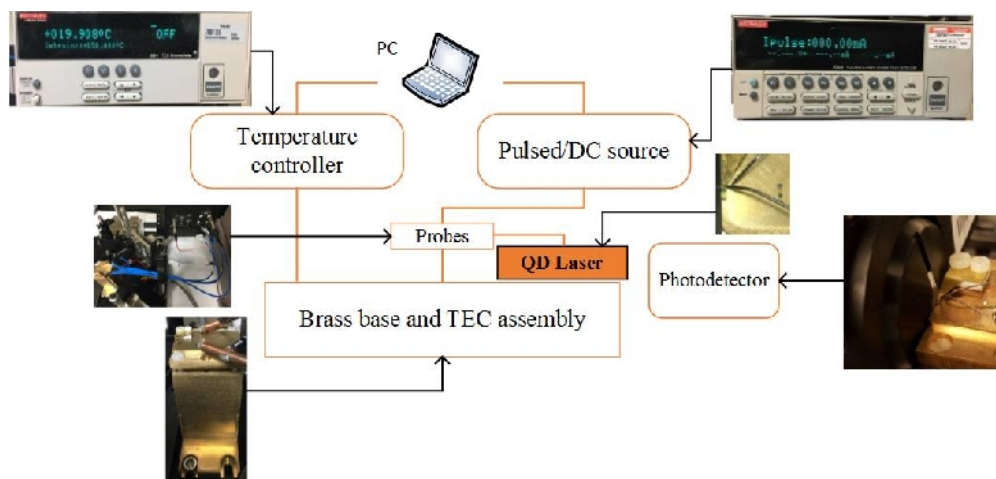


Figure 2.8 Demonstration of laser characterization setup at device level before coupling power into SMF.

## 2.4 Semiconductor Laser Diode Performance Parameters

### 2.4.1 I-V Characteristics

The most essential diode characteristics is its I-V relationship. This characterizes what the current going through a segment is, given what voltage is measured crosswise across it, resistors, for instance, have a basic, linear i-v relationship Ohm's Law. The slope of the I-V curve denotes the dynamic series resistance of the diode. Figure 2.9 shows the I-V curves of 8 different cavity length laser devices. After extracting the slope of each I-V curve, we can find the Ohmic series resistance of the devices which are tabulated in in Table 2.1. In addition, the device turn on voltage is also calculated.

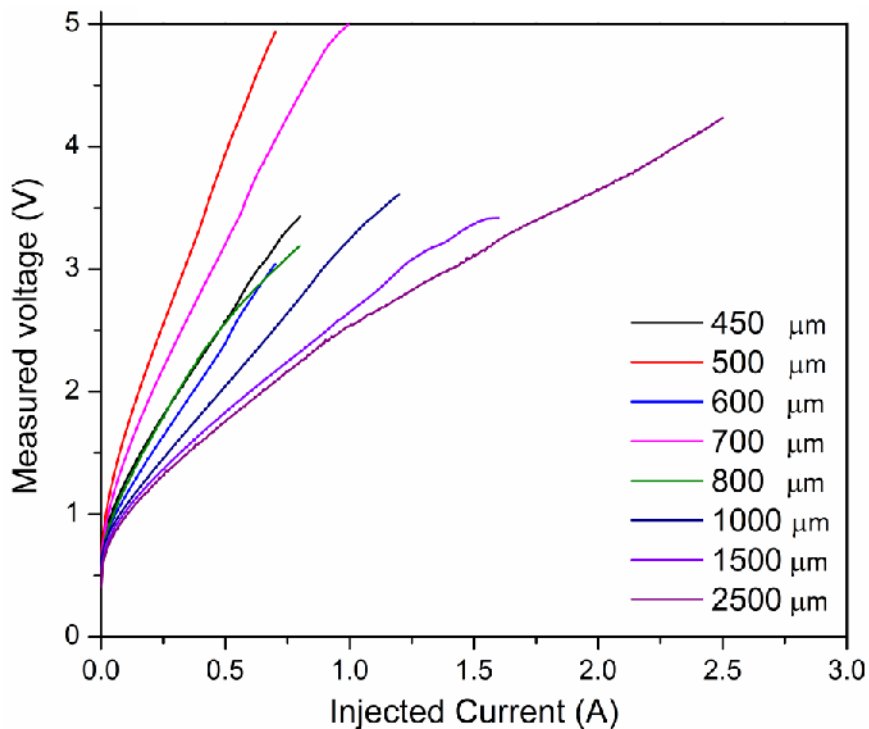


Figure 2.9 I-V characteristics of different cavity length fixed barrier QDash laser diodes.

Table 2.1: Resistance values and turn on voltages of different cavity length lasers.

Cavity Length[ $\mu\text{m}$ ]	450	500	600	700	800	1000	1500	2500
Resistance [ $\Omega$ ]	1	2	3.33	4	4.2	4	3	3.5
Turn on Voltage[V]	0.82	0.81	0.70	0.86	0.67	0.69	0.71	0.70

## 2.4.2 L-I Characteristics

L-I curve of a laser diode is the most significant performance characteristics, which measure the light output power as a function of injection current into device. Figure 2.10 shows the L-I curve of different cavity lengths of the fixed barrier QDash laser. Parameters like threshold current  $I_{th}$ , threshold current density  $J_{th}$  and slope efficiencies can be extracted from L-I curve. The laser first emits in spontaneous regime as small current is being injected into the device, since the gain of the active medium at this point had not overcome the losses, yet. However, as injection current increases, until it starts to emit in stimulated region and this lasing action starts at the threshold current  $I_{th}$  value. It is desirable that threshold current be as low as it could be, for the better efficiency of device. The second parameter threshold current density  $J_{th}$  is obtained by dividing the threshold current by the area of the active region (which is assumed to be the ridge width  $\times$  cavity length). Threshold current density is an indicator of how good the active medium material is; the lower its value the better the material is. Longer cavity length laser device could show a much higher threshold current as compare to shorter cavity length due its larger active area. Certainly, it requires more current for lasing. Therefore, it is more suitable to refer in terms of threshold current density instead of threshold current. Another significant parameter is the slope efficiency that can be extracted from the slope of L-I curve. This

slope indicates how much optical power is being emitted by the laser diode with respect to the injected current. Therefore, a higher value for this slope is desirable and is another direct indicator of the performance of the laser device. Table 2.2 shows the threshold current and threshold current density values, measured slope efficiencies and the equivalent optical slope efficiencies, which is obtained by dividing by the responsivity of the photodetector of these devices which is equal to of 6.52 mA/W (at 1.69  $\mu\text{m}$  wavelength). It can be seen from the Table 2.2 that longer cavity has the lower threshold current density. However, it provides less slopes efficiencies because of small threshold gain.

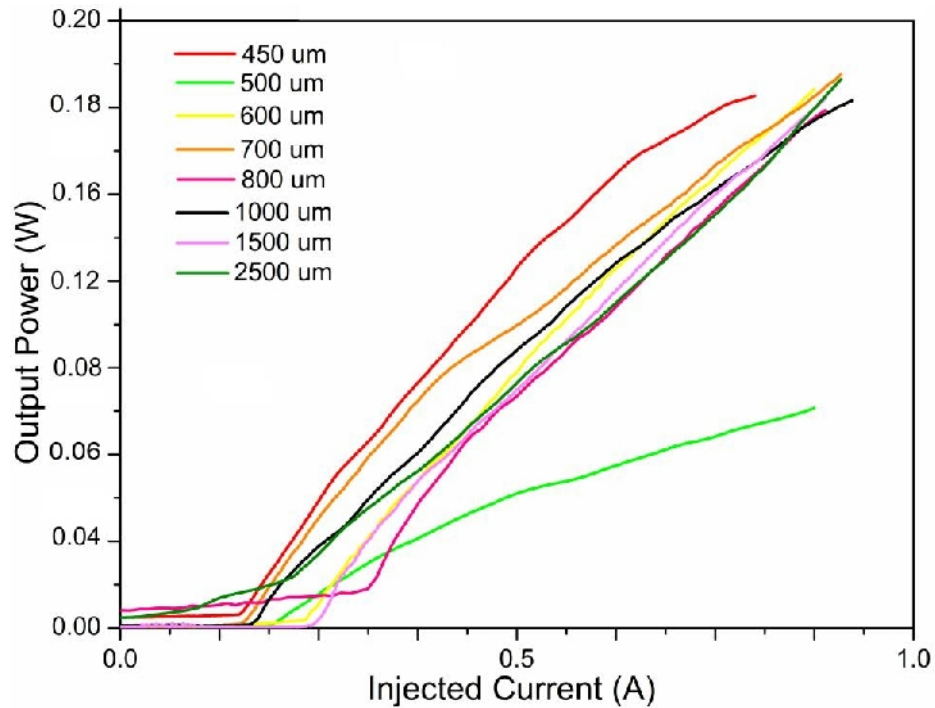


Figure 2.10 L-I characteristics of different cavity length fixed barrier QDash laser diodes.



### 2.4.3 External Differential Quantum Efficiency

The external quantum efficiency (EQE)  $\eta_d$  is another important parameter that represents how much optical power is getting out of the laser diode with respect to the supplied carriers into the device. It can be found by calculating the slope efficiency using the following relation [98].

$$\eta_d = \frac{\Delta P}{\Delta I} \left[ \frac{q\lambda}{hc} \right] \quad (2.1)$$

Where,  $\eta_d$  is the external differential quantum efficiency,  $\frac{\Delta P}{\Delta I}$  is the L-I curve slope efficiency in W/A,  $h$  is Planck's constant equals to  $6.626 \times 10^{-34}$  J.s,  $\lambda$  is the emission center wavelength,  $c$  is the speed of light in a vacuum and equals to  $2.99 \times 10^8$  m/s and  $q$  is the charge of an electron equals to  $1.620022 \times 10^{-19}$  C.

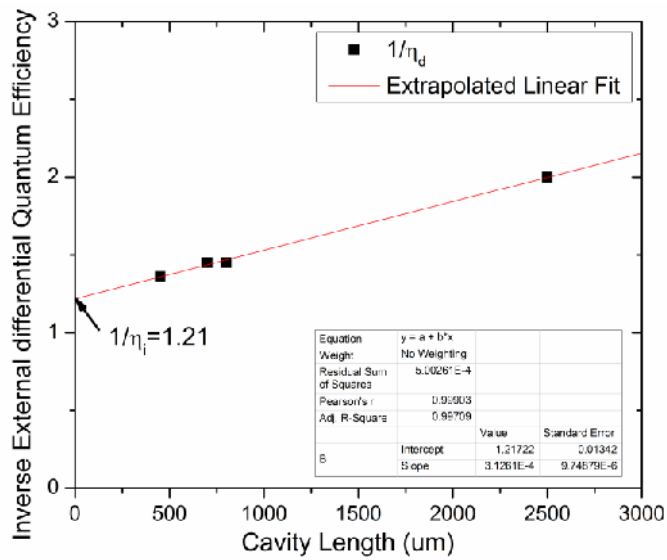


Figure 2.11  $1/\eta_i$  vs different cavity lengths of fixed barrier QDash laser.

**Table 2.2: Threshold current density and efficiency slope of different cavity length fixed barrier QDash laser devices.**

Cavity Length [ $\mu\text{m}$ ]	450	500	600	700	800	1000	1500	2500
Threshold Current [A]	0.145	0.144	0.183	0.166	0.279	0.206	0.428	0.582
Active region area [ $\text{cm}^2$ ]	$1.8 \times 10^{-5}$	$2 \times 10^{-5}$	$2.4 \times 10^{-5}$	$2.8 \times 10^{-5}$	$3.2 \times 10^{-5}$	$4 \times 10^{-5}$	$6 \times 10^{-5}$	$1 \times 10^{-4}$
Threshold Current Density [ $\text{A}/\text{cm}^2$ ]	8277	7230	7658.33	5946.42	8743.75	5172	7143	5822
Optical Efficiency Slope [W/A]	0.54	0.43	0.45	0.508	0.506	0.68	0.72	0.11
Inverse Cavity Length [ $\text{cm}^{-1}$ ]	22.22	20	16.67	14.28	12.50	10	6.67	4
EQE [%]	73.3	58.3	61.09	68.69	68.69	92.31	98.32	14.9
$1/\eta_d$	1.36	1.72	1.63	1.45	1.45	1.08	1.01	2.01

In principle, the slope efficiency with respect to the increasing cavity lengths should decrease hence external quantum efficiency should also go down. However, Table 2.2 shows abrupt behavior in term of threshold current, optical efficiency slope and external quantum efficiency, as observed in L-I characteristics of different cavity lengths (see Figure 2.10), besides the variation in the turn on voltage. This is attributed to the device fabrication process, handling and probing of the bare devices for characterization. For the date of Table 2.2, we selected the best device with low threshold current and high slope efficiency from a number of tested devices. Moreover, we utilized the available several cavity lengths in both CW and pulsed mode for fitting purpose.

#### 2.4.4 Internal Quantum Efficiency

Internal quantum efficiency  $\eta_i$  is a measure of how much of the injected electron-hole pair in the active region is contributing to light emission inside the laser diode structure through radiative recombination. It is a performance parameter of the material of the active region itself regardless of its length unlike external quantum efficiency. External differential quantum efficiency values are plotted against different cavity lengths to find its value. The y-intercept of the extrapolated fitted line indicate the inverse of this value as shown in Figure 2.11. The inverse of this value represents internal quantum efficiency.

Table 2.3: Internal quantum efficiency and Internal loss of fixed barrier QDash laser.

$1/\eta_i$	Internal Quantum efficiency $\eta_i$ [%]	Slope [ $\mu m^{-1}$ ]	Internal loss $\alpha_i$ [ $cm^{-1}$ ]
1.284	82.64	0.00031	8.803

### 2.4.5 Internal Loss

The internal loss  $\alpha_i$  is a parameter that represents the portion of lost generated photons (which are generated in active region) due to re-absorption before exiting the cavity through the mirror facets of the laser diode. The loss inside the optical wave refers to internal loss. Referring to Figure 2.11, the slope of linear fitted curve is used to find the internal loss according to the following [98],

$$1/\eta_d = 1/\eta_i \left[ 1 + \frac{\alpha_i}{\ln(1/R)} L \right] \quad (2.2)$$

Where,  $\eta_d$  is the external differential quantum efficiency,  $\eta_i$  is internal quantum efficiency,  $\alpha_i$  internal loss,  $R$  is the reflectivity of the mirror facets of the laser cavity which equals to 0.31 for as-cleaved facets in typical lasers,  $L$  is the cavity length values. Table lists the value of this extracted parameters.

### 2.4.6 Transparency Current Density

Another important parameter which is measured in Figure 2.12, is the transparency threshold current density  $J_o$ . It is a measure of when the losses in the active region is compensated (i.e. Loss = Gain). Unlike the threshold current density, it does not depend on the length of the active region. Therefore, it does not make sense to use threshold current density  $J_{th}$  for comparison of different quality of semiconductors. The transparency current density  $J_o$  can be obtained as the y-intercept of the linear fit threshold current density  $J_{th}$ , at different cavity length values, against the inverse of these lengths ( $1/L$ ). Figure 2.12

Threshold current density  $J_{th}$  vs. the inverse of different cavity length values. shows a linearly fitted line of the threshold current density values ( $A/cm^2$ ) and the respective inverse cavity length at the inverse of different cavity length values ( $cm^{-1}$ ), which are tabulated in Table 2.3. The extrapolated fitted line shows that the transparency threshold current density of this laser is  $5639 A/cm^2$ .

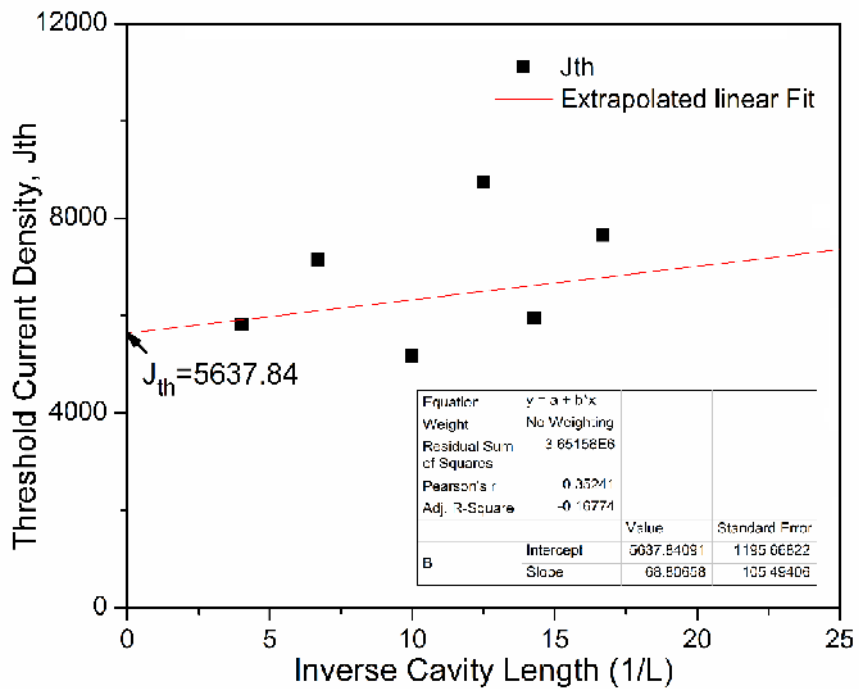


Figure 2.12 Threshold current density  $J_{th}$  vs. the inverse of different cavity length values.

## 2.4.7 Emission Spectrum

To get the laser spectra, three cavity length lasers have been analyzed. All of them shows a central wavelength at  $\sim 1690$  nm. Due to the maximum wavelength limitation of OSA

(Wavelength range: 600 to 1700nm), all these spectrums show high noise at the extreme longer wavelengths. This is due to reduce sensitivity of optical spectrum analyzer (OSA) at these wavelengths. Figure 2.13 (a) – (c) show the emission spectrum of the 600, 800 and 1500  $\mu\text{m}$  cavity length laser at 0.384 ( $2.1 I_{\text{th}}$ ), 0.837 ( $3 I_{\text{th}}$ ) and 1.19 ( $2.8 I_{\text{th}}$ ) injection currents. It can be observed that 800  $\mu\text{m}$  cavity length shows the broadcast emission. It can be observed in Figure 2.13 that as we are increasing the cavity length, the emission gets red shifted. This is ascribed to the decrease in the mirror loss (equation 2.2) which enables achievement of threshold gain at comparatively lower transition energies, thus translating to longer lasing emission.

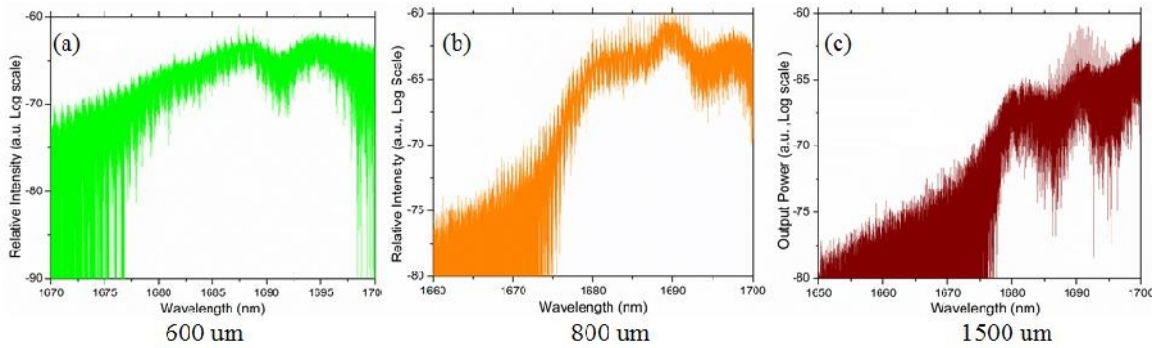


Figure 2.13 Emission spectra of the 4  $\mu\text{m}$  ridge devices of cavity lengths 600, 800 and 1500  $\mu\text{m}$  fixed barrier QDash lasers.

## 2.5 Comparison of Fixed and Chirped barrier QDash Laser

As explained in section 2.4, we utilized fixed barrier InAs/InGaAlAs/InP QDash laser devices for device level characterization. However, for communication experiment, chirped multi-stack InAs/ InGaAlAs /InP QDash laser diode was utilized due to its better

performance in terms of coupled power and lasing emission wavelength as compared to fixed barrier QDash devices. This chirped QDash laser diode laser was grown on n-type InP substrate by MBE technique. The active region is composed of a four stack InAs/InGaAlAs QDash-in-a-well structure where the layers are separated by barrier layers of thickness values of 10 nm, 15 nm, and 20 nm. Varying the barrier layer thickness between different dash ensembles introduces more inhomogeneity thereby introducing wide emission range. Such inhomogeneity is attributed to the variant vertical strain exhibited by each stack during the growth process which has a direct influence on the variation of the dashes height. This intentional chirping the active region increases the inhomogeneous broadening and consequently ultra-broadband lasing emission. A layer-by-layer illustration of the structure of the fixed and chirped barrier Qdash laser diode is shown in Figure 2.14.

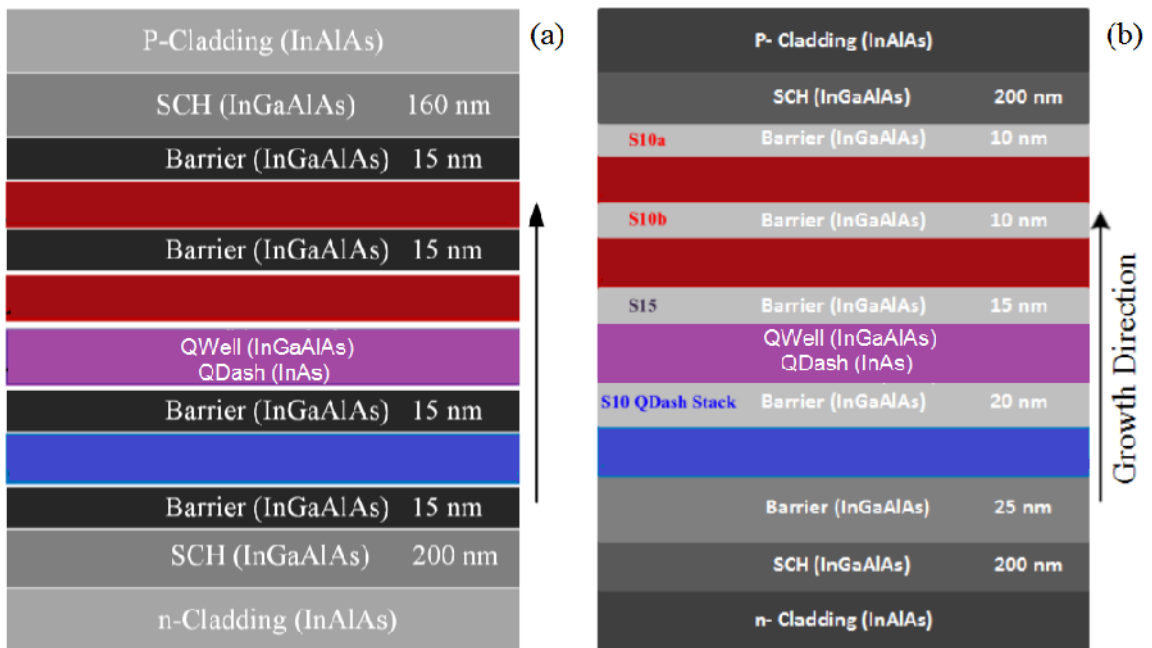
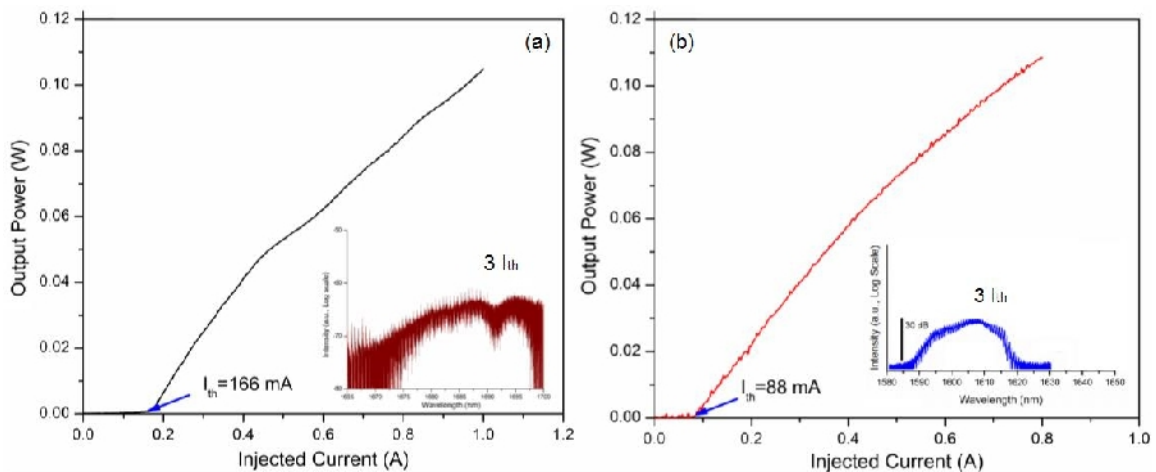
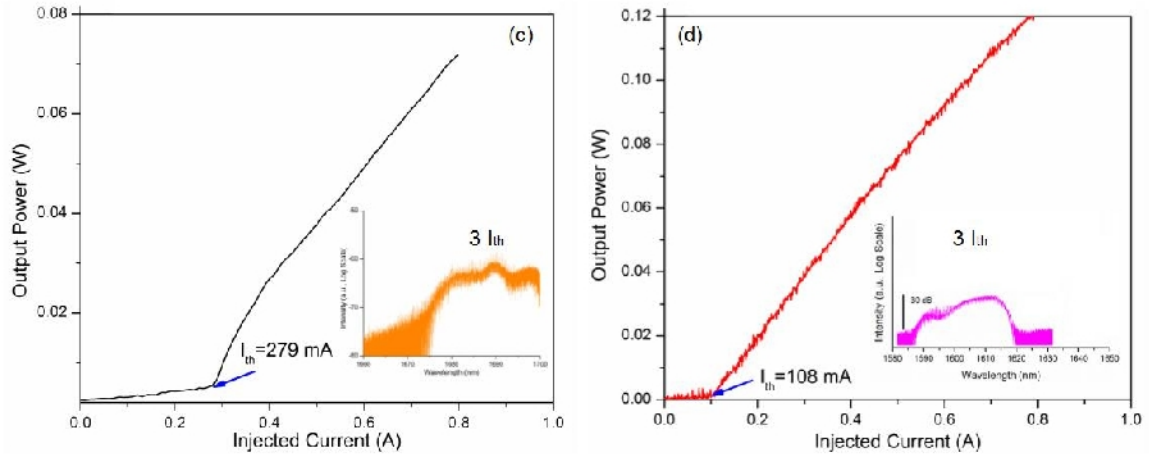


Figure 2.14 QDash Laser diode device structure (a) fixed barrier (b) chirped.

A 4  $\mu\text{m}$  ridge QDash laser diode is utilized with different cavity lengths in both fixed barrier and chirped barrier QDash laser devices. Table 2.4 and Table 2.5 present the comparison of both the above type of laser diodes with 700  $\mu\text{m}$  and 800  $\mu\text{m}$  cavity lengths which have been utilized in system level experiments. It can be observed from both tables that chirped QDash laser has low threshold current which leads to high internal quantum efficiency  $\eta_i$  of 83.62 % as compared to fixed barrier  $\eta_i$  82.6 %. Moreover, the chirped QDash cavity lengths shows better linear fitting, however leads to internal loss of 10.77  $\text{cm}^{-1}$  due to intentionally homogeneity as compared to the fixed barrier QDash cavity lengths which shown 8.6  $\text{cm}^{-1}$  internal loss. Furthermore, Figure 2.15 shows the  $L$ - $I$ - $V$  characteristics of fixed and chirped barrier QDash laser of both 700  $\mu\text{m}$  and 800  $\mu\text{m}$  cavity lengths.







**Figure 2.15: Light output injected current measured voltage (L I V) characteristics of (a) fixed barrier QDash 4x700 μm<sup>2</sup> laser, (b) chirped barrier QDash 4x700 μm<sup>2</sup> laser, (c) fixed barrier QDash 4x800 μm<sup>2</sup> laser, (d) chirped barrier QDash 4x800 μm<sup>2</sup> laser. The corresponding insets show the lasing emission at 3  $I_{th}$  injection current.**

It can be observed that the chirped barrier devices have low threshold currents as compared to the fixed barrier devices. Moreover, the central lasing wavelength of fixed barrier QDash laser was found to be ~1690 nm whereas the chirped barrier QDash laser emission is at ~1610 nm, at room temperature (RT), in both cavity lengths, as shown in the insets of Figure 2.15. Also notice that the emission wavelength range of fixed barrier QDash lasers was beyond the detection limit of various communication equipments, which are in the range of 1528 nm – 1630 nm. This rendered employment of fixed barrier QDash laser diodes in optical communication unfeasible. Hence, the optical communication experiments were accomplished with chirped barrier QDash lasers of two cavity lengths i.e. 700 μm or 800 μm. It is noteworthy to mention that we also reduced the operating temperature from the RT to 14 C° while performing the optical communications experiments to further blue shift the central lasing wavelength of chirped barrier QDash lasers, to be able to reach within the sensitivities of all the equipments/components.

**Table 2.4: Comparison between fixed barrier and chirped  $4 \times 700 \mu\text{m}^2$  ridge QDash laser diode in terms of efficiency parameters.**

Parameters Measurements	Fixed barrier QDash laser	Chirped QDash laser
Threshold Current $I_{th}$ [A]	0.166	0.088
TCD $J_{th}$ [ $\text{A}/\text{cm}^2$ ]	5946	3372
Central lasing Wavelength (nm)	~1690	~1610

**Table 2.5: Comparison between fixed barrier and chirped  $4 \times 800 \mu\text{m}^2$  ridge QDash laser diode in terms of efficiency parameters.**

Parameters Measurements	Fixed barrier QDash laser	Chirped QDash laser
Threshold Current $I_{th}$ [A]	0.279	0.108
TCD $J_{th}$ [ $\text{A}/\text{cm}^2$ ]	8743	3146
Central lasing Wavelength (nm)	~1690	~1610

## **Chapter 3**

### **INJECTION-LOCKING CHARACTERIZATION**

The experimental characterization of injection-locked QDash laser diode is investigated in this chapter. In section 3.1, the objectives and the need for injection-locking is discussed. Following, the basic operation of injection-locking technique and its applications are highlighted in section 3.2 and 3.3, respectively. Injection-locking technique in semiconductor laser is reviewed along with a literature review in section 3.4. The experimental injection-locking setup and characterization experiments are elucidated in sections 3.5 and 3.6, respectively.

#### **3.1 Introduction**

The telecommunication field has been driven by the digital and analogue transmission of data over the past 35 years with substantial improvement towards high transmission capacity and for longer distances. In early 1990s, the development of WDM system significantly increased the communication system bandwidth, where multiple users (wavelength channels or sub-carriers) share single fiber, as explained in chapter 1, Also thanks to the tremendous improvement in the semiconductor laser performance which enabled these achievements, particularly quantum confined active region based devices. However, the performance of semiconductor laser dynamics can be limited in terms of

linewidth, direct modulation and mode stability [99] when it comes to direction modulation in which information signal riding on direct current is injected or pumped in to the light source. Due to low fabrication cost and compactness, directly-modulated lasers are getting attention as promising candidate in optical communications, besides consuming less power as compared to the external modulation (the CW laser light, in this case, is modulated by an information signal through external modulator and is easier in implementation). However, the modulating output power depends on the internal dynamic of the laser which limits the transmission rates (usually low bandwidth), and has been attributed to a high chirp, small relaxation oscillations, etc. [100]. For instance, a directly modulated weak resonant cavity (WRC) lasers are limited to a low transmission rate in the range of 2.5-28 Gb/s [101–102].

To enhance the modulation bandwidth of optical communication system, external modulation of semiconductor laser can be implemented. Besides, injection-locking technique has also been utilized in both external and direction modulation of laser and has shown significant improvement in the laser dynamics and thereby achieving high data rates. The main motivation for injection locking is to improve the laser's linewidth, coherency, and wavelength instabilities [103].

In the subsequent sections, the basic operation of injection-locking technique is discussed and later applied to QDash laser to investigate its performance under injection locking.

This characterization is vital for its successful deployment in optical communication experiments that are discussed in chapter 4 and 5.

### **3.2 Injection-Locking Operation**

The basic operation of injection locking comprises of two optical sources called master and slave lasers. Figure 3.1 (a) depicts one possible configuration of injection-locking in which a master laser (usually tunable single mode laser) is injected into slave laser via one facet and the light output from the slave laser can be collected from the other facet. An optical isolator is usually placed to eliminate back reflection in to the master laser. In the other configuration where access to both the facets of the slave laser is not possible, the tunable master laser with narrow linewidth a CW high power is injected into the slave laser through optical circulator (OC), as shown in Figure 3.1 (b). Thereby, a phase become locked when matching between two frequencies (of master & slave) almost happens. Subsequently the side peaks become suppressed after locking. Physically, when a master laser is injected externally into the slave laser, the light we injected emulates with the emission of the slave laser to get amplified. When the frequency of the external injection light is close to the eigen-frequency or wavelength of the slave laser light, and strong enough in terms of power, it gets amplified due to the availability of gain provided by slave laser. Simultaneously, the gain of the other modes become saturate and suppress all the remaining free-running modes [104]. An optical circulator is placed so that only output light goes to the photodetector. To match the polarization states of master and slave laser, which helps

in improving the injection locking efficiency, polarization controller could be used within the setup.

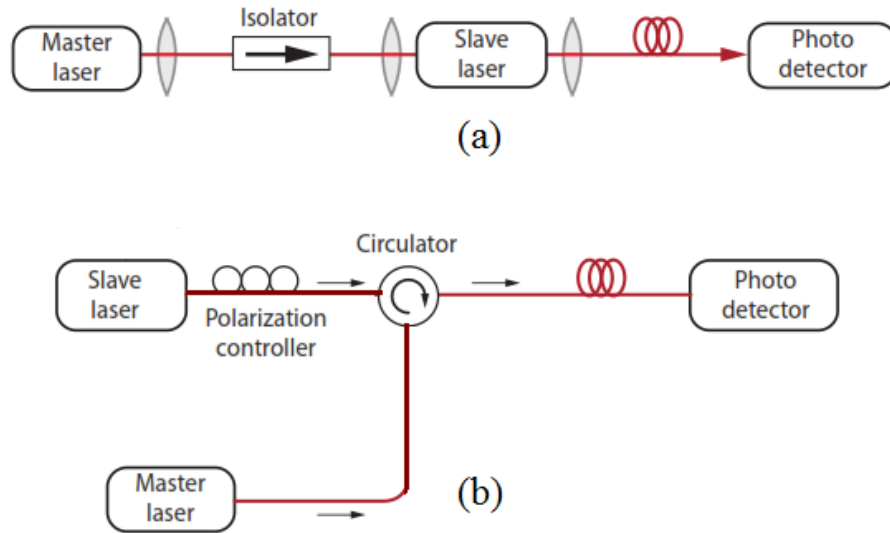


Figure 3.1 Typical schematics for injection-locking system (a) transmission style, (b) reflection-style [105].

Typically, the master laser are commercially available laser sources such as wide wavelength tunability external cavity laser with high linearity and DFB laser of high power, exhibiting small laser linewidths in the range of MHz to kHz. The important parameters for injection locking consists of injection ratio  $\eta$  and locking range (frequency detuning)  $\Delta f$ . The injection ratio, defined as  $\left(\frac{P_{master}}{P_{slave}}\right)$ , determines the optical power ratio of master laser over the salve laser, while the frequency detuning is the difference between master frequency and slave laser frequency, whilst maintaining locking condition (i.e. slave laser should remain injection locked). Following are some advantages of the injection-locking;

- Injection-locking (IL) assists in reducing the linewidth of Fabry- Perot (FP) laser (i.e.~ GHz to ~ kHz range).
- Reduced phase noise and relative intensity noise [106].
- Reduced frequency (wavelength) chirp [107].
- Increase modulation bandwidth [108].

In addition, injection locking have been utilized to reduce dispersion effects caused in long distances of single mode fiber (SMF) [108]. It has been shown that under stable injection-locking, a communication system can communicate over substantial length of SMF. Stability is an important factor for an injection-locked (IL) laser system and the, stability properties have been tested for a weak injection-locking by Mogensen *et al.* in 1985 [109]. The authors found that injection-locking is stable under negative frequency detuning ( $\lambda_{master} < \lambda_{slave}$ ) instead of positive detuning which created chaotic behavior. Figure 3.2 shows different stability regions in terms of frequency detuning and injection power. We can observe that un-shaded area other than stable and un-stable locking regime where four-wave mixing and other oscillations could occur while the shaded area represents either locking or unlocking operation. The hatched part shows the instability for positive frequency detuning with strong injection. On the other hand, the negative frequency detuning shows stable injection-locking for weak injection power.

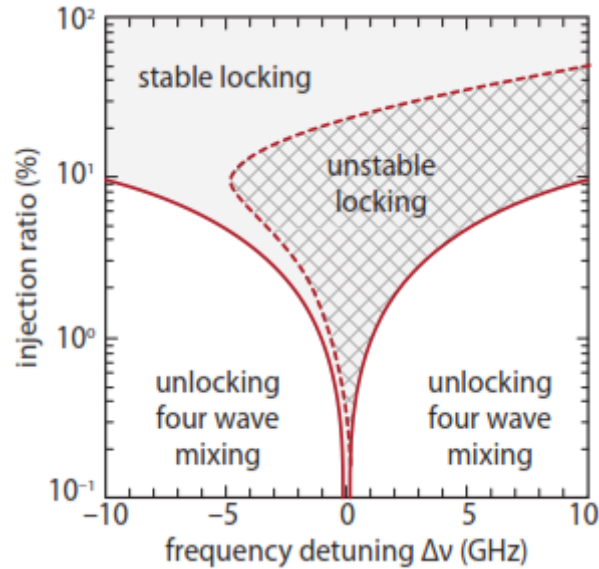


Figure 3.2 Frequency detuning vs. injection power for different stability conditions [105].

### 3.3 Applications of Injection-Locking

The method of injection locking was implemented in many state-of-the-art applications. For instance, to improve the directly modulated laser characteristics was one of the first application to improve the modulation bandwidth via injection locking [110–116]. Moreover, injection-locking has a wide range of applications in all-optical signal processing [117], millimeter-wave generation [118], power amplifiers [19] and multi-wavelength mode locked lasers [120]. Meanwhile, the wavelength-division-multiplexed passive optical network (WDM-PON) concept was proposed due to rapid demand of high transmission in optical technology and, injection-locking has found various applications in optically IL colorless WDM-PON transmitter (a CW injection locked Fabry-Perot laser diode (FP-LD) for achieving high speed WDM-PON at 10 Gb/s upstream and downstream transmission [121].



On the other hand, injection-locking was also realized in Radio-over-fiber (RoF) applications. A directly modulated injection-locked DFB laser was demonstrated in RoF communication channel for 155 Mb/s transmission [122], cable access TV applications (CATV) [123], and free-space optical communication for both visible and infra-red (IR) regions. In visible region, an injection-locked 680 nm VCSEL has been demonstrated to increase the transmission rate up to 40 Gb/s for optical wireless communication applications such light-fidelity (LiFi). Similarly, an IL laser diode transmitter based on 405 nm blue light is demonstrated to improve the bandwidth performance of underwater optical wireless communication from 2.3 Gb/s to 9.6 Gb/s [124–125]. Moreover, an injection-locked FSO transmission in IR regions will be discussed in chapter 05, in detail.

### **3.4 Injection-Locking in Semiconductor Laser**

Researchers have worked on the idea of frequency locking between two oscillators for centuries. Locking phenomena can happen between oscillators of any sort, and was demonstrated first on two pendulum clocks which were synchronized by Huygens in 1665. He found that two pendulum clock could synchronize to each other even with different initial parameters [126]. Later, Van der Pol created forced electronic oscillator using Huygens phenomena in 1927 [127]. Moreover, R. Adler in 1945 further made a development to this technique in electronics and communication [128]. He addressed locking phenomena theoretically in electric oscillators.

After the invention of laser in 1960s, for the first time in 1966, Stover and Steier successfully injection-locked two HeNe lasers [129]. In 1976, Buczek and Freiberg successfully demonstrated the injection locking in CO<sub>2</sub> lasers [130]. Finally, after the development of semiconductor lasers, employing injection-locking technique on them has been the focus of several researchers. In fact, it was found that injection locking with external modulation helped in reduce the linewidth and noise in lasers [131–132]. This was found to be one of the most important advantage of injection-locking. In addition, injection locking in direct modulation was also realized for coherent optical communication, with the advancement in active materials and laser designs [133–134]. However, direct modulation still limits the transmission capacity in optical communication links.

Several investigations were performed to enhance the modulation bandwidth of semiconductor laser diodes. In 1980's, Kobayashi *et al.* demonstrated injection locking on GaAs/AlGaAs double heterostructure lasers for single-mode operation [135]. In this paper, the authors reported the interference pattern between master laser and slave laser using phase injection-locking technique which could be used as an amplifier or oscillator in coherent transmission. Subsequently, the suppression of side modes to get a single mode via injection-locking with low partition noise at 1550 nm wavelength was demonstrated by Iwashita *et al.* [132]. In 1982, various theoretical works were published by Lang *et al.* on detail characterization of injection locking in semiconductor lasers [136]. Recently, using slave DFB at 1.55  $\mu\text{m}$ , Lee *et al.* showed enhancement in the modulation bandwidth of up to 28 GHz [137] via injection locking compared to 20 GHz without injection locking. In 2003, Cheng *et al.* demonstrated VCSEL injection locking at 1.55  $\mu\text{m}$  for the first time [138], [139] and demonstrated the enhancement of analog transmission. On the other hand,

digital transmission is also demonstrated by directly modulated VCSELs with transmission rate of 2.5 Gb/s over 50 km SMF.

Quantum confined active region based laser has also been explored via injection-locking. An injection-locked Qwell laser was demonstrated for small-signal modulation enhancement. The injection-locking showed twofold improvement in 3dB modulation bandwidth of IL- FP laser (10.5 GHz) as compared to free-running (5.3GHz) [140]. Lately, three dimensional confined Qdots based lasers have been investigated at 1.33  $\mu\text{m}$  and 1.55  $\mu\text{m}$  applications. Terry *et al.*, reported the four times modulation bandwidth (16.3 GHz) enhancement in Qdot laser via injection-locking at 1.3  $\mu\text{m}$  [141]. In addition, InAs/GaAs Qdot mode-locked lasers (MLL) have shown much advancement in improving the pulsewidths and RF linewidths. Sub picoseconds pulse widths have been reported using single-section 1.55- $\mu\text{m}$  Qdot MLL up to 346 GHz repetition rates with few KHz radio frequency (RF) linewidths [142]. Similarly, QDash-based laser has also been explored in injection-locking for ultra-high speed and short-pulses generation. Very recently, Sooudi *et al.*, in 2011, reported optical injection-locking in 21-GHz single-section and two-section InAs/InP 1.5  $\mu\text{m}$  QDash mode-locked lasers [143]. The single-section laser only operates as a self-mode-locked laser while the two-section laser could operate as both a self-mode-locked laser (SMLL) and saturable-absorber mode-locked laser (SAMLL). Figure 3.3 (a) and (c) show the optical and corresponding RF spectra of the SMLL while for the SAMLL, the locked and free running optical and RF spectra are shown in Figure 3.3 (b) and (d). Figure 3.3 (c) shows the injection-locked RF linewidth of 160 KHz as compared to  $\sim$ 100 KHz free running in SMLL while  $\sim$ 165 KHz linewidth was found in SAMLL in Figure 3.3 (d). More than 1 GHz locking range is found in both cases with wide frequency tuning

range (~270 MHz) of MLL. The authors also proposed dual-mode injection-locking QDash for two section SAMLL.

Very recently, an injection-locked QD-MLL is utilized for the reduction of the noise from mode locked laser to get narrow linewidth optical combs for coherent communication [144], [96]. The InP QD-MLL acts as slave laser whereas external tunable laser is used as master laser in injection-locking process. Likewise, the multi-wavelength coherent seeding source is proposed for injection-locked FP-LD using QD-MLL [22]. So, the novel quantum-dash laser diode can meet the requirements of future high speed communication through an injection-locking, hence could be route towards next generation optical networks.

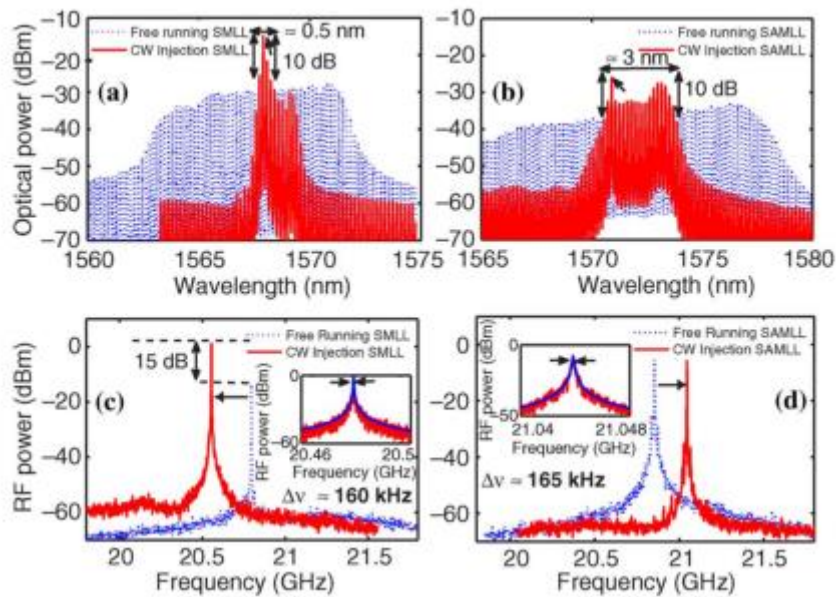


Figure 3.3 (a) Optical spectrum of the SMLL at free running (dashed-line/blue) and locked (solid-line/red) (b) Optical spectrum of the SAMLL. (c), (d) RF spectrum corresponding to (a) and (b) [143].

### 3.5 Experimental Optical Injection Setup

Figure 3.4 shows the experimental setup for characterization IL QDash laser. The setup consists of high quality narrow linewidth (less than  $\sim 100$  KHz,) tunable laser (master), isolator, 3 port optical circulator, polarization controller (PC), chirped QDash laser (slave) and Agilent 86142B optical spectrum analyzer (OSA). The TLS is connected to port 1 of OC through isolator to prevent the TLS from back reflections. The QDash slave laser is injected into the port 2 of the OC via APC/FC connector. PC is placed to improve the injection-locking efficiency and maximize the output power. Port 3 of the OC is connected to optical spectrum analyzer to analyze the injection-locking.

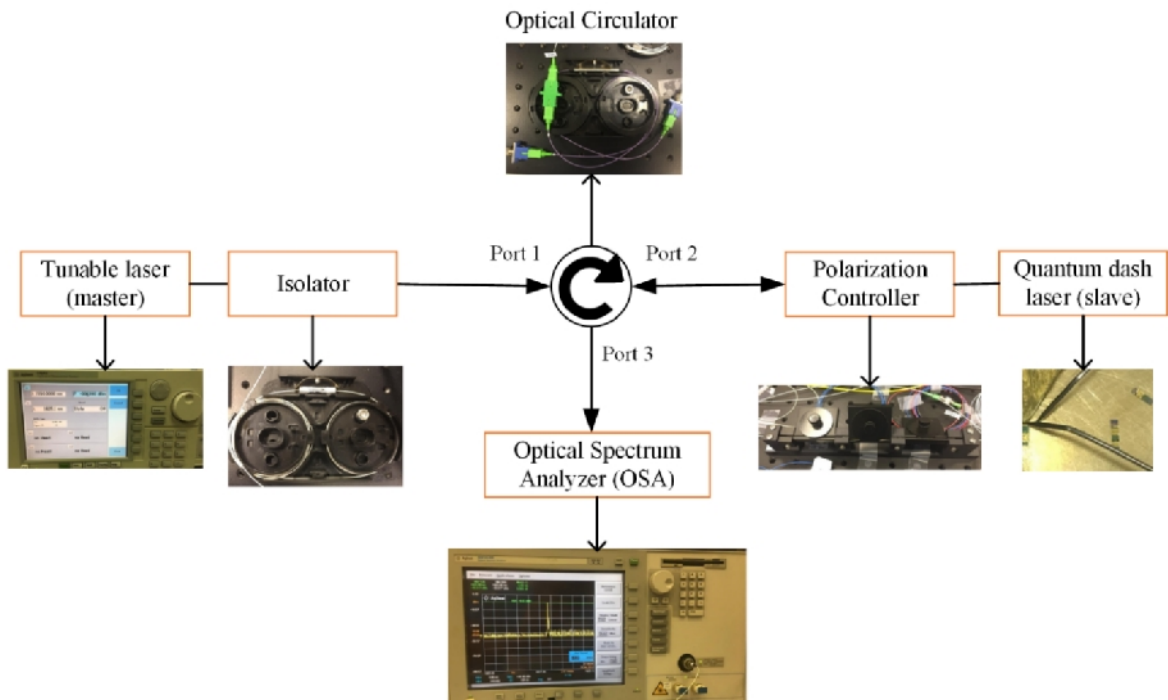


Figure 3.4 Experimental setup for the injection-locking of QDash laser diode.

### 3.5.1 Tunable Master laser

The single mode continuous wave TLS has a wider wavelength tunability of 1461–1635 nm with -7 to +7 dBm power range. The TLS was manufactured by Keysight technologies having a model number agilent 8146B. The controller is attached to tune the wavelength up to four decimal digits' accuracy. Figure 3.5 shows the single mode (carrier) of the TLS at ~1621 nm. This TLS carrier is injected into port 1 of OC which is observed (100 %) using OSA with a 0.06 nm resolution having an integrated power of ~ -5 dBm from 1614 nm to 1628 nm wavelengths which is displayed on OSA. The associated -3 dB (-15 dB) bandwidth at ~1621 nm is measured to be ~0.06 (~0.16) nm. The reason to select this particular wavelength is because our injection-locked mode utilized for optical communication is at around ~ 1621 nm and is discussed in chapter 4.

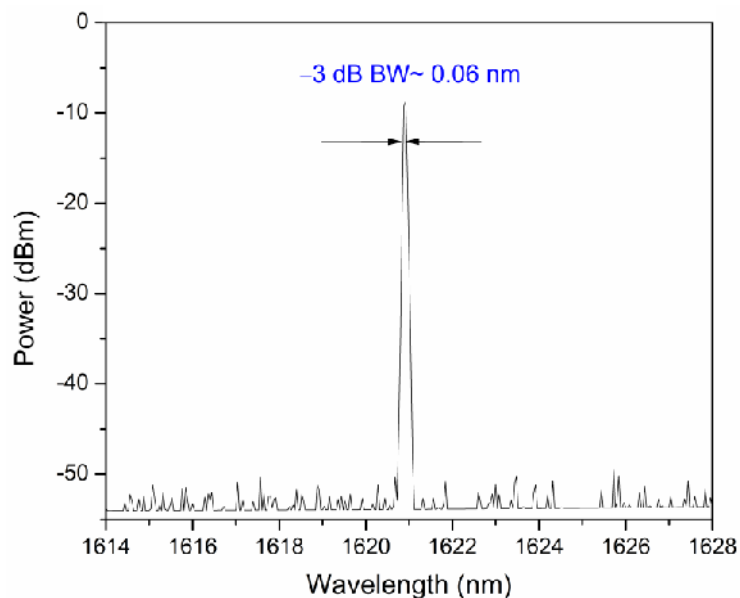


Figure 3.5 Single mode TLS carrier at 1621 nm.

### 3.5.2 Slave (QDash) Laser

A bare  $4 \times 800 \mu\text{m}^2$  ridge-waveguide QDash Fabry-Perot laser diode (QD-LD) is utilized for injection locking characterization. It is mounted on a brass base with p-side up configuration as shown in the insets of Figure 3.6. The device temperature is controlled by Keithley-2510 temperature controller and a CW of 250 mA is injected through Keithley-2520 laser diode test system. The single laser facet optical power is then coupled into a lensed single mode fiber (SMF) at  $14^\circ\text{C}$  temperature. A maximum optical power up to  $\sim 1.0$  mW ( $\sim 0$  dBm) is measured at the fiber end before roll off. After coupling the maximum power, the SMF is connected to the OSA to check the free running QDash lasing spectrum, as shown in Figure 3.6. The spectrum shows the emission centered at  $\sim 1625$  nm with  $\sim 9$  nm lasing -3dB bandwidth. The longitudinal mode spacing is 0.35 nm (40 GHz). This slave laser optical power is injected into port 2 of the OC to get an injection-locked mode at port 3 of OC after fine tuning of master laser wavelength for injection-locking to occur.

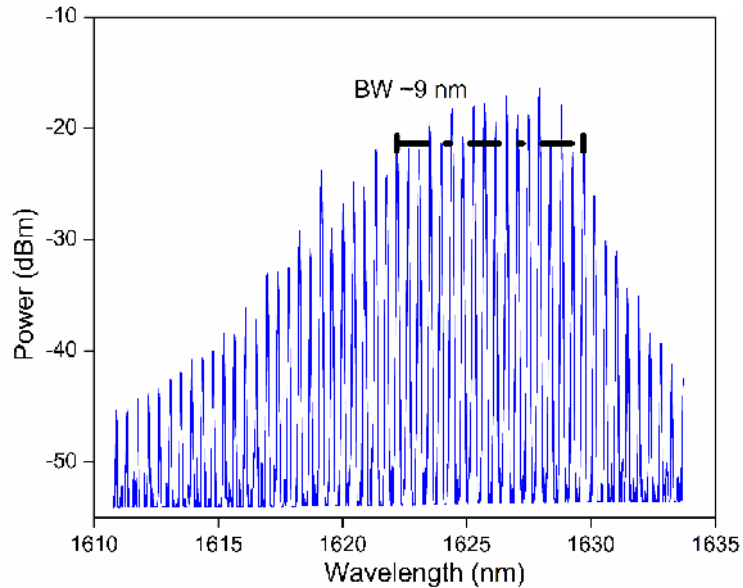


Figure 3.6 Free running QDash laser spectrum centered at 1625 nm.

In addition, the stability of the QDash laser has been examined in terms of output optical power and emission center wavelength. The stability test is conducted for an observation time of ~60 minutes. By focusing on a single FP mode at ~1621 nm, (the mode that was injection-locked), both the fluctuations in the output power and shifts in the emission center wavelength are tracked every 5 minutes, with 3 reading per min for the first 7 minutes. Figure 3.7 shows the variation in the measured output power and the emission center wavelengths as functions of time, with corresponding fluctuations of ~1.5 dB and ~0.05 nm. In the subsequent section, via injection locking, these variations were considerably reduced, thus improving the mode characteristics to be used as a sub-carrier in optical communication experiments.

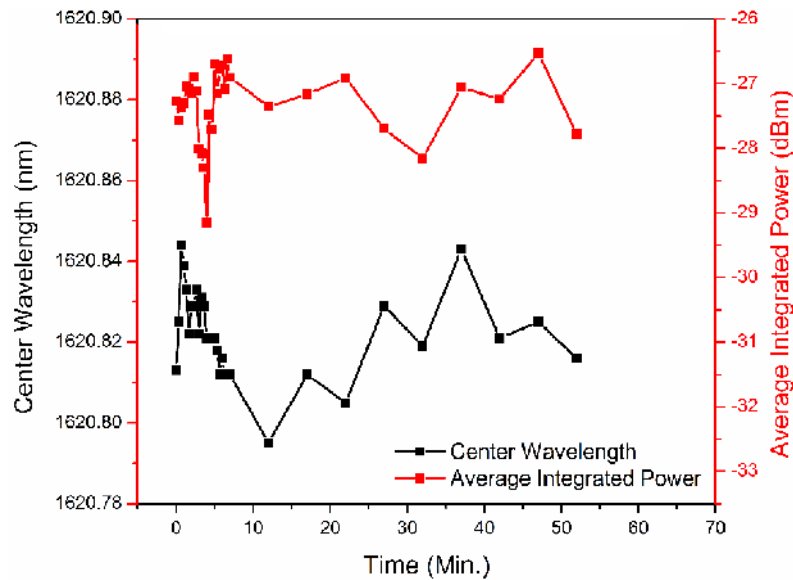


Figure 3.7 Emission center wavelength and average integrated power as functions of times.



### 3.5.3 Injection-Locked Mode

An optical spectrum analyzer was connected at port 3 of OC for the measurement of IL-FP mode. A TLS CW injection light, fixed at 5 dBm external injection power, is transmitted through an isolator to an OC and PC, and into the QD-LD. The output spectra of the injection-locked QD-LD is observed using OSA. Figure 3.8 shows the optical spectrum without TLS injection and with injection and tuned to lock at  $\sim 1621$  nm longitudinal mode with  $\sim \pm 10$  pm locking range. The measured single mode output power and side-mode suppression ratio (SMSR) are  $-7.8$  dBm and 38 dB, respectively. In addition, a 9 dB gain is exhibited by injection-locking besides reducing the phase noise.

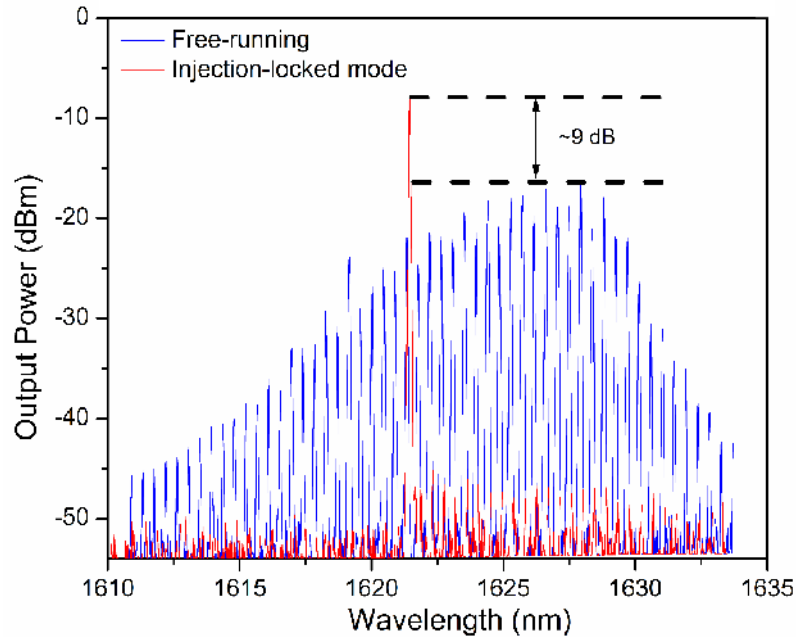


Figure 3.8 QDash laser characteristics under free running mode and injection locked mode.

## 3.6 Characterization of Injection-Locked Modes

### 3.6.1 Tunability

The slave QDash could be characterized to check the tunability from shortest to longest wavelength Fabry-Perot mode that could be injection locked. Moreover, the performance of all the injection locked QD-LD modes should be similar, if employed as sub-carriers in the WDM-PON architecture.

In injection-locking characterization, the tunability experiment of the QD-LD is performed using the same  $4 \times 800 \mu\text{m}^2$  QDash Fabry-Perot laser diode. The fixed CW injection power of 5 dBm is launched into each longitudinal mode of the QD-LD at different TLS wavelengths. The results are plotted in Figure 3.9 which shows a wavelength tunability of  $\sim 23$  nm from  $\sim 1611$  nm to  $\sim 1634$  with 1.31 nm tuning steps. A fluctuation of  $\sim 3.2$  dB and  $\sim 3$  dBm in SMSR and output power, respectively, is observed across the  $\sim 1613.6 - 1634$  nm wavelengths tuned IL modes. However, mode-to-mode power variation increases from  $\sim 3$  dBm to 5.5 dBm after including  $\sim 1611$  nm IL mode. This is attributed to the high fluctuation of Fabry-Perot mode power towards shorter and longer wavelengths of the QDash slave laser free-running spectrum which has a central wavelength of  $\sim 1625$  nm. If we exclude this IL mode, the wavelength tunability will be  $\sim 21$  nm. It is worth to be noted that the output power and SMSR of each of the IL mode could be unified by varying the injection power besides changing the TLS wavelengths since this has been fixed at  $\sim 5$  dBm in our case. Figure 3.10 shows the output power and the side-mode suppress ratio (SMSR)

versus the different lasing wavelengths with  $\sim 1$  nm tuning step in the same wavelengths range mentioned above.

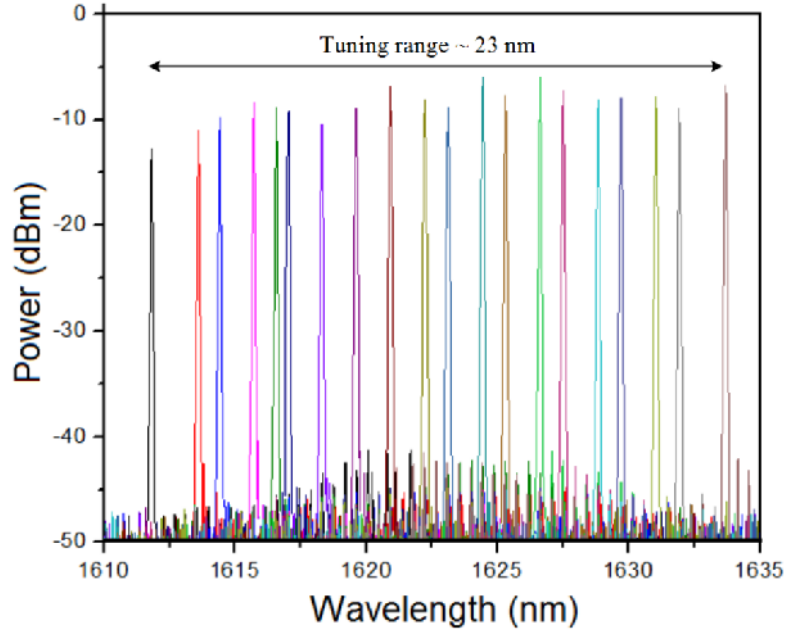


Figure 3.9 Tuning range (1611–1634 nm) of injection-locked modes of a QDash laser at different wavelengths, and at a fixed CW external injection of  $\sim 5$  dBm.

It can be observed that the output power and SMSR variation between  $\sim 1619.6$ – $1627.5$  nm is minimal, whereas, these fluctuations increase towards the shorter and longer wavelength extremes. This might be due to the smaller output powers of QD-LD Fabry-Perot modes that reside at the edges of the  $-3$  dB lasing spectrum (see Figure 3.8), as discussed above. These variations could be unified by varying the TLS CW power at each wavelength locked mode, as explained earlier. Moreover, an improved QD-LD optical power (by optimized device design and packaging) would enable working at lower current

bias point which might help in lowering down the CW injection power and improve the locking range [145,146].

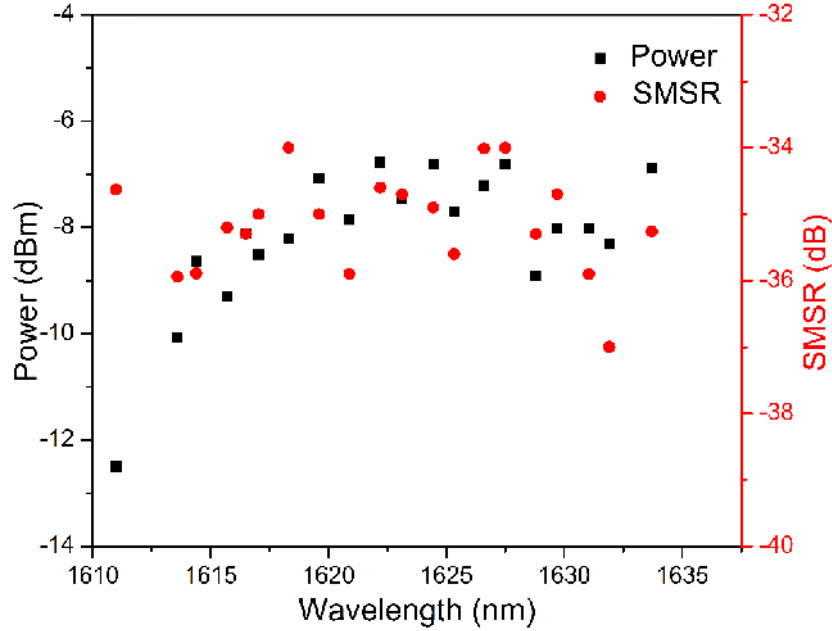


Figure 3.10 Output power and SMSR versus different lasing wavelength with tuning steps of ~1 nm.

### 3.6.2 Short-Term Stability

A short-term stability of the injection-locked QD-LD mode is also conducted and found to be stable throughout the observation time of 24 minutes. The IL mode was at 1619.68 nm with -5.7 dBm output power. The power, SMSR and wavelength variations of IL QD-LD mode are found to be ~0.5 dB, ~2.5 dB and 0 nm, respectively, as shown in Figure 3.11 (a) and (b). The laser source has performed well in terms of output power and SMSR stability.

An injection-locked mode is sustained for ~24 minutes thus affirming the stability of injection-locking and hence its potential application in optical communication.

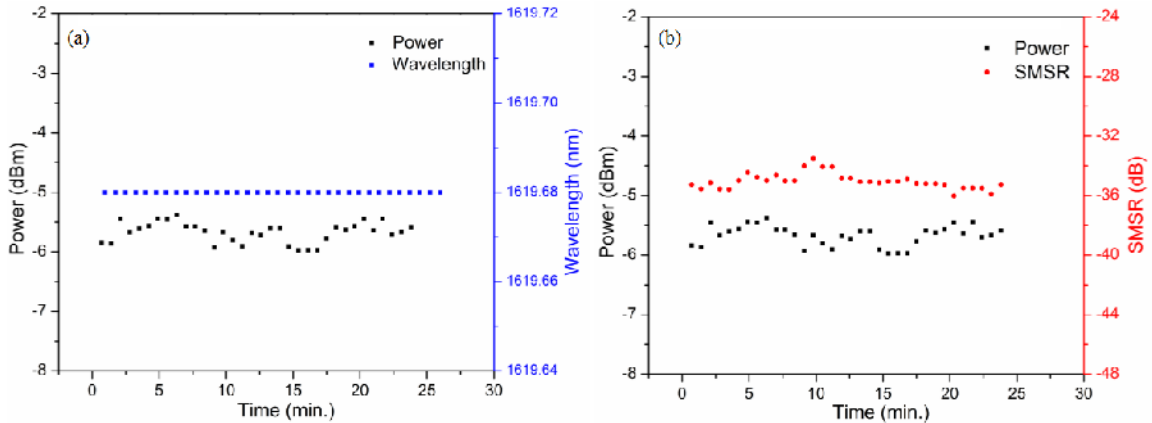


Figure 3.11 Short term stability test of the 1619.68 nm IL mode (a) in terms of wavelength and output power variations, (b) in terms of output power and SMSR variations.

### 3.6.3 Injection-Locked Hysteresis

Figure 3.12 illustrates hysteresis curve of the injection locked 1621.01 nm mode. By varying the external injection power of the TLS from 7 to 3 dBm (reducing) and then 3 to 7 dBm (increasing), the injection-locked single FP mode and its output power was measured. It can be seen that injection-locking was maintained till 4.2 dBm starting from + 7 dBm, afterwards the mode was unlocked which was observed till 3 dBm. Similarly, on increasing the external injection power from +3dBm, the mode was unlocked till 5.8 dBm and then injection-locking again occurred at 6 dBm which was measured up to 7 dBm.

It was found that injection-locking could be achieved above 4.2 dBm TLS injection power. Also, increasing the injection power more than 6 dBm does not appreciably improve the

output power of the injection locked mode. Moreover, the power variation in the injection locked mode, which is observed at high injected power i.e.  $> 6$  dB, might be the effect of variation in gain which might be possible in highly inhomogeneous active region QDash lasers.

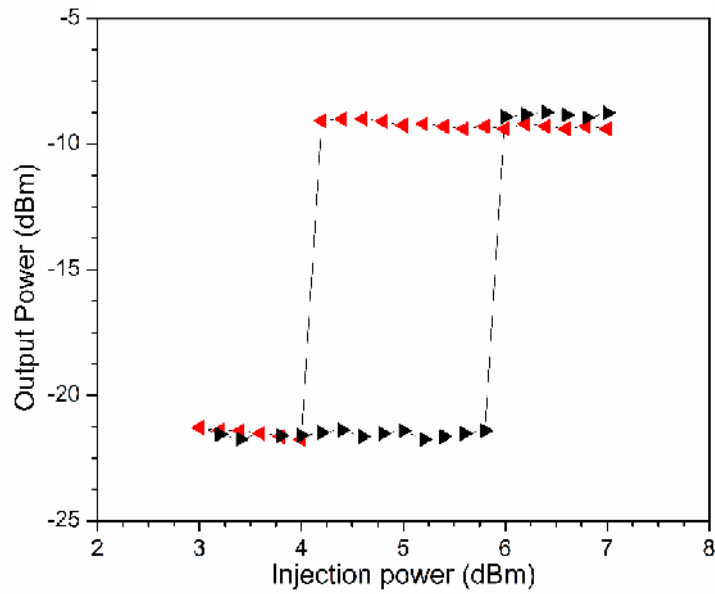


Figure 3.12 Injection powers vs. output powers of the injection-locked QD-LD. The IL mode is fixed at 1621.01 nm.

## **Chapter 4**

# **INJECTION-LOCKED QUANTUM DASH LASER IN OPTICAL FIBER COMMUNICATION**

The experimental transmission of an externally modulated far L-band injection-locked QDash laser diode is demonstrated in this chapter. In section 4.1, an injection-locked conventional transmitter and the need for a unified WDM-PON transmitter for next generation is discussed. Following, the device level laser characterization setup is demonstrated in section 4.2. The single channel transmission using injection-locked QDash laser is explained in section 4.3. In section 4.4, the proposed WDM-PON upstream and downstream transmitter is discussed.

### **4.1 Introduction**

The explosive increase in the demand for high speed internet and mobile connectivity at the user end, driven recently by existing WDM based optical access networks, will soon experience difficulties meeting up with the extraordinary increase in the transmission capacity in near future [147,148]. The next generation passive optical networks (NG-PON)

solutions such as 100Gbit-PON has been considered as a promising solution for ever-increasing number of subscribers and their broad-band services demand [149]. Besides, this trend dictates a need in the expansion of upstream and downstream transmission window beyond the current C- and near L- bands ( $< \sim 1610$  nm) which is leveraging on low optical fiber attenuation and amplification opportunity, to achieve cost effective and upgrade flexibility PON [147,150].

Indeed, the recently proposed colorless PON to realize wavelength independent communication, by employing spectrum sliced and injection locked transmitters is garnering attention. Furthermore, semiconductor optical amplifiers (SOA) [149,151], Fabry-Perot laser diodes (FP-LD) [152] and weak-resonant-cavity laser diode (WRC-FPLD) [153] based transmitters has appeared to be promising candidates compared to costly externally tunable lasers and DFB or DBR lasers [17]. However, directly modulated SOAs are found to be limited by transmission capacity with a maximum of 25 Gb/s transmission over 120 km single mode fiber (SMF) [149]. On the other hand, conventional FP-LDs are typically narrow band and limits on the number of subscribers in PONs and bulk production of transceivers in ONUs.

Therefore, a unified transmitter exhibiting all these essential requirements is decisive for mass deployment. Various WDM-PON transmission reports are available in literature using IL FP-LD [154-155]. In general, most of the reported works exploit direct modulation scheme for simple and cost-effective Gigabit-PONs, nonetheless the bandwidth will be limited by the fundamental properties of the transmitter light source active region (*i.e.*



carrier dynamics) which could pose a bottleneck for next generation 100Gbit-PONs, which has been standardized, and 400Gbit-PONs, which is under consideration.

In this chapter, we intend to employ an injection locked QDash FP laser mode as a single channel for binary phase shift keying (BPSK) and quadrature phase shift keying (QPSK) transmission experiments via SMF. We evaluated the externally modulated QDash FP-LD IL mode, without any signal amplification, in terms of maximum transmission data rates and longest fiber length possible.

## **4.2 CW Characteristics of Chirped QDash Laser Diode**

To meet the requirement of the different system elements, different QDash laser devices were identified that operated at shorter central lasing wavelengths and with high power, under CW injection. The device temperature has been set at 14° C with the objective of blue shifting the lasing spectrum and improving the output optical power. However, reducing the temperature further caused the formation of frost over the brass base that could damage the laser diode, hence the 14 degrees operating temperature was selected and fixed throughout the experiment. The selected 4×800  $\mu\text{m}^2$  chirped QDash laser diode shows a good performance in terms of consistency, optical coupling power and stability for system level work.

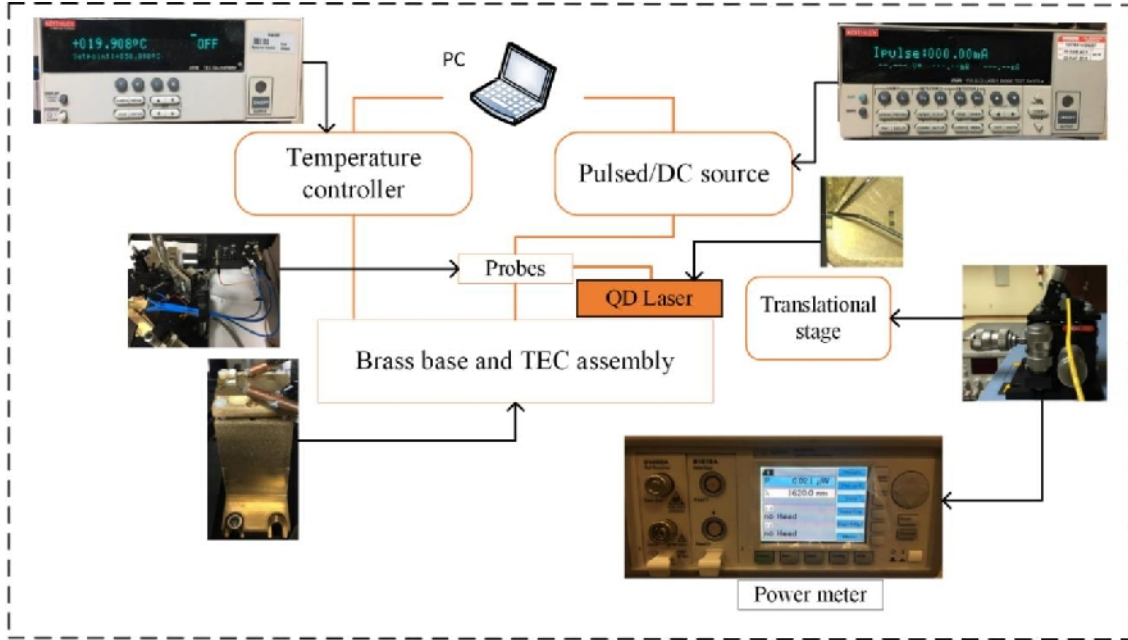


Figure 4.1 Demonstration of laser characterization setup at device level.

Figure 4.1 illustrates the bare laser characterization setup by including all pictures of the components. The bare  $4 \times 800 \mu\text{m}^2$  ridge-waveguide QDash FP-LD (QD-LD) is mounted on a brass base with p-side up configuration. Two probes are used where the cathode one connected to the brass base while the anode probe is placed over an isolated gold plated clamp that touches the p-contact of the laser. First, the device is characterized under a short pulse width (SPW) current operation with a pulse width of  $0.5 \mu\text{s}$  and a delay width of  $250 \mu\text{s}$  (0.2% duty cycle). After safely current probing the laser using Keithley 2520, the voltage drop across the diode is measured. In addition, the optical power from one of the facets is also measured via integrating sphere with InGaAs photodiode. For injection locking characterization and communication experiment, the single laser facet optical power is coupled into a lensed SMF. The facet end  $L$ - $I$ - $V$  characteristics under pulsed and

CW operation, are shown in Figure 4.2 (a), (b) at 14°C while the SMF fiber end  $L$ - $I$ - $V$  characteristic under CW operation, and at 14°C, is shown in Figure 4.3. The SMF was mounted on a three-axis manual translational stage for aligning purpose and the other end of the SMF was connected to an optical lightwave multimeter, as shown in Figure 4.1, which helped in alignment.

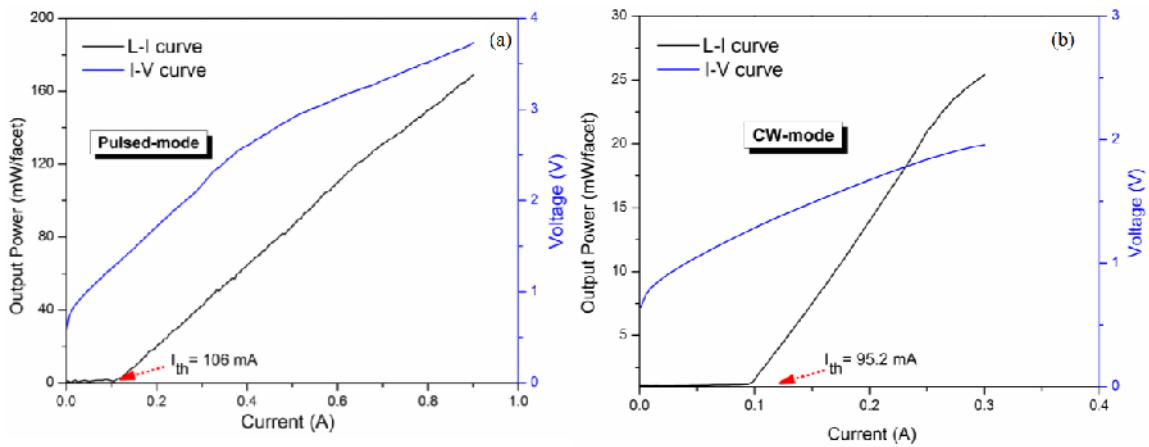


Figure 4.2 The facet end L-I-V characteristics (a) pulsed operation and, (b) CW operation.

An optical power up to  $\sim 1.0$  mW ( $\sim 0$  dBm) is measured at 240 mA maximum injected CW current through the SMF end. A huge degradation in the laser performance is observed under the CW mode compared to pulsed current operation (see Figure 4.2) which is expected since the device active region design is not optimized. With proper growth optimization, the laser performance could be substantially improved, and would be comparable to the pulsed operation [156]. Moreover, an optimized design laser would enable realization of ultra-broadband lasing bandwidth of  $>50$  nm and power  $> 100$  mW in CW operation.

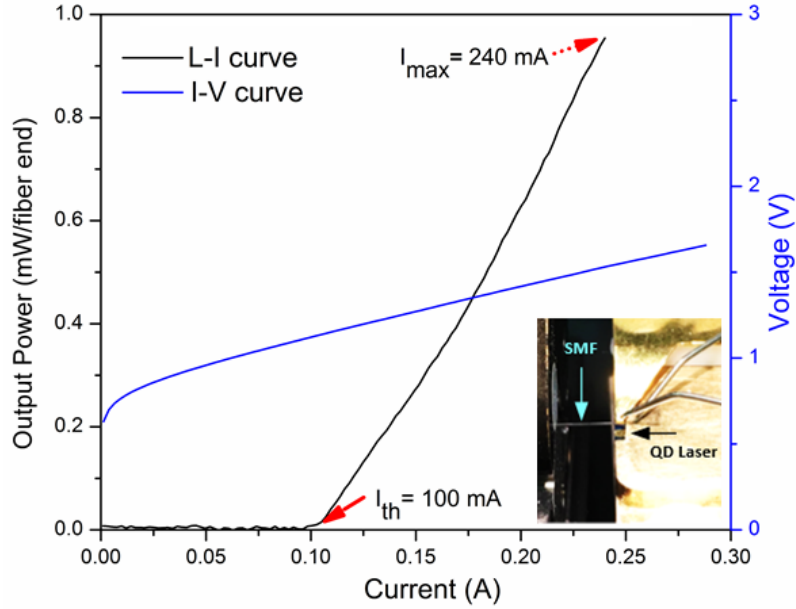


Figure 4.3 L-I -V characteristic of free running QDash laser, measured at the SMF end. The inset shows the bare QDash FP-LD power coupled to a lensed SMF.

### 4.3 Injection-locked Optical Communication

After setting up the experiment, we performed an optical fiber transmission experiment using only a single channel injection-locked QDash laser, at different transmission rates, via back-to-back (BtB) as a reference case and over a fiber link. In the previous chapter, we successfully showed an injection locked wavelength tunability of  $\sim 23$  nm which covers  $\sim 50$  sub-carriers, showing its potential usage in PON. Thus, the performance of all the injection locked QD-LD modes in PON-WDM system will not be affected appreciably, provided the channels (i.e. the injection locked modes) exhibit similar power and SMSR.

### 4.3.1 Optical Fiber Transmission Setup

Figure 4.4 represent the data transmission experimental setup. The QDash laser spectrum of the  $4 \times 800 \mu\text{m}^2$  QDash laser is observed on OSA as shown in Figure 4.5. The OSA is used for characterizing the injection-locking characteristics and also to monitor the injection-locked mode while performing communication experiments.

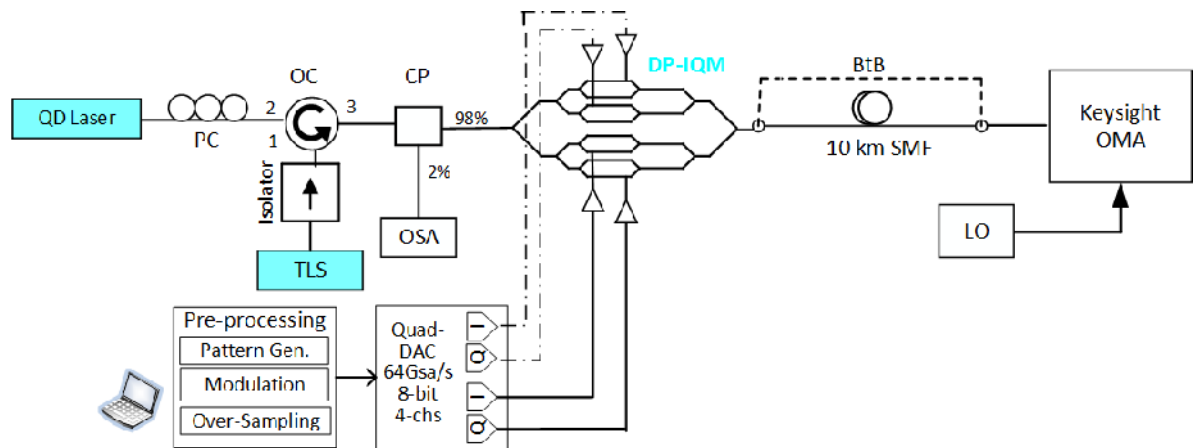


Figure 4.4 Experimental setup of DP-QPSK WDM transmission via injection locked QDash FP-LD. The signal transmission is characterized first in a back-to-back (BtB) configuration and then over a 10 km single mode fiber (SMF).

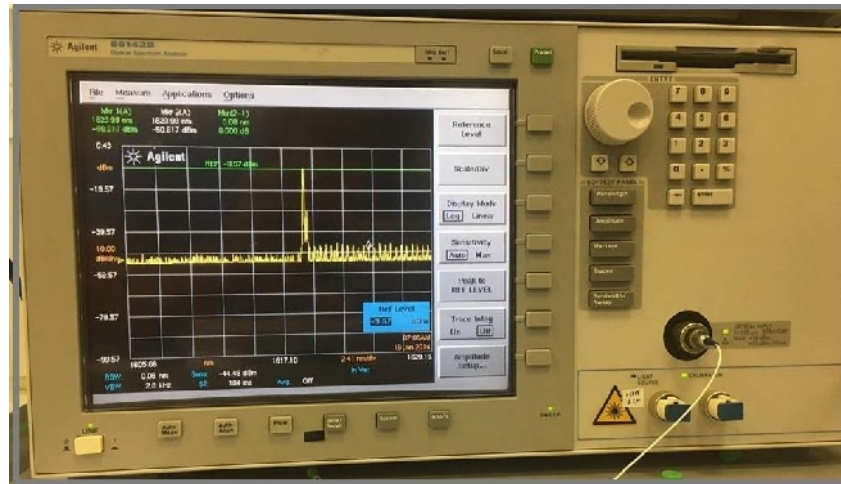


Figure 4.5 Agilent optical spectrum analyzer for characterization of an injection-locking.

The measured free running lasing spectrum of QDash laser is shown in Figure 4.6 with ~8–10 nm lasing bandwidth at a CW current injection of 240 mA centered at ~1625 nm (calculated at the full width at half maximum). When the wavelength of the tunable master laser source was tuned to one of longitudinal mode (~1621 nm) of the QDash laser while keeping a fixed external CW injection of 5 dBm, injection-locking occurs, as shown in the insets of Figure 4.6. The longitudinal mode spacing and threshold current are 0.35 nm (40 GHz) and 100 mA, respectively.

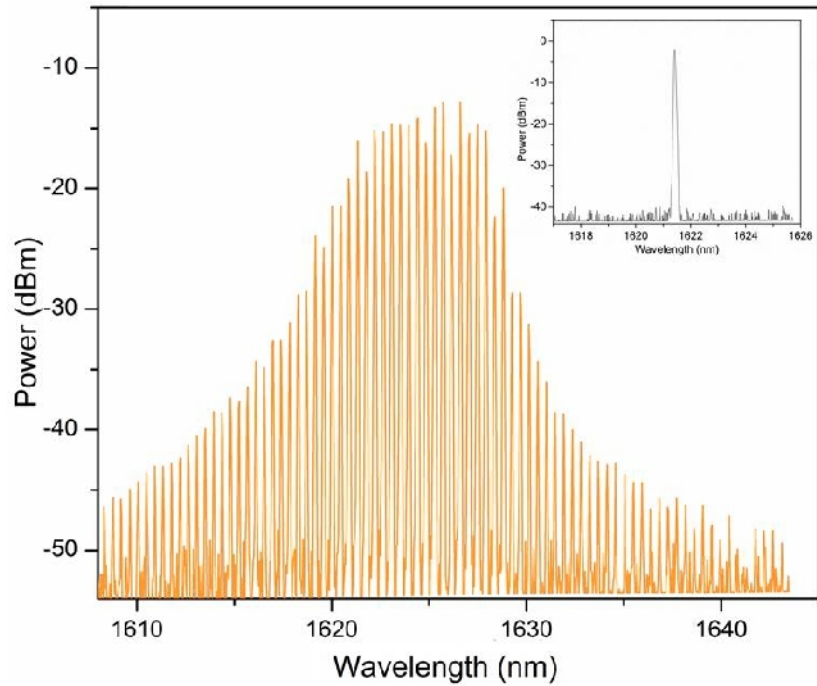


Figure 4.6 Free-running lasing spectra of the bare  $4 \times 800 \mu\text{m}^2$  QDash laser. The inset shows an injection-locked single FP mode of the broadband QDash laser at  $\sim 1621 \text{ nm}$ .

During the injection-locking process, an optical circulator, polarization controller and isolator are utilized, which are shown in Figure 4.7. Isolator and PC are used to protect the TLS and improve the injection-locking efficiency, respectively.

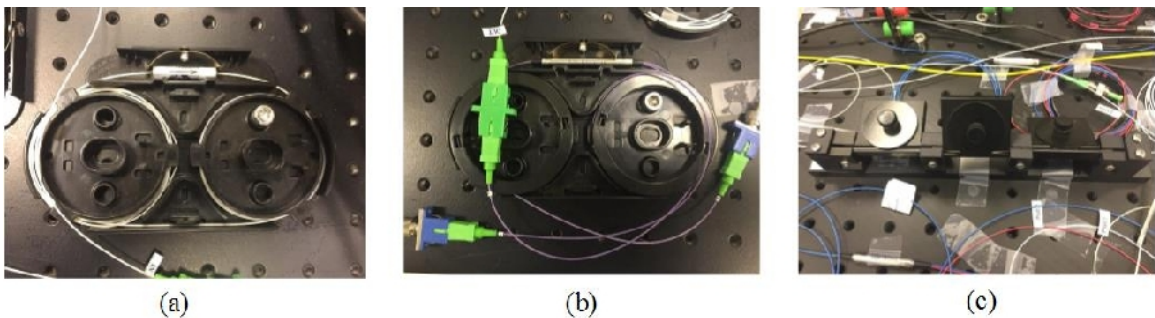


Figure 4.7 Optical isolator (b) 3-port optical circulator (OC), and (c) polarization controller (PC).

Afterwards, the output spectra of the injection-locked QD-LD is observed at the 2% output of a 2/98 optical coupler (CP) while remaining 98% is fed into the modulator for transmission experiments. The 98% of the injection-locked mode at  $\sim 1621$  nm is fed into dual polarization In-phase Quadrature-phase modulator (DP-IQM) for modulation. Figure 4.8 depicts complete electronic circuitry of the optical modulation that includes Quad digital-to-analog converter (DAC), four amplifiers, two Mach-Zehnder IQ modulator (MZM) and one phase modulator.

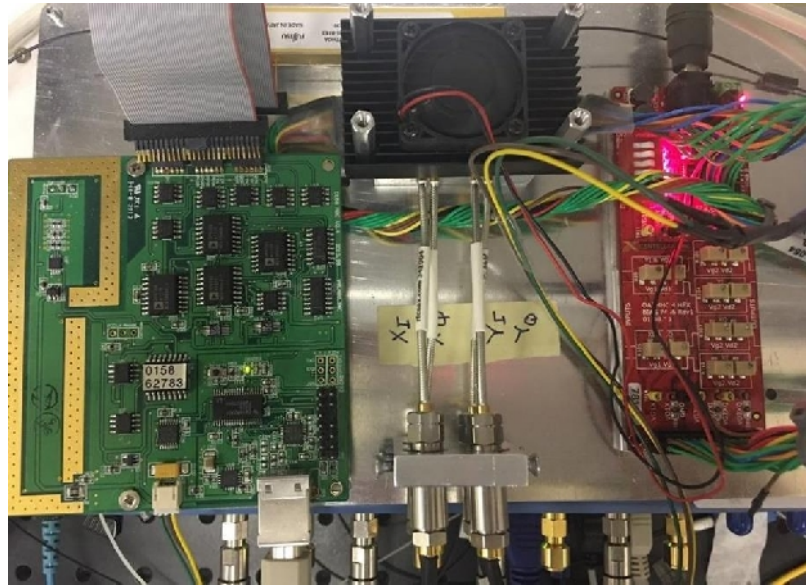


Figure 4.8 The optical modulation circuit utilized during communication experiments.

After DP-IQ modulator, we employed a variable optical attenuator (VOA) before sending the signal into OMA for detection, as shown in Figure 4.9. After transmission, different bit error rate (BER) values can be measured by attenuating the optical received power using VOA to reach forward error correction (FEC).





**Figure 4.9 Variable optical attenuator (VOA).**

For signal detection and analysis, we used Keysight optical modulation analyzer (OMA-N4391A), as shown in Figure 4.10, in order to demodulate the signal and extract constellation diagrams, I-Q eye diagrams, received baseband signal, Q-factor, received optical power, BER values etc. Figure 4.11 shows an illustration of the whole communication system in which the QDash-LD has been employed.

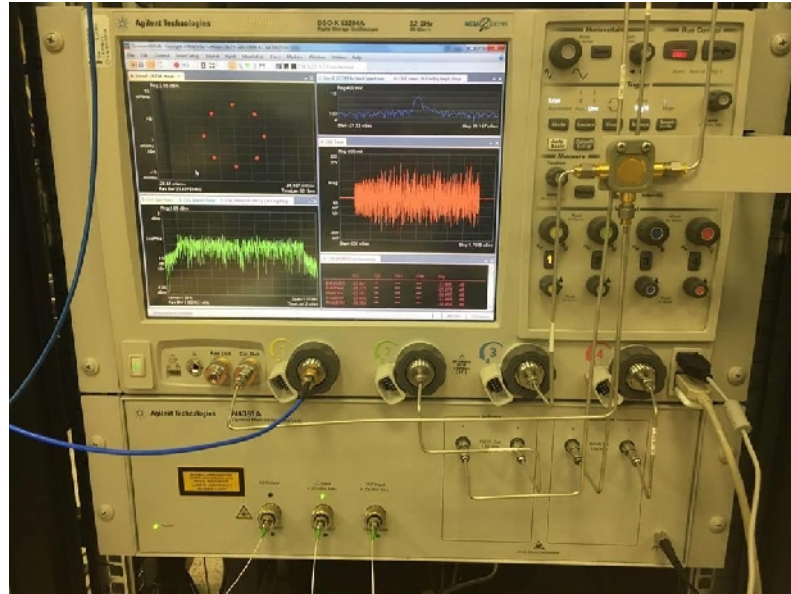


Figure 4.10 Keysight optical modulation analyzer (OMA).

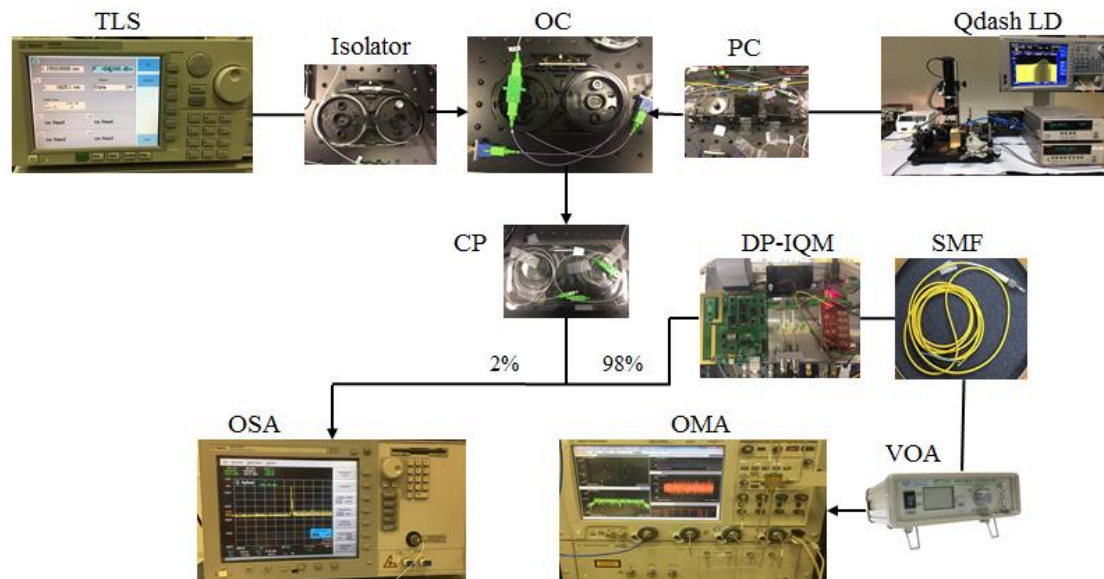


Figure 4.11 A complete illustration of an experimental optical communication setup via injection-locking technique showing all the system and device level components.

### 4.3.2 Transmission Experiments

Once, the QD-LD is injection locked with an external injection of  $\sim 5$  dB, the selected sub-carrier with mode power -5dBm is fed to the dual polarization IQ (DP-IQ) modulator and modulated with DP-QPSK scheme at 8, 16 and 25 Gbaud. Pre-processing of the signal was performed using MATLAB by generating a pseudo random binary sequence (PRBS) with a length of  $2^{11}-1$  and mapped into QPSK constellation by an arbitrary wave generator (Keysight AWG M8195A). A sampling rate of 64 GSa/s is used to generate four channels multi-level signal, two channel for individual polarization, employed as a digital to analog converter (DAC). The output of four signals are driven, through a four channels linear amplifier of 20 dB gain over 32GHz flat bandwidth, into the four RF inputs of DP-IQ modulator. A far L-band sub-carrier at  $\sim 1621$  nm (see inset of Figure 4.6) is selected for DP-QPSK signal transmission with root raised cosine (RRC) pulse shaping filter having 0.35 roll-off factor. The signal transmission is characterized first in a back-to-back (BtB) configuration and then over a 10 km SMF for all transmission rates.

### 4.3.3 32/64 Gb/s DP-QPSK WDM-PON Transmission

The DP-QPSK signal is transmitted at 8 and 16 Gbaud transmission which corresponds to 32 and 64 Gb/s, characterized first in a BtB configuration and then over a 10 km SMF. In order to evaluate the performance of the communication system, the bit error rate (BER) is estimated. BER is a measure that quantifies the probability of erroneous data in decoding a digital signal. Figure 4.12 presents the variation of BER with the received signal sensitivity. To achieve  $3.8 \times 10^{-3}$  FEC threshold (ITU-Criterion [157]), received power of -18.7 (-19.7) dBm are required for 64 (32) Gb/s in BtB case. On the other hand, a receiver sensitivity of -18.4 and -16.7 dBm is observed for 32 and 64 Gbit/s respectively, after 10 km SMF transmission, with power penalties of ~1.3 dB and ~2 dB respectively, under the FEC threshold. This might be loss incurred by the fiber due to extreme far L-band wavelength (~1621 nm) operation.

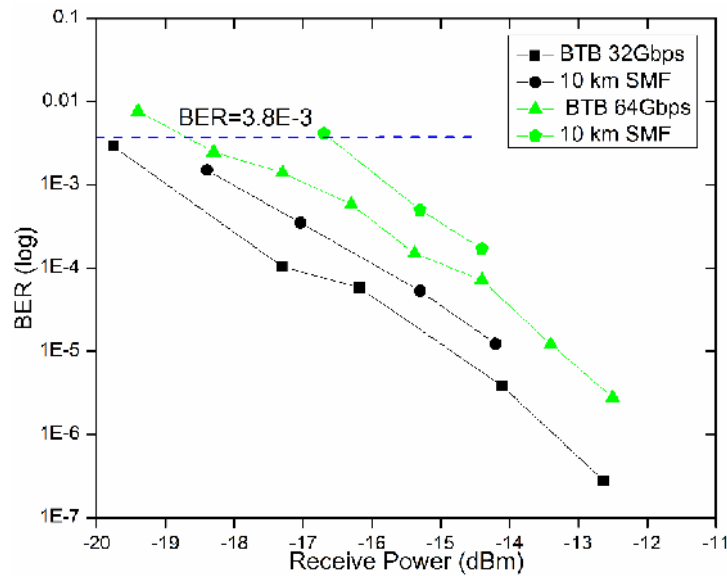


Figure 4.12 BER versus received optical power at 32 and 64 Gbit/s under BtB and after 10 km SMF transmission.

The eye diagrams and constellation are also measured to evaluate the overall optical system performance. The opening of an eye diagram, both vertically and horizontally, is a direct indication of the quality of the recovered signal. The horizontal openness of an eye diagram (eye width) reflects how well aligned both the rise and fall times of each bit are. As the transmission rate is increased, reflections, chromatic dispersion, signal distortion, and inter-symbol interference (ISI) play a major role. On the other hand, the vertical eye openness (eye height) of the eye, plays a significant role in received bit decision making between 0 and 1. Moreover, the vertical opening of the eye diagram is affected by the optical output power of the QDash laser in addition to different losses that occur at different elements of the communication system while Horizontal opening is affected mainly at high rates by pulse spreading due to chromatic dispersion and reflections.

Figure 4.13 (a), (b) show the eye diagrams and QPSK constellations for BtB and 10 km transmission of 32 Gbit/s data rate at -19.7 dBm received power for BtB transmissions while -18.4 dBm received power for 10 km SMF transmission, respectively. Similarly, Figure 4.14 (a), (b) show the eye diagrams for 64 Gbit/s at -18.3 dBm and -16.3 dBm for BtB and 10 Km transmissions, respectively, just below the FEC threshold.

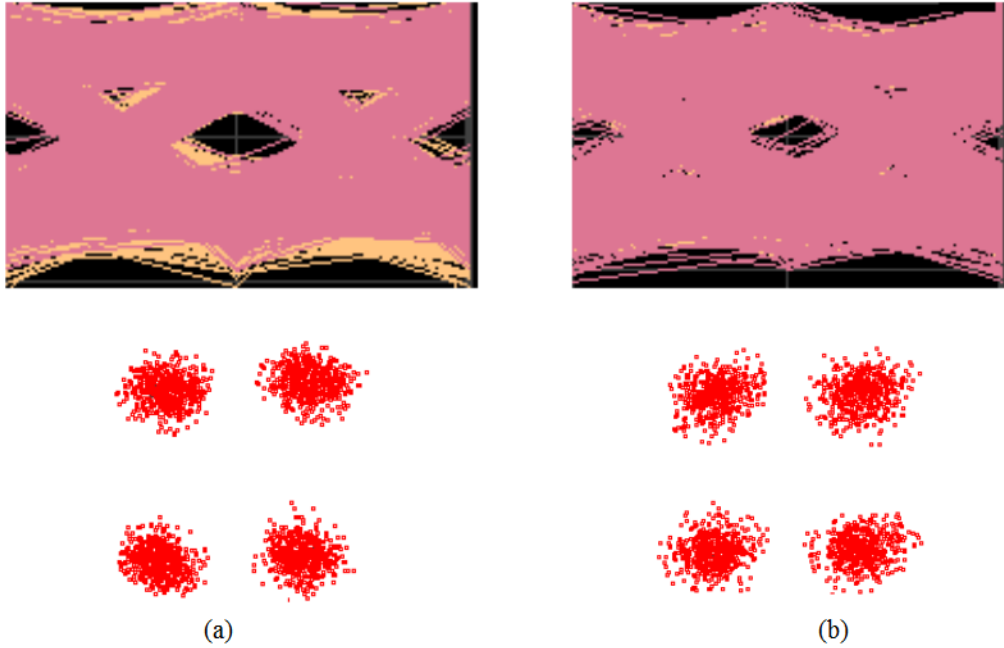


Figure 4.13 Eye diagrams and QPSK constellations of 32 Gb/s data rate (a) BtB and, (b) 10 km SMF transmission, at FEC threshold.

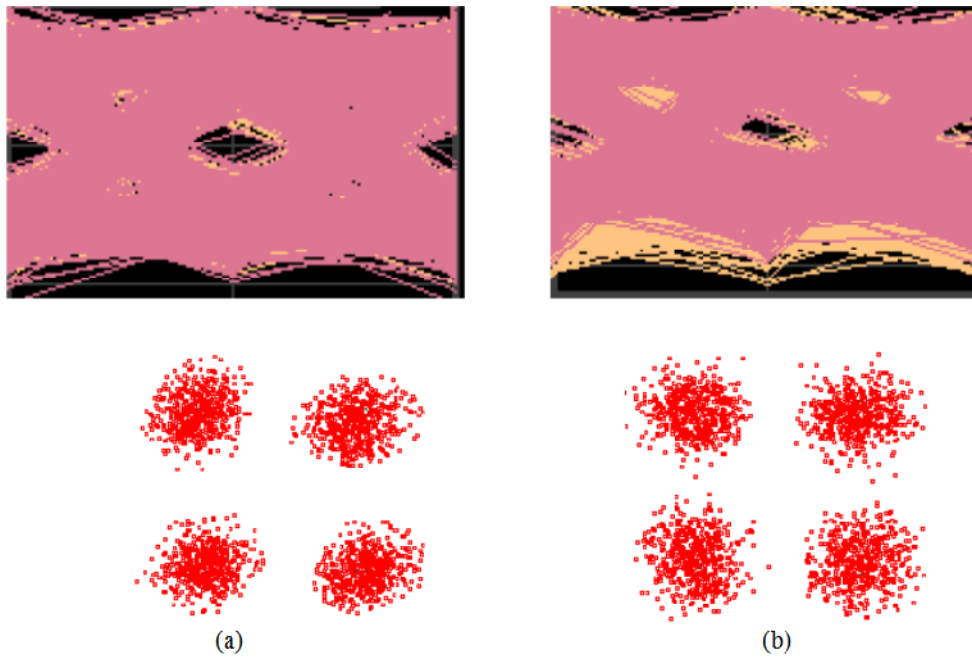


Figure 4.14 Eye diagrams and QPSK constellations of 64 Gbit/s data rate for (a) BtB and, (b) over 10 km transmission.

#### 4.3.4 100 Gb/s DP-QPSK WDM-PON Transmission

The corresponding error vector magnitude (EVM) BER results at 25 (100) Gbaud (Gb/s) transmission in both configurations are presented in Figure 4.15. To achieve a BER of  $3.8 \times 10^{-3}$  (FEC threshold), a received power of -17.2 dBm is required for 100 Gb/s data rates, in BTB case. On other front, the corresponding receiver sensitivity of -17.4 dBm is noted after 10 km transmission, with power penalty of ~0.2 dB. This also might be attributed to the variations in the OMA sensitivity because of the extreme far L-band wavelength operation, as explained earlier. In addition, since the measurements are performed with a bare QD-LD by coupling the light into a lensed SMF, any transmitter (injection-locked mode) power variation could also lead to receiver sensitivity fluctuations. Table 4.1 displays the measured Q-factor values for all transmission rates at their maximum received optical power. The Figure 4.16 shows the eye diagrams and QPSK constellations for 100 Gbit/s at -16.2 (-16.02) dBm received powers for 10 km (BtB) transmission.

A clear open eye with no eye compression in above eye diagrams without any signal amplification of all transmission rates that affirms the potential of QDash laser transmitter in WDM-PONs.

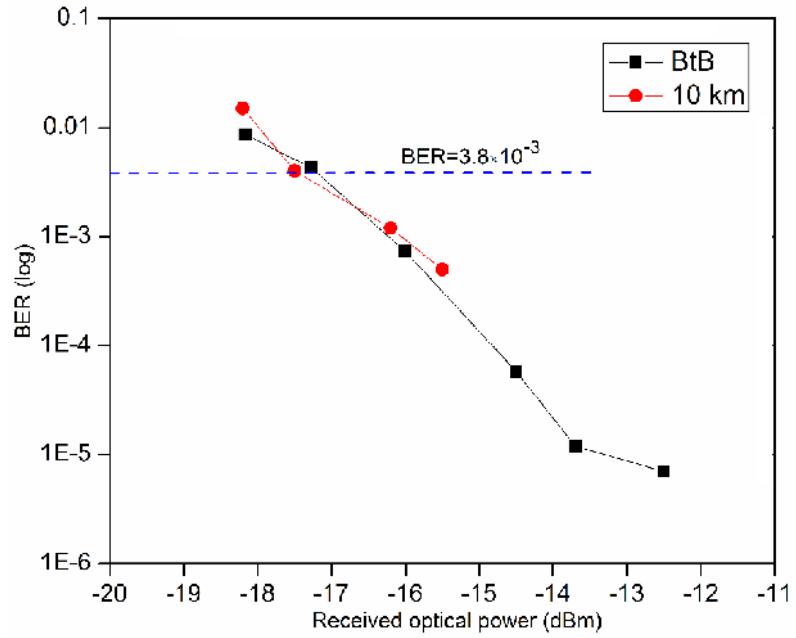


Figure 4.15 Bit error rate as a function of received optical power for 100 Gbit/s after 10 km SMF transmission.

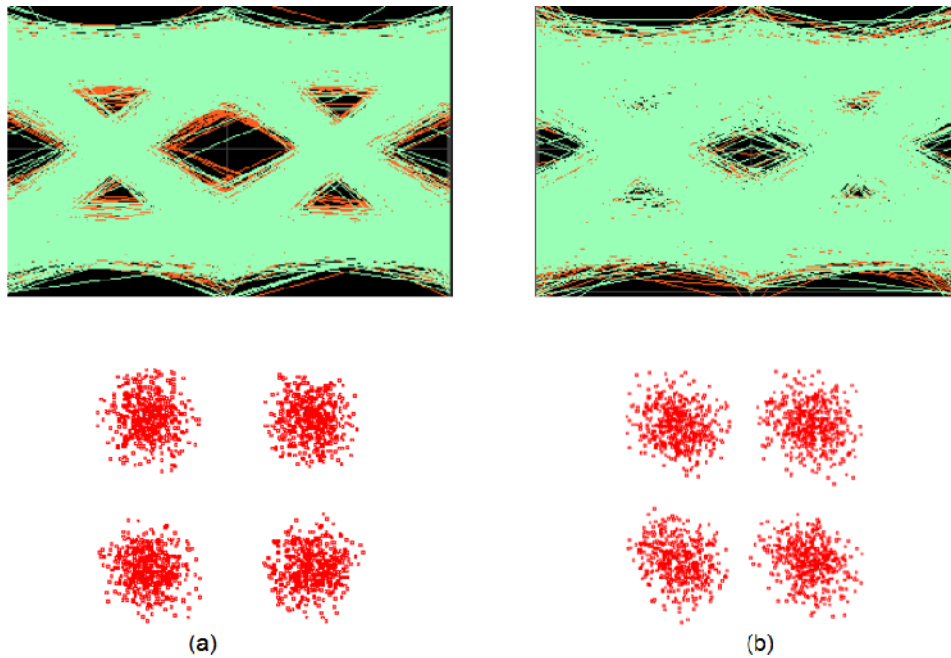


Figure 4.16 Eye diagrams and QPSK constellations for 100 Gbit/s transmission (a) BtB and, (b) over 10 km SMF.



Table 4.1: The maximum received powers and their corresponding Q-factors over 10 km fiber.

Transmission rate (Gbps)	32	64	100
Received Power (dBm)	-15.2	-14.4	-15.5
Q-factor (dB)	6.323	5.725	5.183

#### 4.4 Proposed Transmitter for NG WDM-PON

We propose a possible next generation WDM-PON capable of more than 100 Gb/s transmission capacity, and is depicted in Figure 4.17. The proposed scheme exclusively includes Qdash based active devices *i.e.* ultra-broadband QD-LDs as unified transmitters, possible Qdash based broadband photodiodes (QD-PDs) as unified receivers, and broadband QD-MLL as external seeding light sources. Two QD-MLLs are utilized, one at the OLT situated at CO and other at the RN. The former is used as an external source of injection-locking at the OLT for down transmission while the latter is used to realize injection-locking at the ONU for up transmission via different wavelength band compared to the downstream signal wavelength band, to avoid any crosstalk. A single SMF could serve as a channel for bi-directional transmission without any crosstalk [147-149] since two different lasing wavelength bands, from the ultra-broadband emission of the QD-LD, could be used for down traffic and up traffic, as illustrated in the inset of Figure 4.17. Moreover, this architecture would enable utilization of identical transceivers in ONUs and



~14 dB, circulator of ~2 dB, the U/D multiplexer/de-multiplexer and other connectors loss of ~2.5 dB). The power budget for the proposed NG WDM-PON is displayed in Table 4.2. In addition, the power budget of 100 Gb/s experimental transmission is also estimated and the results are summarized in the Table 4.3.

**Table 4.2: Proposed NG-PON power budget employing a 20 dB far L-band amplifier at CO (Downstream) and RN (Upstream).**

<b>Transmission Type</b>	<b>Transmitted Power</b>	<b>Power budget</b>	<b>Receiver sensitivity</b>
Downstream	5 dBm	22.4 dB	-17.4 dBm
Upstream	5 dBm	22.4 dB	-17.4 dBm
Estimated Channel Loss	~14 dB (2 multiplexer/de-multiplexers) + ~2 dB (OC) + ~2.4 (Fiber loss including connectors) + ~2.5 dB (U/D multiplexer/de-multiplexer and/other connectors)		~20.9 dB

**Table 4.3: Estimated power budget of 100 Gb/s transmission without including any amplifier.**

<b>Transmitted Power</b>	<b>Channel loss</b>	<b>Receiver sensitivity</b>
-5 dBm (injection locked mode power), -10 dB (modulator loss) = -15 dBm	~2.4 dB for 10 km fiber attenuation and connector losses	-17.4 dB

The experimental demonstration for 100 Gbps transmission did not utilize any single amplification. We have used L-band EDFA (Amonics; Model: AEDFA-L-18B-R) but unfortunately it was not helpful in amplifying ~1621 nm signal because of its wavelength limitation (maximum up to 1603 nm). Thus, the power budget does not include any

amplifier in 100 Gb/s transmission experiments. However, a far L-band amplifier of 20 dB gain is included in the power budget of the proposed WDM-PON. An optimized QD-LD device design along with appropriate signal amplifier and the availability of the L-band multiplexer/de-multiplexer (wavelength tunability ~1611 to 1634 nm) would potentially boost the power budget of the QD-LD and hence the proposed NG-PON architecture, enabling not only longer transmission distances but also higher transmission rates.

It is noteworthy to mention that the mode spacing of the injection-locked modes (see Figure 3.9) of the QD-LD, and hence the PONs, could be altered to align with WDM standards (coarse-WDM or dense-WDM) by essentially selecting a proper cavity length and current injection. Hence, with a tunability of ~50 sub-carriers, can be seen in Figure 4.6, a single QD-LD would provide a transmission capacity of ~5 Tb/s if all these modes are simultaneous IL by an external seeding QD-LD working under mode locked scheme (QD-MLL) [96], when deployed at OLT for down streaming. Concurrently, a QD-LD in the ONU would enable 100 Gb/s upstreaming, thus facilitating a possible route towards next generation 100Gbit-PONs.

## **Chapter 5**

# **INJECTION-LOCKED QUANTUM DASH LASER IN OPTICAL WIRELESS COMMUNICATION**

In section 5.1, the potential of optical wireless communication as an indoor and outdoor free space communication is discussed. The single channel FSO transmission using injection-locked QDash laser over 4 m and 2 m free space channel, is explained in section 5.2. In section 5.3, a comparison between IL slave QDash laser and tunable master laser, as an independent carrier, is discussed.

### **5.1 Introduction**

The massive surge in the commercial demand for unlimited and high-speed broadband wireless access, to accommodate the ever-increasing demands of individual users, has prompted extraordinary growth in the internet traffic demand in the recent decade. This relentless continuous growth necessitates development of higher bandwidth and capacity systems and is pushing the current RF systems into bandwidth limitations and ultimately to traffic congestion.

Optical wireless communication (OWC) has been identified as a promising complement to the existing wireless RF solutions, providing large bandwidth and higher data rates with low deployment costs and infrastructure maintenance [158]. OWC in the form of FSO relies on line of sight (LOS) communication and can be used in both indoor and outdoor environments, thus, is highly attractive because of its affordability and license free spectrum. In fact, recent demonstrations of FSO in outdoor building-to-building LOS communication, indoor data centers for intra/inter-rack communication, and radio over free space optics (RoFSO) [159 – 161], substantiate the viability of this alternate solution.

Some of the recent FSO achievements regarding outdoor FSO work, which has been considered as a promising solution in mobile-wireless backhaul, disaster recovery, metro ring extensions and many more, typically employs near infra-red commercial laser diodes. For instance, the longest 1–1.5 km FSO link was presented in [162], achieving 100 Gb/s transmission using polarization multiplexed QPSK scheme. A 212 m FSO link based on wavelength division multiplexed 32 distributive feedback LDs in C-band (1535.7–1560.5 nm) has been demonstrated in [163] using OOK and 40 Gb/s/channel data rate. Likewise, 100 Gb/s transmission capacity per carrier, using 1550 nm LDs, has been reported in [164] and [159] on 120 m and 80 m FSO links, respectively. While the former utilized orbital angular momentum (OAM) multiplexing and QPSK modulation scheme, the latter was based on WDM) and DP-QPSK format. Very recently, a record capacity FSO of 320 Gb/s using a single 1550 nm DFB-LD as a carrier and DP-QPSK modulation, has been reported, over 11.5 m outdoor link [165].

On the other hand, indoor FSO demonstration with VLC as well as infra-red LDs has been reported. VLC has a potential in addressing indoor light-based wireless communication (LiFi) applications and solid-state lighting (SSL) concurrently [166–168] and hence is taking center stage in indoor FSO solutions. In contrast, interior FSO employing C-band LDs is garnering attention for data centers interconnections and high performance computing (HPC) networks which are currently bandwidth overloaded with fiber technology and suffering from flexibility issue for cable rerouting after deployment. In this respect, references [169] – [171] addressed long indoor communication over 150 m and 20 m free-space link based on C-band light source, and reported 10–40 Gb/s per channel transmission. Short communication channels of 1 m, 2m, and 6 m are considered in [172] – [174], respectively, with corresponding successful transmission of 100 Gb/s (OAM DP-QPSK), 37.2 Gb/s and 10 Gb/s data signals on C-band sub-carriers. Very recently, experimental demonstration of indoor FSO link of up to 30 cm for card-to-card 40 Gb/s flexible interconnection [175] stems the potential of FSO as a promising solution for varied wireless applications.

After employing the injection-locked QDash laser diode in optical fiber communication, we explored the feasibility of employing same IL broadband laser diode as a potential source in indoor FSO link. In this chapter, we investigated the high speed indoor FSO communication via single channel and quadrature phase shift keying (QPSK) transmission scheme. The far L-band ( $\sim 1621$  nm) injection-locked wavelength mode is externally modulated through different indoor free-space channels. Furthermore, a comparison of

optical communication via injection locked slave quantum-dash laser and with the corresponding master laser, as independently carriers, is also performed.

## 5.2 Injection-locked Indoor Communication

Figure 5.1 illustrates the optical spectra of QD-LD without injection and with injection at ~1613 nm. A clear master tunable laser source (TLS) line is visible before injection locking, while after injection locking, all the side modes of QD-LD are suppressed, leading to a high power IL single mode operation [143].

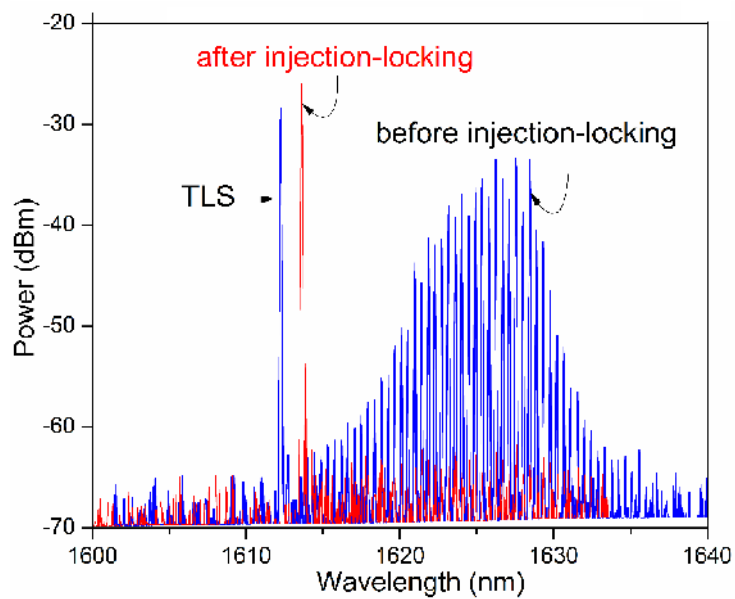


Figure 5.1 The optical spectra of QD-LD with/without injection locking. The master TLS laser linewidth is visible.



Figure 5.2 depicts the 1621.42 nm IL mode of the QD-LD when the TLS is wavelength tuned with a CW injection power of  $\sim 4.5$  dBm. The measured single mode output power and SMSR of this IL single FP mode is  $-5.34$  dBm and 31 dB, respectively.

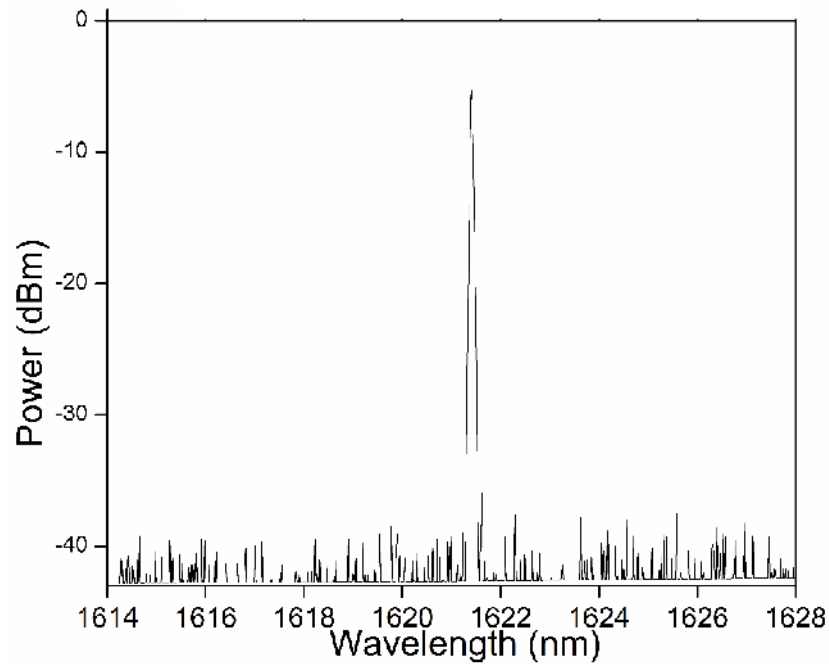
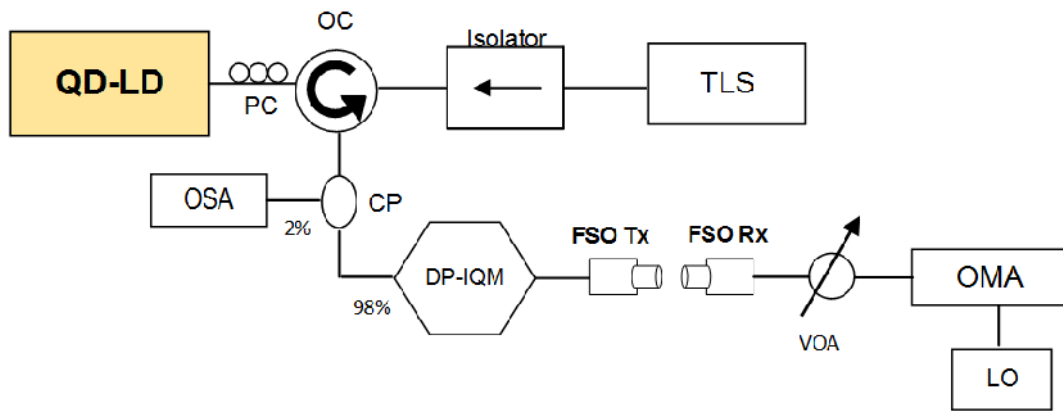


Figure 5.2 Injection-locked mode (1621.42 nm) of the QD-LD.

### 5.2.1 Optical Wireless Transmission Setup

Figure 5.3 depicts the block diagram of FSO setup. A master TLS at fixed  $\sim 4.5$  dBm external power is injected into an OC via an isolator, and through a PC into the slave QD-LD. The 1621.42 nm IL QD-LD mode is observed at the 2% output of a 2/98 power splitter and combiner (CP) using OSA. The remaining 98%, which corresponds to mode power of

$\sim -5.2$  dBm, is fed in to a dual-polarization in-phase and quadrature (DP-IQ) modulator for modulation purpose. Pre-processing (pattern generator, modulation, over-sampling) of the signal was performed using MATLAB. We have used a  $2^{11}-1$  PRBS data stream in QPSK format. These signals are driven into the DP-IQ modulator whose process is already described in chapter 4 and later the modulated signals are detected using OMA.



**Figure 5.3 Experimental setup of DP-QPSK transmission employing externally modulated IL QD-LD.**

Figure 5.4 and Figure 5.5 show the indoor laboratory FSO setup for 2 and 4 meter free-space channel, respectively. The FSO channel is composed of two SMF collimators, one is utilized for transmitting the modulated laser beam into the free space and the other is used for reception of the beam. The collimator includes aspheric lens operating in the wavelength range of 1050 –1620 nm, and has a beam diameter of 3.6 mm. The beam divergence and focal length are  $0.032^\circ$  and 18.75 mm, respectively. Initial alignment of the FSO links have been accomplished manually using visible green light laser (520 nm). Later, two-dimensional translation stages are used to further fine align the signal into the reception collimator SMF and to check the error margin under misalignment conditions.

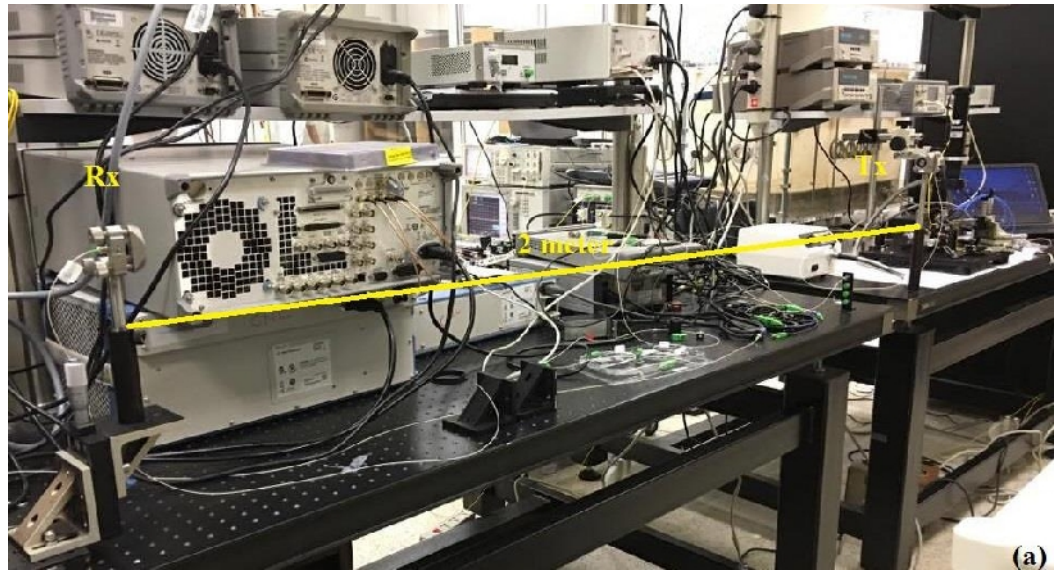


Figure 5.4 2 m indoor laboratory FSO setup.

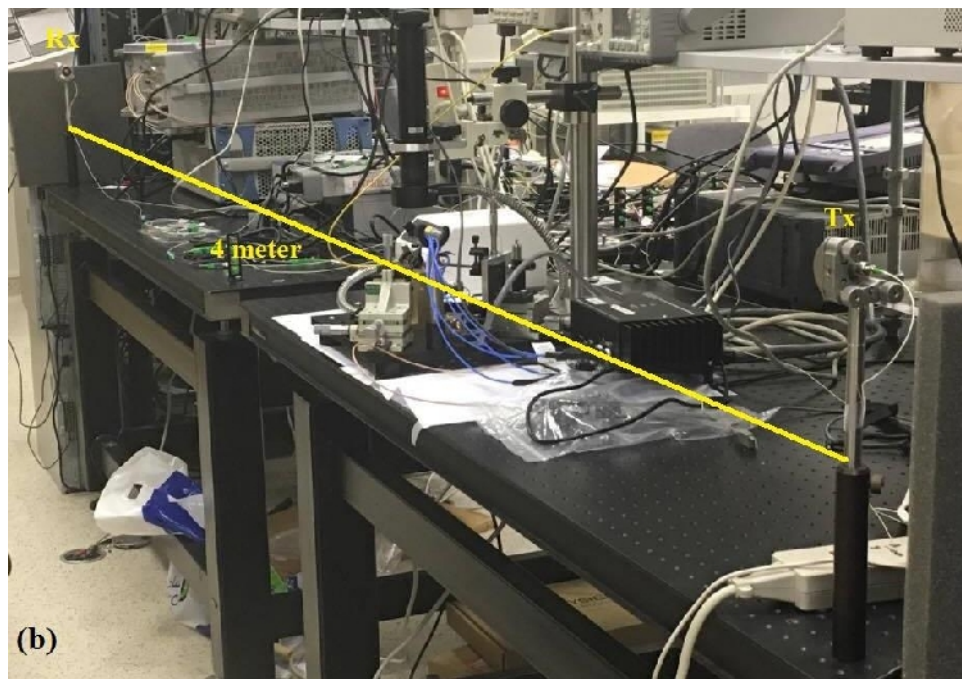


Figure 5.5 4 m indoor laboratory FSO setup.

The signal transmission is characterized over a 2-m and 4-m free-space link. We measured the free space channel loss over 2 m and 4 m distance by transmitting a known power of 5.5 dBm using 1550 nm laser, as shown in Figure 5.6 (b). The received power after the reception collimator is measured using optical power meter, as shown in Figure 5.6 (a), and the loss is deduced. The values are  $\sim 0.5$  dB and  $\sim 2.5$  dB for 2 m and 4 m channels, respectively. This high channel loss with increasing channel distance is primarily attributed to the manual alignment system which can be further improved by precise alignment or piezo alignment techniques. After signal coupling into the reception collimator SMF, a VOA is employed before sending the signal into OMA for detection. All the FSO system level experiments were performed in the Communication and Networking laboratory (CNL), King Saud University, Riyadh.

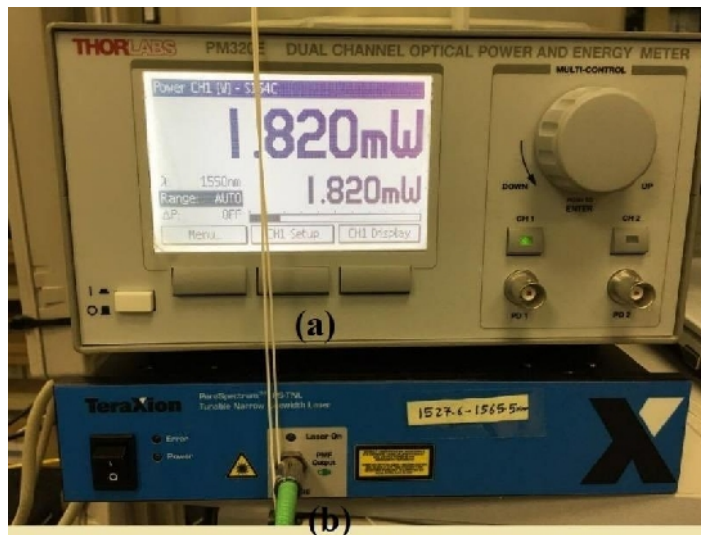


Figure 5.6 (a) Optical power meter (b) 1550 nm tunable narrow linewidth laser

## 5.2.2 Eye Safety Standards

Laser safety standards is one of the important part to be considered in FSO experiments. High power and focused laser beam could adversely damage the eye, particularly at shorter wavelengths. Several standards for laser safety have been developed by different countries such as American National Standards Institute (ANSI) and the European Committee for Electrotechnical Standardization (CENELEC) [27]. The permissible emission levels and laser classifications for 850 nm and 1500 nm wavelengths, is shown in Table 5.1. Indoor FSO communication system is well-suited in Class 1 bands with no warning labels. However, Class 3B can be utilized for outdoor FSO communication with certain precautions regarding transmitter locations, where high power budget is required. Class 4 devices are dangerous to the eyes and skin due to very high emission power.

**Table 5.1: Classification of Laser safety and permissible emission ranges for 850 nm and 1550 nm wavelengths [27].**

	<b>850 nm</b>	<b>1550 nm</b>
Class 1	Up to 0.78 mW	Up to 10 mW
Class 1M	Up to 0.78 mW	Up to 10 mW
Class 2	Band reserved for visible light wavelengths (400-700 nm)	
Class 3R	0.22–2.2 mW	10–50 mW

Class 3B	2.2–50 mW	50–500 mW
Class 4	>500 mW	>500 mW

The eye-safety limit of the laser beam in free space can be calculated by the accessible emission limit (AEL) [172],

$$AEL = MPE \times \pi r^2 \quad (5.1)$$

Where *MPE* is maximum permissible exposure and  $\pi r^2$  is the beam area. For a 4 m distance, the beam area is 0.14309 cm<sup>2</sup> and *MPE* is 0.1 W/cm<sup>2</sup> [176] (see Table 5.2), thus, the maximum AEL is ~14.3 mW (~11.55 dBm). Similarly, the maximum AEL for 2 m distance is ~ 11.2 mW (~10.49 dBm) with 0.1121 cm<sup>2</sup> beam area. In our experiment the estimated maximum transmitted optical power is -13 to -16 dBm which is way below the AEL eye-safety limit.

**Table 5.2: Maximum permissible exposure (MPE) for 850 nm and 1550 nm wavelengths [173].**

Exposure Time (s)	1	2	4	10	100	1000	10000
MPE (W/cm <sup>2</sup> ) at 850 nm	0.0036	0.0030	0.0025	0.002	0.0011	0.00065	0.00036
MPE (W/cm <sup>2</sup> ) at 1550 nm	0.560	0.330	0.19	0.1	0.1	0.1	0.1

### 5.2.3 4 m DP-QPSK Indoor FSO Communication

We transmitted a CW 1621.42 nm IL (see Figure 5.2) DP-QPSK signal into the indoor 4 m FSO link with different Gbaud rates (8, 16 and 25 Gbauds). A root raised cosine (RRC) pulse shaping filter with roll-off factor of 0.35 is used at both the transmitter and receiver ends. The maximum achieved baud rate over 4 m free space channel is 25 Gbaud corresponding to 100 Gb/s with 2.96 b/s/Hz spectral efficiency. The corresponding signal constellation and the eye diagram is shown in Figure 5.7 (a) and (b), respectively, at an optical received power of -17.2 dBm. The Figure 5.8 (a) and (b), show the eye diagrams and QPSK constellations for 64 Gbit/s at -18.8 dBm received power. In Figure 5.9, the measured error vector magnitude (EVM) BER versus the received signal power at 16 (64) and 25(100) Gbaud (Gb/s) is presented. To achieve a BER FEC threshold of  $3.8 \times 10^{-3}$ ,

received powers of -17.5 dBm and -19 dBm are required for 100 and 64 Gb/s transmission rate, respectively.

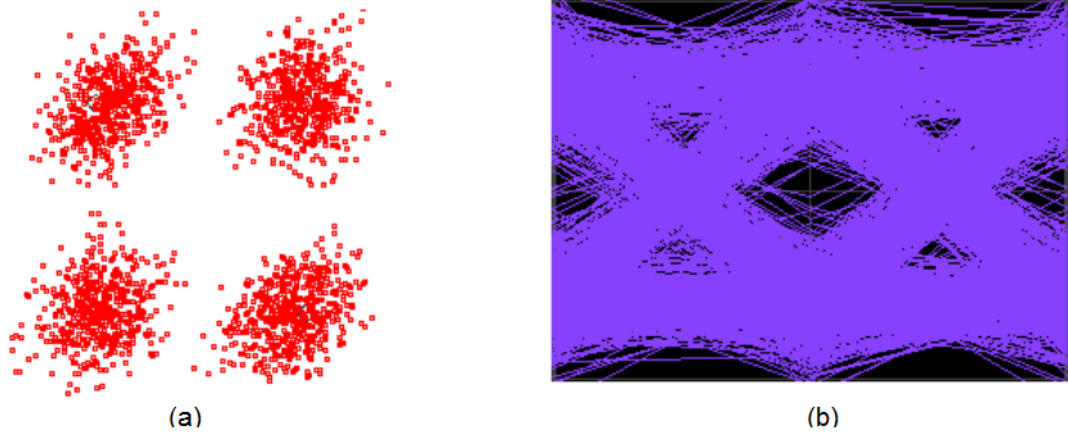


Figure 5.7 (a) Constellation diagram and, (b) eye diagram, for 4-m/100 Gb/s transmission rate.

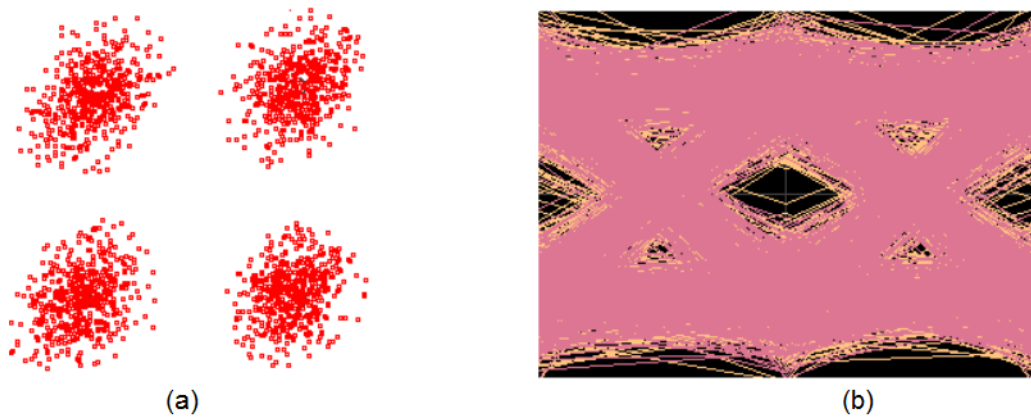


Figure 5.8 (a) Constellation diagram and, (b) eye diagram, for 4-m/64 Gb/s transmission rate.



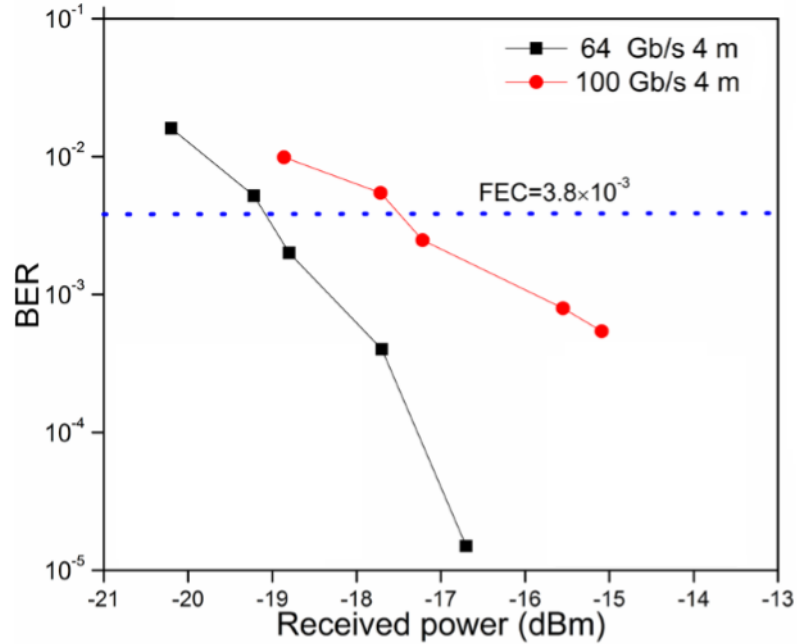


Figure 5.9 Measured BER curves of the IL QD-LD-based FSO link over 4 m channel length, and at transmission rate of 64 and 100 Gb/s.

#### 5.2.4 2 m DP-QPSK Indoor FSO Communication

The performance of DP-QPSK 100 Gb/s and 64 Gb/s QD-LD IL modulated signal is tested over different channel length scenarios. The Figure 5.10 and Figure 5.11 show the eye diagrams and QPSK constellations for 64 Gb/s and 100 Gbit/s at -19.2 and -17.2 dBm received powers, respectively, below FEC threshold. The corresponding BER results at 64 and 100 Gb/s transmission over 2 m free space link is presented in Figure 5.12. To achieve a BER of  $3.8 \times 10^{-3}$  (FEC threshold), a received power of -17.94 dBm is required for 100 Gb/s data rate.

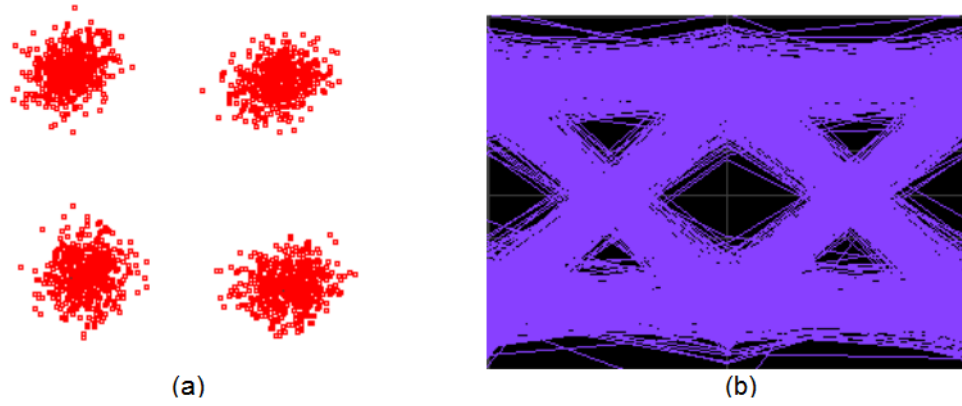


Figure 5.10 (a) Constellation diagram and, (b) eye diagram, for 2-m/64 Gb/s transmission rate.

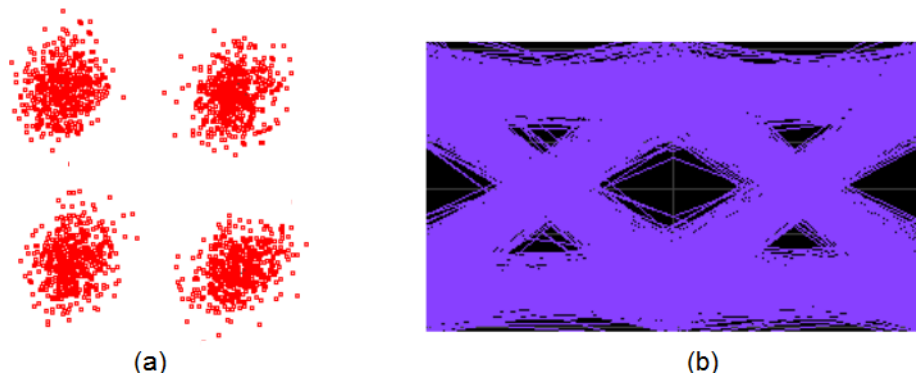


Figure 5.11 (a) Constellation diagram and, (b) eye diagram, for 2-m/100 Gb/s transmission rate.

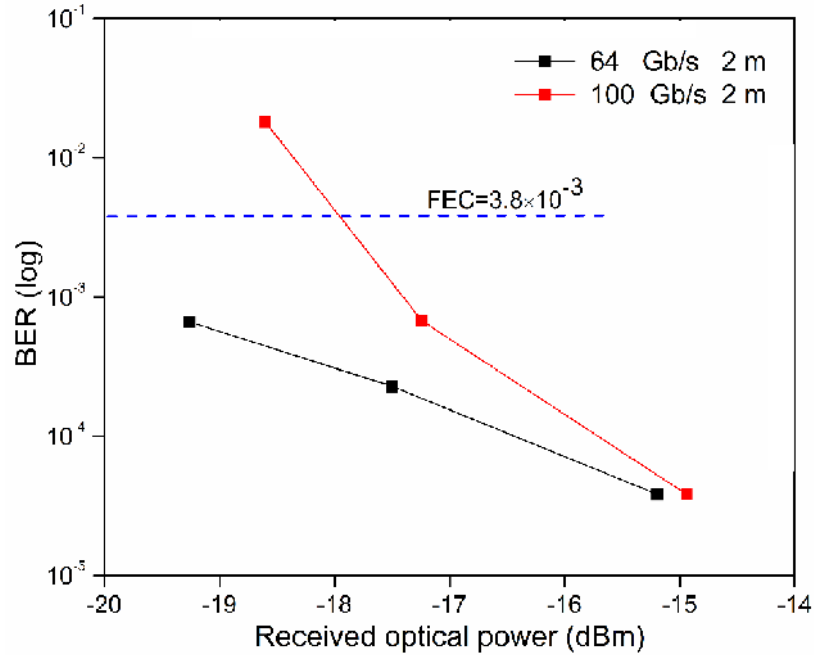


Figure 5.12 Bit error rate as a function of received optical power of IL QD-LD-based FSO link over 2 m channel length, and at transmission rate of 64 and 100 Gb/s.

### 5.2.5 2 m & 4 m FSO BER curves Comparison

Figure 5.13 shows the comparison of measure BER curves over 2 m and 4 m free space channels, and at 100 Gb/s transmission. A receiver sensitivity of -18.3 (-17.3) dBm is noted over 2 m (4 m), translating to ~1.0 dB received power improvement at FEC threshold compared to the long channel (4 m). Reducing the channel length from 4 m to 2 m noticeably improved the transmission performance, as a result of higher received optical power level, and affirms the wide open eye (see Figure 5.10 and Figure 5.11) and better BER for the 2 m link case. It is noteworthy to mention that by precise collimators' alignment, the free space channel loss could further be reduced, thereby enabling to realize longer indoor FSO link within the available ~0 dBm power budget of the QD-LD.

Moreover, with improved power budget by employing a proper far L-band amplifier in the system, QD-LD has a potential to address not only long indoor channels but also long outdoor communication links.

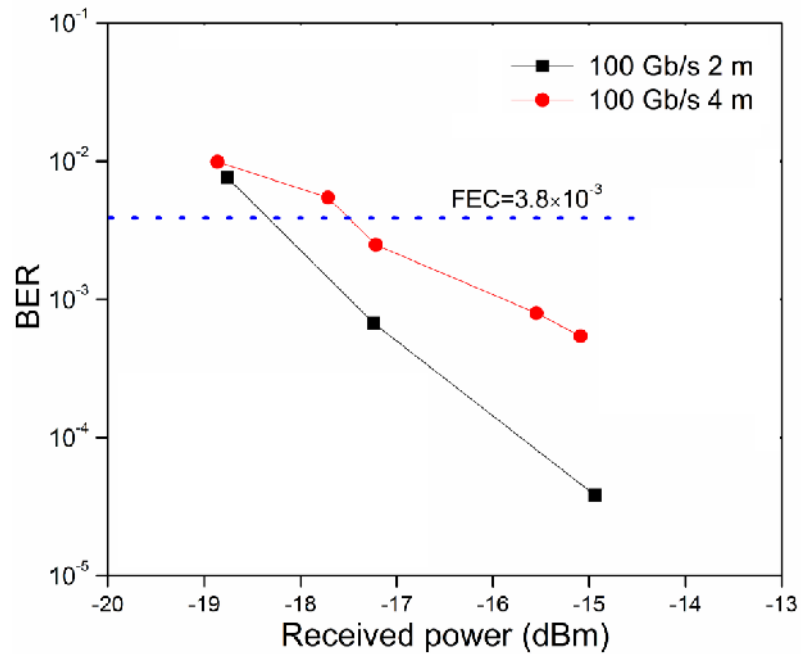


Figure 5.13 Comparison of the measured BER curves of the IL QD-LD-based FSO link over 2 m and 4 m long free space channels, and at 100 Gb/s transmission

### 5.2.6 Laser Beam Misalignment

A laser beam propagates through the free-space channel between the SMF collimators as if the fibers were connected smoothly. In practice, this is not the case and we expect misalignment to occur. To estimate the error margin of this optical misalignment on 4 m/64

Gb/s FSO transmission system, we intentionally moved the reception collimator horizontally and vertically with a step size of 0.2 mm and measured the BER. The results are shown in Figure 5.14 (a) and (b). The measured BER values are found to increase exponentially under increasing horizontal misalignment of optical beam while a disrupt behavior is observed in misaligning vertically. In general, the horizontal and vertical misalignment should provide similar results however, this behavior is attributed to the stability of injection-locked mode and fluctuation of DC power in QD-LD at that particular experimental time. To achieve BERs below the FEC limit, we estimated the maximum horizontal and vertical beam displacement to be ~1.6 mm and ~ 2.4 (~42% and ~ 66% of the beam diameter), respectively, that can be tolerated. The two-dimensional translation stage into the reception collimator SMF is shown in Figure 5.15 for laser beam misalignments.

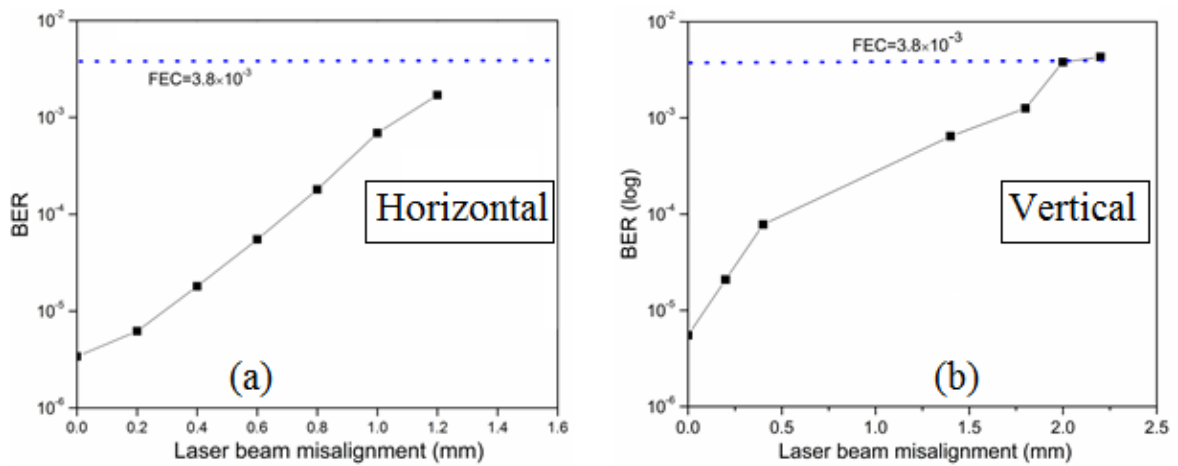


Figure 5.14 BER values of 4 m/64 Gb/s IL QD-LD FSO link under different laser beam misalignment conditions.

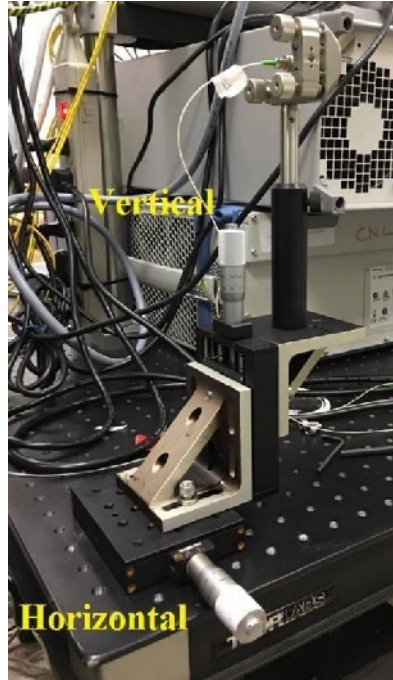


Figure 5.15 Setup of two-dimensional translation stage into the reception collimator SMF for different beam misalignments.

### 5.3 Comparison of IL QD-LD and TLS Carrier

To show the effectiveness of employing IL QD-LD for better transmission, we compared 100 Gb/s DP-QPSK transmission over 1621.42 nm injection-locked QD-LD and 1620.90 nm TLS, which are operated individually, as shown in Figure 5.16 (a). We set the carrier

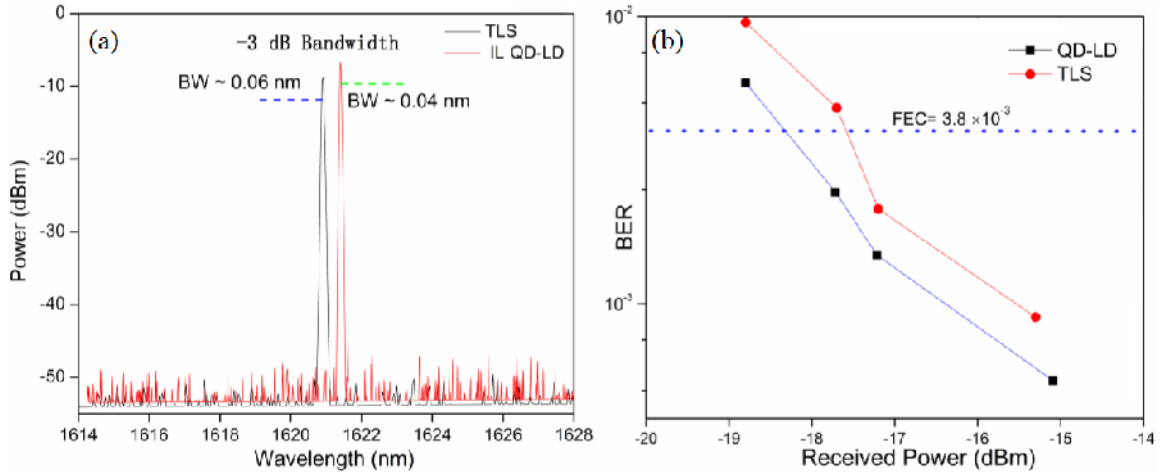


Figure 5.16 (a) 1621.42 nm IL QD-LD and 1620.90 nm TLS carrier, (b) measured BER comparison of IL QD-LD and TLS, for 4 m/100 Gb/s transmission system.

signal power similar for both cases before sending into the DP-IQ modulator, and compared the BER values at an identical received power (using VOA), before demodulation. The results are illustrated in Figure 5.16 (b) which shows surprisingly transmission performance with an IL QD-LD source compared to TLS counterpart.

The comparison showed superior performance of the IL slave QD laser light source, achieving a power improvement of ~1.0 dB at FEC threshold. However, it is to be noted that the shown TLS mode was not the one that has been utilized for injection locking QDash laser diode and hence a direct comparison of the performance is void. When we measured the linewidth of the sources we found an improved coherency of IL QD-LD 1621.42 nm mode with -3 dB (-15 dB) linewidth of ~0.04 (~0.12) nm. The associated -3 dB (-15 dB) linewidth of 1620.90 nm TLS is measured to be ~0.06 (~0.16) nm. Hence, we believe that TLS mode that was utilized for IL should have linewidth of less than or equal to the IL QD-LD mode.

## Chapter 6

# CONCLUSION AND FUTURE WORK

### 6.1 Thesis Conclusion

In this thesis, characterization and performance of InAs/InP quantum dash (QDash) laser is evaluated at device and system level. We experimentally investigated QDash laser devices in pulse and CW injection in order to extract the different laser parameters and their emission spectrum profiles at device level. At system level, we evaluated the QDash laser performance over an optical fiber and optical wireless communication systems. Here we summarize the most significant conclusions from this work.

- Firstly, we characterized the fixed barrier InAs/InGaAlAs/InP QDash laser at room temperature with different cavity lengths. A 4  $\mu\text{m}$  ridge width device was utilized during characterization of eight different cavity lengths. The internal quantum efficiency was found to be 77.8 % and internal loss  $8.8 \text{ cm}^{-1}$ . The transparency current density showed a high value of  $\sim 5639 \text{ A/ cm}^2$ . Moreover, the  $4 \times 800 \mu\text{m}^2$  device displayed a broadest lasing emission as compared to the other cavity lengths, however, a detailed spectral analysis was not possible owing to the wavelength limitation of the OSA.



- Later, the fixed barrier InAs/InGaAlAs/InP QDash laser performance was compared with a chirped multi-stack InAs/ InGaAlAs /InP QDash laser. The internal quantum efficiency and transparency current density was found to be superior in the latter case with values reaching 83.62 % and 3146 A/cm<sup>2</sup>. Besides, the central lasing wavelength of fixed barrier QDash laser was found to be ~1690 nm whereas the chirped barrier QDash laser emission was at ~ 1610 nm, at room temperature. Based on the comparison results, the chirped QDash laser diode was selected for subsequent transmission experiments., In particular, a 4×800 um<sup>2</sup> chirped QDash laser diode is selected, providing a CW SMF fiber coupled optical power up to ~1.00 mW (~0 dBm), at an injection current of 240 mA.
- Afterwards, the injection locking characteristics of chirped 4×800 um<sup>2</sup> QDash laser diode is investigated to improve the laser sub-carrier performance in terms of linewidth, coherency and wavelength instabilities for its deployment in optical communication experiments. Wavelength tunability, short-term stability, and injection-locked hysteresis experiments were performed in characterization of an injection-locked QDash laser diode. An injection locked mode wavelength tunability of ~23 nm was accomplished from ~1611 nm to ~1634. In short-term stability test, a particular injection-locked QD-LD mode (1619.68 nm one of the mode from tuning range) was found to be stable throughout the observation time of 24 minutes. Finally, it was observed that injection-locking hysteresis was maintained till 4.2 dBm starting from + 7 dBm injection power, afterwards injection-locked mode was unlocked and similar behavior was observed till 3 dBm external injection power.

- Then, we performed fiber transmission experiment using a single injection-locked Fabry-Perot mode of a QDash laser as a sub-carrier. We demonstrated a single channel 32, 64 and 100 Gb/s dual-polarization quadrature phase shift keying (DP-QPSK) transmission at ~1621 nm by employing external modulation. The signal transmission was characterized first in a back-to-back (BtB) configuration and then over a 10 km single mode fiber (SMF) for all transmission rates. We also proposed a next generation WDM-PON with a unified upstream and downstream transmitter capable of more than 100 Gb/s transmission capacity, and based on exclusively ultra-broadband QD-LDs as unified transmitters, possible QDash based broadband photodiodes as unified receivers, and broadband QD-MLL as external seeding light sources.
- Finally, the potential of tunable injection locked far L-band quantum-dash laser as a promising light source in both indoor and outdoor future high speed free space optical communication, is investigated. We experimentally demonstrated an indoor 64 Gb/s and 100 Gb/s free space optical communication using single channel injection locked (~1621 nm) quantum-dash laser. The far L-band injection-locked wavelength mode is externally modulated over 2 m and 4 m indoor free-space links using DP-QPSK scheme. Moreover, we estimated the maximum horizontal and vertical beam displacement and found to be ~1.6 mm and ~ 2.4 (~ 42% and ~ 66% of the beam diameter), respectively, that can be tolerated.

## 6.2 Future Work

The following are some future work possibilities:

- Self-injection locking of QDash laser can be employed instead of external injection-locking for its potential deployment in optical communication. Tuning of the locked mode could be performed by changing the bandpass filter center wavelength.
- Possibility of employing Quantum dash laser as a gain medium and for injection-locking, while modulating the master laser signal, could be explored.
- Self-homodyne detection method could be utilized in any proposed future work to mitigate the sub-carrier coherency issue at the detection side, instead of employing heterodyne detection technique. However, the transmission capacity could be reduced appreciably as a copy of local oscillator is also transmitted along with the modulated signal.
- High transmission rate can be achieved through high order modulation formats under external modulation, such as 16-Quadrature phase shift keying (QPSK), M-ary Quadrature amplitude modulation (QAM) and orthogonal frequency division multiplexing (OFDM), provided the SMF coupled optical power of QDash laser diode is improved
- To enable future high speed and long distance optical wireless communication, the length of free-space channels can be increased with the expense of higher power budget of QDash laser device, and its performance in outdoor FSO could be investigated. Performance of directly modulated QDash laser in next generation PON can be investigated via external or self-injection locking. It will not require

any external modulator and an amplifier hence, a cost effective solution for colorless WDM-PON.

## REFERENCES

- [1] The Electromagnetic Telegraph. (n.d.). Retrieved December 20, 2016, from <https://mysite.du.edu/~jcalvert/tel/morse/morse.htm>.
- [2] Elisha Gray. (n.d.). Retrieved December 20, 2016, from <http://www.oberlin.edu/external/EOG/OYTT-images/ElishaGray.html>.
- [3] Hall, R. N., Fenner, G. E., Kingsley, J. D., Soltys, T. J., & Carlson, R. O. (1962). Coherent Light Emission from GaAs Junctions. *Physical Review Letters*, vol. 9, no.9, pp.366–368, 1962.
- [4] Ujager, F. S., Zaidi, S. M. H., & Younis, U, “A review of semiconductor lasers for optical communications”, In *7th International Symposium on High-capacity Optical Networks and Enabling Technologies*, pp. 107–111, 2010.
- [5] Encyclopedia of Laser Physics and Technology - optical fiber communications, data transmission, capacity, telecom windows, C band, L band, WDM. (n.d.). Retrieved December 20, 2016, from [https://www.rp-photonics.com/optical\\_fiber\\_communications.htm](https://www.rp-photonics.com/optical_fiber_communications.htm).
- [6] Fiber Optic Communications. (n.d.). Retrieved December 20, 2016, from [http://www.olson-technology.com/mr\\_fiber/FO\\_Communications.htm](http://www.olson-technology.com/mr_fiber/FO_Communications.htm)
- [7] Cisco Visual Networking Index: Global Mobile Data Traffic Forecast update 2015-2020 White paper, <http://www.cisco.com/c/en/us/solutions/collateral/service-provider/visual-networking-index-vni/mobile-white-paper-c11-520862.pdf> (Accessed December 20, 2016).
- [8] Vujicic, V, “*Optical multicarrier sources for spectrally efficient optical networks* (doctoral)”, Dublin City University. School of Electronic Engineering, March 2016, Retrieved from <http://doras.dcu.ie/20981/>.
- [9] Ragheb, A., & Fathallah, H, “Candidate modulation schemes for next generation-passive optical networks (NG-PONs)”, In *High Capacity Optical Networks and Emerging/Enabling Technologies*, pp. 226–231, 2012.
- [10] Zhou, R, “*Optical frequency comb source for next generation access networks* (doctoral)”, Dublin City University. School of Electronic Engineering, November 2014, Retrieved from <http://doras.dcu.ie/20213/>.
- [11] 10G-PON FTTH solution - Huawei Solutions. (n.d.). Retrieved December 20, 2016, from [http://www1.huawei.com/ilink/en/solutions/broader-smarter/HW\\_453305](http://www1.huawei.com/ilink/en/solutions/broader-smarter/HW_453305).

- [12] Pfeiffer, T, "Evolution of optical access network technologies," Vol. 7607, pp. 760716-760716-12, 2010.
- [13] Mbah, A. M. "*Hybrid fibre and free-space optical solutions in optical access networks* (doctoral)". University of Nottingham, July 2016, Retrieved December 20, 2016, from <http://eprints.nottingham.ac.uk/32572/>.
- [14] Dong, T, "*Wavelength division multiplexed passive optical networks* (Thesis)" The Hong Kong Polytechnic University, 2013 Retrieved from <http://ira.lib.polyu.edu.hk/handle/10397/6167>.
- [15] Alhalani, M, "Performance Improvement of Wavelength Division Multiplexing Passive Optical Networks (WDM PONs)". The Islamic University of Ghaza, March 2014, Retrieved December 20, 2016, from <http://library.iugaza.edu.ps/thesis/112782.pdf>.
- [16] Lin, G. R., Liao, Y. S., Chi, Y. C., Kuo, H. C., Lin, G. C., Wang, H. L., & Chen, Y. J, "Long-Cavity Fabry Perot Laser Amplifier Transmitter with Enhanced Injection-Locking Bandwidth for WDM-PON Application," *Journal of Lightwave Technology*, vol. 28, no. 20, pp. 2925–2932, 2010.
- [17] Z Xu, Y. J. Wen, W. Zhong, C. Chae, X. Cheng, Y. Wang, C. Lu, and J. Shankar, "High-speed WDM-PON using CW injection-locked Fabry-Pérot laser diodes," *Opt. Express*, vol. 15, no. 6 pp. 2953-2962, 2007.
- [18] Shin, D. J., Jung, D. K., Shin, H. S., Kwon, J. W., Hwang, S., Oh, Y., & Shim, C, "Hybrid WDM/TDM-PON with wavelength-selection-free transmitters," *Journal of Lightwave Technology*, vol. 23, no. 1, pp. 187–195, 2005.
- [19] Feng, M., Luo, Q., & Bai, C, "Colorless ONU implementation for WDM-PON using direct-detection optical OFDM". *Optoelectronics Letters*, Vol. 9. no. 2, pp.135–138, 2013.
- [20] Su, C.-F., Wang, L., Liaw, S.-K., & Huang, Y.-S, "A colorless WDM-PON system using multi-wavelength light sources for optically-injection-locked transmitters." *Optical Fiber Technology*, vol. 16, no. 1, pp.1–4, 2010.
- [21] Q. T. Nguyen *et al.*, "Bidirectional transmission in colourless WDM-PON based on injection-locked Fabry-Perot laser at 2.5 Gbit/s using low-cost seeding source," *2009 35th European Conference on Optical Communication*, Vienna, pp. 1-2, 2009.
- [22] Nguyen, Q. T *et al.*, "16x2.5 Gbit/s Downstream Transmission in Colorless WDM-PON Based on Injection-Locked Fabry-Perot Laser Diode Using a Single Quantum Dash Mode-Locked Fabry-Perot Laser as Multi-Wavelength Seeding Source". In *Optical Fiber Communication Conference and National Fiber Optic Engineers Conference*, p. OThA3, 2009. Optical Society of America.

- [23] Z Xu, Y. J. Wen, W. Zhong, C. Chae, X. Cheng, Y. Wang, C. Lu, and J. Shankar, "High-speed WDM-PON using CW injection-locked Fabry-Pérot laser diodes," *Opt. Express*, vol. 15, no. 6 pp. 2953-2962, 2007.
- [24] A. Emsia *et al.*, "Cost-efficient Upstream Transmitter Using Injection Locked Fabry-Perot Laser Diodes for Multi-Gbit/s WDM-PON," *Photonic Networks; 17. ITG-Symposium; Proceedings of*, Leipzig, Germany, pp. 1-8, 2016.
- [25] Batagelj, B., Janyani, V., & Tomažič, S., "Research Challenges in Optical Communications Towards 2020 and Beyond." *Informacije MIDE M*, vol. 44, no. 3, pp.177–184, 2012.
- [26] H. Kaushal; G. Kaddoum, "Optical Communication in Space: Challenges and Mitigation Techniques," in *IEEE Communications Surveys & Tutorials*, vol. PP, no.99, pp.1-1, 2016.
- [27] Abisayo, A. "Optically amplified free-space optical communication system (doctoral)". University of Nottingham, July 2013, Retrieved December 20, 2016, from <http://eprints.nottingham.ac.uk/13304/>.
- [28] Mansour, A., Mesleh, R., & Abaza, M, "New challenges in wireless and free space optical communications." *Optics and Lasers in Engineering*, vol. 89, pp. 95–108, 2017.
- [29] LASER World of PHOTONICS | Trade Fair Laser Photonics Industry. (n.d.). Retrieved December 20, 2016, from <http://www.world-of-photonics.com/index-2.html>.
- [30] M. Lu, L. Liu and S. Hranilovic, "Raptor-coded free-space optical communications experiment," in *IEEE/OSA Journal of Optical Communications and Networking*, vol. 8, no. 6, pp. 398-407, June 2016.
- [31] Free Space Optics (FSO) and Visible Light Communication (VLC) Market - 2020 |MarketsandMarkets. (n.d.). Retrieved December 20, 2016, from <http://www.marketsandmarkets.com/Market-Reports/visible-light-communication-market-946.html>.
- [32] Ghassemlooy, Zabih, Shlomi Arnon, Murat Uysal, Zhengyuan Xu, and Julian Cheng. "Emerging optical wireless communications-advances and challenges." *IEEE Journal on Selected Areas in Communications*, vol. 33, no. 9, pp. 1738-1749, 2015.
- [33] Parca, Giorgia, Ali Shahpari, Valeria Carrozzo, Giorgio Maria Tosi Beleffi, and Antonio L. J. Teixeira. "Optical wireless transmission at 1.6-Tbit/s (16×100 Gbit/s) for next-generation convergent urban infrastructures." *Optical Engineering*, vol. 52, no. 11, pp.116102–116102, 2013.

- [34] Hamza, Abdelbaset S., Jitender S. Deogun, and Dennis R. Alexander. "Free space optical data center architecture design with fully connected racks" in *IEEE Global Communications Conference*, pp. 2192-2197, 2014.
- [35] Bohata, J., S. Zvanovec, P. Pesek, T. Korinek, M. Mansour Abadi, and Z. Ghassemlooy. "Experimental verification of long-term evolution radio transmissions over dual-polarization combined fiber and free-space optics optical infrastructures." *Applied Optics*, vol. 55, no. 8, pp. 2109–2116, 2016.
- [36] S. Arnon, Ed., *Visible Light Communication*. Cambridge, U.K.: Cambridge Univ. Press, Feb. 2015.
- [37] Pang, T. Kwan, C.-H. Chan, and H. Liu, "LED traffic light as a communications device," in *Proc. IEEE/IEEE/JSAI Int. Conf. Intell. Transp. Syst.*, Tokyo, Japan, pp. 788–793, 1999.
- [38] K. Kulhavy, Home: RONJA, Retrieved December, 21, 2016 <http://ronja.twibright.com>.
- [39] Tanaka, S. Haruyama, and M. Nakagawa, "Wireless optical transmissions with white colored led for wireless home links," in *Proc. 11th IEEE Int. Symp. PIMRC*, London, U.K., vol. 2, pp. 1325–1329, 2000.
- [40] J. Grubor, S. Randel, K. D. Langer, and J. W. Walewski, "Broadband information broadcasting using LED-based interior lighting," *J. Lightw. Technol.*, vol. 26, no. 24, pp. 3883–3892, 2008.
- [41] *Short-Range Wireless Optical Communication Using Visible Light*, IEEE Standard for Local and Metropolitan Area Networks-Part 15.7 Std., 2011.
- [42] Y. Suh, C.-H. Ahn, and J. K. Kwon, "Dual-codeword allocation scheme for dimmable visible light communications," *IEEE Photon. Technol. Lett.*, vol. 25, no. 13, pp. 1274–1277, 2013.
- [43] S. Wu, H. Wang, and C.-H. Youn, "Visible light communications for 5G wireless networking systems: From fixed to mobile communications," *IEEE Netw.*, vol. 28, no. 6, pp. 41–45, 2014.
- [44] D. Tsonev, S. Videv, and H. Haas, "Light fidelity (Li-Fi): Towards all-optical networking," in *Proc. SPIE*, 2013, vol. 9007, 2013.
- [45] A. T. Hussein and J. M. H. Elmirghani, "High-speed indoor visible light communication system employing laser diodes and angle diversity receivers," *2015 17th International Conference on Transparent Optical Networks (ICTON)*, Budapest., pp.1-6,2015.



- [46] D. Bykhovsky and S. Arnon, "An experimental comparison of different bit-and-power-allocation algorithms for DCO-OFDM," *J. Lightw. Technol.*, vol. 32, no. 8, pp. 1559–1564, Apr. 2014.
- [47] G. Cossu, A. M. Khalid, P. Choudhury, R. Corsini, and E. Ciaramella, "3.4 Gbit/s visible optical wireless transmission based on RGB LED," *Opt. Exp.*, vol. 20, no. 26, pp. B501–B506, 2012.
- [48] J. Vucic *et al.*, "230 Mbit/s via a wireless visible-light link based on OOK modulation of phosphorescent white LEDs," in *Proc. Opt. Fiber Commun./Nat. Fiber Opt. Eng. Conf.*, pp. 1–3, 2010.
- [49] A. Burton, H. Le Minh, Z. Ghassemlooy, E. Bentley, and C. Botella, "Experimental demonstration of 50-Mb/s visible light communications using  $4 \times 4$  MIMO," *IEEE Photon. Technol. Lett.*, vol. 26, no. 9, pp. 945–948, 2014.
- [50] C. B. Naila, K. Wakamori, M. Matsumoto, A. Bekkali, and K. Tsukamoto, "Transmission analysis of digital TV signals over a radioon-FSO channel," *IEEE Commun. Mag.*, vol. 50, no. 8, pp. 137–144, 2012.
- [51] P. Mandl, P. Schrotter, and E. Leitgeb, "Hybrid systems using DVB-T, WLAN and FSO to connect peripheral regions with broadband Internet services," in *Proc. 10th Int. ConTEL*, pp. 67–71, 2009.
- [52] J. C. Juarez, D. W. Young, J. E. Sluz, J. L. Riggins II, and D. H. Hughes, "Free-space optical channel propagation tests over a 147-km link," in *Proc. SPIE, Atmos. Propag. VIII*, 2011, Art. ID. 80380B.
- [53] M. O. Zaatari, "Wireless optical communications systems in enterprise networks," *Telecommun. Rev.*, pp. 49–57, 2003.
- [54] E. Ciaramella *et al.*, "1.28 terabit/s ( $32 \times 40$  Gbit/s) WDM transmission system for free space optical communications," *IEEE J. Sel. Areas Commun.*, vol. 27, no. 9, pp. 1639–1645, 2009.
- [55] Y. Arimoto *et al.*, "320 Gbit/s ( $8 \times 40$  Gbit/s) double-pass terrestrial free-space optical link transparently connected to optical fibre lines," in *Proc. 34th ECOC*, pp. 1–2, 2008.
- [56] Chen, S. Chang, S. Shuen-Te Ji, H. Lin, H. Tsay, P. Huang, W. Chiang, W. Lin, S. Lee, H. Tsao, *et al.*, "Demonstration of 16 channels 10 Gb/s WDM free space transmission over 2.16 km," *IEEE/LEOS Summer Topical Meetings, 2008 Digest of the*, pp. 235–236, 2008.

- [57] G. Parce, A. Shahpari, V. Carrozzo, G. M. T. Beleffi, and A. L. Teixeira, "Optical wireless transmission at 1.6-Tbit/s ( $16 \times 100$  Gbit/s) for next generation convergent urban infrastructures," *Opt. Eng.*, vol. 52, no. 11, 2013.
- [58] Connolly, C, "A Transparent Unidirectional Wave Division Multiplexing Passive Optical Network Architecture (doctoral)", National University of Ireland. December 2011, Retrieved from <http://hdl.handle.net/10379/3026>.
- [59] Maged A. Esmail, Amr Ragheb, H. Fathallah, and M-S Alouini. "Experimental demonstration of outdoor 2.2 Tbps super-channel FSO transmission system." in *IEEE International Conference on Communications Workshops (ICC)*, pp. 169-174, 2016.
- [60] Lee, K., Lim, S. D., Jhon, Y. M., Kim, C. H., Ghelfi, P., Nguyen, A. T., ... Lee, S. B., "Broadcasting in colorless WDM-PON using spectrum-sliced wavelength conversion." *Optical Fiber Technology*, vol. 18, no. 2, pp. 112–116, 2012.
- [61] S.-M. Lee, K-M. Choi, S.-G. Mun, J.-H. Moon, C.-H. Lee, "Dense WDM-PON based on wavelength-locked Fabry-Perot laser diodes", *IEEE Photonics Technology Letters*, vol. 17, no. 7, pp. 1579-1581, 2005.
- [62] K. Y. Cho, U. H. Hong, Y. Takushima, A. Agata, T. Sano, M. Suzuki, and Y. C. Chung, "103-Gb/s long-reach WDM PON implemented by using directly modulated RSOAs," *IEEE Photonics Technology Letters* vol. 24, no. 3, pp. 209–11, 2012.
- [63] Nguyen, Q. T., Besnard, P., Bramerie, L., Shen, A., Garreau, A., Vaudel, O., ... Simon, J.-C, "Using optical injection of Fabry-Perot lasers for high-speed access in optical telecommunications," *Proc. SPIE, Semiconductor Lasers and Laser Dynamics IV*, vol. 7720, p. 77202D–77202D–10, 2010.
- [64] Ki-Man Choi, Jin-Serk Baik and Chang-Hee Lee, "Color-free operation of dense WDM-PON based on the wavelength-locked fabry-Pe/spl acute/rot laser diodes injecting a low-noise BLS," in *IEEE Photonics Technology Letters*, vol. 18, no. 10, pp. 1167-1169, 2006.
- [65] C. H. Yeh, H. C. Chien and S. Chi, "Cost-Effective Colorless RSOA-Based WDM-PON with 2.5 Gbit/s Uplink Signal," *Conference on Optical Fiber Communication/National Fiber Optic Engineers Conference*, San Diego, CA, 2008, pp. 1-3.
- [66] H. Y. Chen, C. H. Yeh, C. W. Chow, J. Y. Sung, Y. L. Liu and J. Chen, "Investigation of Using Injection-Locked Fabry-Pérot Laser Diode with 10% Front-Facet Reflectivity for Short-Reach to Long-Reach Upstream PON Access," in *IEEE Photonics Journal*, vol. 5, no. 3, pp. 7901208-7901208, 2013.

- [67] M. Cheng, T. Cheng-Ting, C. Yu-Chieh, and L. Gong-Ru, "Direct QAM-OFDM encoding of an L-Band master-to-slave injection-locked WRC-FPLD Pair for  $28 \times 20$  Gb/s DWDM-PON transmission." *Journal of Lightwave Technology*, vol. 32, no. 17, pp. 2981–88, 2014.
- [68] C. H. Yeh, C. W. Chow, Y. F. Wu, S. P. Huang, Y. L. Liu, and C. L. Pan. "Performance of long-reach passive access networks using injection-locked Fabry-Perot laser diodes with finite front-facet reflectivities." *Journal of Lightwave Technology*, vol. 31, no. 12, pp. 1929–34, 2013.
- [69] Lin, G. R., Liao, Y. S., Chi, Y. C., Kuo, H. C., Lin, G. C., Wang, H. L., & Chen, Y. J, "Long-Cavity Fabry Perot Laser Amplifier Transmitter with Enhanced Injection-Locking Bandwidth for WDM-PON Application," *Journal of Lightwave Technology*, vol. 28, no. 20, pp. 2925–2932, 2010.
- [70] Lin, G.-R., Cheng, T.-K., Chi, Y.-C., Lin, G.-C., Wang, H.-L., & Lin, Y.-H, "200-GHz and 50-GHz AWG channelized linewidth dependent transmission of weak-resonant-cavity FPLD injection-locked by spectrally sliced ASE," *Opt. express*, vol. 17, no. 20, pp. 17739-17746, 2009.
- [71] Y. F. Wu, C. H. Yeh, C. W. Chow, Y. L. Liu, and J. Y. Sung, "2.5–10 Gbit/s laser source based on two optical-injection Fabry–Perot laser diodes," *Optical Fiber Technology*, vol. 19, no. 6, pp. 579–82, 2013.
- [72] Z. Alferov, "Double heterostructure lasers: early days and future perspectives," *IEEE Journal of Selected Topics in Quantum Electronics*, vol. 6, no. 6, pp. 832–840, 2000.
- [73] Kroemer, H. (1963). "A proposed class of heterojunction lasers," *Proc. IEEE*, vol. 51, pp. 1782-1783, 1963.
- [74] Woodall, J. M., Rupprecht, H., and Petti, G. D, "Solid state device conference, June 19, 1967, Santa Barbara, California." [Abstract reported in *IEEE Trans. Electron. Devices* ED-14, 630 (1967).
- [75] Zory, Peter S. Quantum well lasers. Academic Press, 1993.
- [76] Miller, R.C., et al. "Laser oscillation with optically pumped very thin GaAs Al<sub>x</sub>Ga<sub>1-x</sub>As multilayer structure and conventional double heterostructures." *Journal of Applied Physics* vol. 47, no. 10, pp. 4509-4517, 1976.
- [77] Holonyak, N., Kolbas, R. M., Laidig, W. D., Vojak, B. A., Dupuis, R. D., & Dapkus, P. D, "Low-threshold continuous laser operation (300–337 °K) of multilayer MO-CVD Al<sub>x</sub>Ga<sub>1-x</sub>As-GaAs quantum-well heterostructures". *Applied Physics Letters*, vol. 33, no.8, pp. 737–739, 1978.

- [78] Nelson, R. J., Wright, P. D., Barnes, P. A., Brown, R. L., Cella, T., & Sobers, R. G, "High-output power InGaAsP ( $\lambda=1.3 \mu\text{m}$ ) strip-buried heterostructure lasers." *Applied Physics Letters*, vol. 36, no.5, pp. 358–360, 1980.
- [79] Wright, P. D., Nelson, R. J., & Cella, T. "InGaAsP double heterostructure lasers ( $\lambda=1.3 \mu\text{m}$ ) with etched reflectors." *Applied Physics Letters*, vol.36, no.7, pp.518–520,1980.
- [80] Ng, W., Hong, C. S., Manasevit, H., & Dapkus, P. D. "Low-threshold 1.3- $\mu\text{m}$  GaInAsP/InP buried heterostructure lasers by liquid phase epitaxy and metalorganic chemical vapor deposition" *Applied Physics Letters*, vol. 39, no.3, pp.188–189, 1981.
- [81] Koren, U., Miller, B. I., Su, Y. K., Koch, T. L., & Bowers, J. E. "Low internal loss separate confinement heterostructure InGaAs/InGaAsP quantum well laser." *Applied Physics Letters*, vol. 5, no.21, pp.1744–1746, 1987.
- [82] J. J. Coleman, J. D. Young and A. Garg, "Semiconductor Quantum Dot Lasers: A Tutorial," in *Journal of Lightwave Technology*, vol. 29, no. 4, pp. 499-510, 2011.
- [83] Huffaker, D. L., Park, G., Zou, Z., Shchekin, O. B., & Deppe, D. G, "1.3  $\mu\text{m}$  room-temperature GaAs-based quantum-dot laser." *Applied Physics Letters*, vol. 73, no. 18, pp. 2564–2566, 1998.
- [84] G. Park, D. L. Huffaker, Z. Zou, O. B. Shchekin and D. G. Deppe, "Temperature dependence of lasing characteristics for long-wavelength (1.3- $\mu\text{m}$ ) GaAs-based quantum-dot lasers," in *IEEE Photonics Technology Letters*, vol. 11, no. 3, pp. 301-303, 1999.
- [85] K. Mukai, Y. Nakata, K. Otsubo, M. Sugawara, N. Yokoyama and H. Ishikawa, "1.3- $\mu\text{m}$  CW lasing of InGaAs-GaAs quantum dots at room temperature with a threshold current of 8 mA," in *IEEE Photonics Technology Letters*, vol. 11, no. 10, pp. 1205-1207, 1999.
- [86] Alghoraibi *et al.*, "InAs self-assembled quantum dot and quantum dash lasers on InP for 1.55  $\mu\text{m}$  optical telecommunications," *2006 2nd International Conference on Information & Communication Technologies*, Damascus, pp. 2085-2090, 2006.
- [87] Bauer, E. "Phänomenologische Theorie der Kristallabscheidung an Oberflächen. II." *Zeitschrift Für Kristallographie*, 110(1–6), pp. 395–431, 1958.
- [88] Saito, H., Nishi, K., & Sugou, S. "Ground-state lasing at room temperature in long-wavelength InAs quantum-dot lasers on InP (311) B substrates." *Applied Physics Letters*, vol. 78, no. 3, pp. 267–269, 2001.

- [89] K. Akahane, N. Yamamoto, and T. Kawanishi, "The dependence of the characteristic temperature of highly stacked InAs quantum dot laser diodes fabricated using a strain-compensation technique on stacking layer number," in *Semiconductor Laser Conference (ISLC), 2012 23rd IEEE International*, 2012, pp. 82-83, 2012.
- [90] Wang, R. H., et al. "Room-temperature operation of InAs quantum-dash lasers on InP [001]." *Photonics Technology Letters*, IEEE 13.8, pp. 767-769, 2001.
- [91] R. Schwertberger, D. Gold, J. Reithmaier, and A. Forchel, "Longwavelength InP-based quantum-dash lasers," *IEEE Photonics Technology Letters*, vol. 14, pp. 735-737, 2002.
- [92] Huolei, Wang, et al. "InGaAs/GaAs quantum well laser with broad spectrum of stimulated emission at 1.06  $\mu\text{m}$ ." *CLEO: QELS Fundamental Science*. Optical Society of America, 2014.
- [93] Somers, W. Kaiser, J. Reithmaier, and A. Forchel, "InP-based quantum dash lasers for broadband optical amplification and gas sensing applications," in *International Conference on Indium Phosphide and Related Materials*, 2005., pp. 56-59, 2005.
- [94] M. Z. M. Khan, T. K. Ng, C.-S. Lee, P. Bhattacharya, and B. S. Ooi, "Investigation of Chirped InAs/InGaAlAs/InP Quantum Dash Lasers as Broadband Emitters," *IEEE Journal of Quantum Electronics*, vol. 50, pp. 5161, 2014.
- [95] A. Akrouf *et al.*, "Separate Error-Free Transmission of Eight Channels at 10 Gb/s Using Comb Generation in a Quantum-Dash-Based Mode-Locked Laser," in *IEEE Photonics Technology Letters*, vol. 21, no. 23, pp. 1746-1748, 2009.
- [96] J. Pfeifle *et al.*, "Coherent terabit communications using a quantum-dash mode-locked laser and self-homodyne detection," *2015 Optical Fiber Communications Conference and Exhibition (OFC)*, Los Angeles, CA, pp. 1-3, 2015.
- [97] Z. Mi, J. Yang and P. Bhattacharya, "Growth and characteristics of P-doped InAs tunnel injection quantum-dash lasers on InP," in *IEEE Photonics Technology Letters*, vol. 18, no. 12, pp. 1377-1379, 2006.
- [98] Mobarhan, K. S. Test and characterization of laser diodes: determination of principal parameters. *Newport Corporation*, 1996.
- [99] Naderi, N. A. "External control of semiconductor nanostructure lasers (doctoral)." The University of New Mexico, 2007 Retrieved from <http://repository.unm.edu/handle/1928/13160>.
- [100] Azawe, M. I. *Chaotic Dynamics of Semiconductor Lasers for Secure Optical Communication*, 2012.

- [101] M. Cheng, T. Cheng-Ting, C. Yu-Chieh, and L. Gong-Ru, "Direct QAM-OFDM encoding of an L-Band master-to-slave injection-locked WRC-FPLD Pair for  $28 \times 20$  Gb/s DWDM-PON transmission." *Journal of Lightwave Technology*, vol. 32, no. 17, pp. 2981–88, 2014.
- [102] Chi, Y.-C., Li, Y.-C., Wang, H.-Y., Peng, P.-C., Lu, H.-H., & Lin, G.-R, "Optical 16-QAM-52-OFDM transmission at 4 Gbit/s by directly modulating a coherently injection-locked colorless laser diode," *Opt. Express*, vol. 20 no. 18, pp. 20071–20077, 2012.
- [103] Pochet, M., Naderi, N. A., Grillot, F., Terry, N., Kovanis, V., & Lester, L. F. "Modulation response of an injection locked quantum-dash Fabry Perot laser at 1550nm". In *SPIE proc. 7211, Physics and Simulation of Optoelectronic Devices XVII*, vol. 7211, 2009.
- [104] Jin, X., & Chuang, S.-L. "Bandwidth enhancement of Fabry-Perot quantum-well lasers by injection-locking." *Solid-State Electronics*, vol. 50, no. 6, pp. 1141–1149, 2006.
- [105] Krstić, Marko M. "Statical and dynamical characteristics of injection-locked Fabry-Pérot laser diodes(doctoral)", University of Belgrade, School of Electrical Engineering, March 2016, Retrieved December 21, 2016, from [https://phaidrabg.bg.ac.rs/detail\\_object/o:12216?tab=0#mda](https://phaidrabg.bg.ac.rs/detail_object/o:12216?tab=0#mda).
- [106] I. Petitbon, P. Gallion, G. Debarge, C. Ghabran, "Locking Bandwidth and Relaxation Oscillation of an Injection-Locked Semiconductor Laser," *IEEE Journal of Quantum Electronics*, Vol. 24, No. 2, pp. 148-154, 1988.
- [107] J. M. Liu, H. F. Chen, X. J. Meng, T. B. Simpson, "Modulation Bandwidth, Noise, and Stability of a Semiconductor Laser Subject to Strong Injection Locking," *IEEE Photonics Technology Letters*, No. 9, Vol. 10, pp. 1325-1327, 1997.
- [108] F. Mogensen, H. Olesen, G. Jacobsen, "Locking Conditions and Stability Properties for a Semiconductor Laser with External Light Injection," *IEEE Journal of Quantum Electronics*, Vol. QE-21, No. 7, pp. 784-793, 1985.
- [109] F. Mogensen, H. Olesen, G. Jacobsen, *Journal of Quantum Electron.*, vol. QE-21, pp. 784-793, 1985.
- [110] T. B. Simpson, J. M. Liu, "Enhanced modulation bandwidth in injection-locked semiconductor lasers," *IEEE Photonics Technology Letters*, vol. 9, no. 10, pp. 1322–1324, 1997.
- [111] J. Wang, M. K. Haldar, L. Lin, F. V. C. Mendis, "Enhancement of modulation bandwidth of laser diodes by injection locking," *IEEE Photonics Technology Letters*, vol. 8, pp. 34–36, 1996.

- [112] J. M. Liu, H. F. Chen, X. J. Meng, and T. B. Simpson, "Modulation bandwidth, noise, and stability of a semiconductor laser subject to strong injection locking," *IEEE Photonics Technology Letters*, vol. 9, pp. 1325–1327, 1997.
- [113] L. Chrostowski, X. Zhao, C. J. Chang-Hasnain et al., "50-GHz optically injection-locked 1.55- $\mu\text{m}$  VCSELs," *IEEE Photonics Technology Letters*, vol. 18, pp. 367–369, 2006.
- [114] E. K. Lau, H. Sung, M. C. Wu, "Frequency response enhancement of optical injection-locked lasers," *IEEE Journal of Quantum Electronics*, vol. 44, no. 1, pp. 90–99, 2008.
- [115] Y. Hong and K. A. Shore, "Locking characteristics of a side-mode injected semiconductor laser," *IEEE Journal of Quantum Electronics*, vol. 35, pp. 1713–1717, 1999.
- [116] Zlitni, A. G. R., Krstić, M. M., & Gvozdić, D. M, "Modulation response and bandwidth of injection-locked Fabry–Pérot laser diodes," *Physica Scripta*, pp. 14033, 2012.
- [117] Y. Onishi, and F. Koyama, "All-optical regeneration using a vertical-cavity surface-emitting laser with external light injection," *IEICA Transactions on Electronics*, vol. E87C, no. 3, pp. 409-415, 2004.
- [118] M. Al-Mumin, X. H. Wang, W. M. Mao, S. A. Pappert, and G. F. Li, "Optical generation and sideband injection locking of tunable 11-120GHz microwave/millimeter signals," *Electronics Letters*; vol. 36, no.18, pp. 1547-1548, 2000.
- [119] C. Henry, "Theory of spontaneous emission noise in open resonators and its application to lasers and optical amplifiers," *Journal of Lightwave Technology*, vol. 4, pp. 288-297, 1986.
- [120] T. Jung, S. Ji-Lin, D. T. K. Tong, S. Murthy, M. C. Wu, T. Tanbun-Ek, W. Wenshen, R. Lodenkamper, R. Davis, L. J. Lembo, and J. C. Brock, "CW injection locking of a mode-locked semiconductor laser as a local oscillator comb for channelizing broad-band RF signals," *IEEE Transactions on Microwave Theory and Techniques*, vol. 47, pp. 1225-1233, 1999.
- [121] Z Xu, Y. J. Wen, W. Zhong, C. Chae, X. Cheng, Y. Wang, C. Lu, and J. Shankar, "High-speed WDM-PON using CW injection-locked Fabry–Pérot laser diodes," *Opt. Express*, vol. 15, no. 6 pp. 2953-2962, 2007.
- [122] A. Kaszubowska, P. Anandarajah, and L. P. Barry, "Improved performance of a hybrid radio/fiber system using a directly modulated laser transmitter with external injection," *IEEE Photonics Technology Letters*, vol. 14, pp. 233–235, 2002.

- [123] L. Hai-Han, H. Hsu-Hung, S. Heng-Sheng, and W. Ming-Chuan, "Fiber optical CATV system-performance improvement by using external light-injection technique," *IEEE Photonics Technology Letters*, vol. 15, pp. 1017–1019, 2003.
- [124] Lu, H.-H., Li, C.-Y., Chu, C.-A., Lu, T.-C., Chen, B.-R., Wu, C.-J., & Lin, D.-H. (2015). 10 m/25 Gbps LiFi transmission system based on a two-stage injection-locked 680 nm VCSEL transmitter. *Optics Letters*, vol. 40, no. 19, pp. 4563–4566.
- [125] H. H. Lu *et al.*, "An 8 m/9.6 Gbps Underwater Wireless Optical Communication System," in *IEEE Photonics Journal*, vol. 8, no. 5, pp. 1-7, 2016.
- [126] Pikovsky, A., Rosenblum, M., & Kurths, J, "*Synchronization: A Universal Concept in Nonlinear Sciences*. Cambridge University Press, 2003.
- [127] B. van der Pol, "Forced oscillations in a circuit with non-nonlinear resistance," *Philos. Mag.*, iii, 65–80, 1927.
- [128] R. Adler, "A study of locking phenomena in oscillators," in *Proc. IRE*, 34, 351–357, 1946.
- [129] H. L. Stover and W. H. Steier, "Locking of laser oscillators by light injection," *Appl. Phys. Lett.*, 8, pp. 91–93, 1966.
- [130] C. J. Buczek, and R. J. Freiberg, "Hybrid injection locking of higher power CO lasers," *IEEE Journal of Quantum Electronics*, vol. QE-8, no. 7, pp. 641–650, 1972.
- [131] P. Gallion, H. Nakajima, G. Debarge, and C. Chabran, "Contribution of spontaneous emission to the linewidth of an injection-locked semiconductor laser," *Electronics Letters*, vol. 21, no. 14, pp. 626-628, 1985.
- [132] K. Iwashita and K. Nakagawa, "Suppression of mode partition noise by laser diode light injection," *IEEE Journal of Quantum Electronics*, vol. 18, no. 10, pp. 1669-1674, 1982.
- [133] N. A. Olsson, H. Temkin, R. A. Logan, L. F. Johnson, G. J. Dolan, J. P. van der Ziel, and J. C. Campbell, "Chirp-free transmission over 82.5 km of single mode fibers at 2 Gbit/s with injection locked DFB semiconductor lasers," *Journal of Lightwave Technology*, vol. 3, no. 1, pp. 63-67, 1985.
- [134] Y. Yamamoto and T. Kimura, "Coherent optical fiber transmission systems," *IEEE Journal of Quantum Electronics*, vol. 17, no. 6, pp. 919-935, 1981.
- [135] S. Kobayashi and T. Kimura, "Coherence on injection phase-locked AlGaAs semiconductor laser," *Electron. Lett.* Vol.16, 668–670, 1980.



- [136] R. Lang, "Injection locking properties of a semiconductor laser," *IEEE J. Quantum Electron.*, vol. QE-18, 976–83, 1982.
- [137] Lee, H. L. T., et al. "Bandwidth enhancement and chirp reduction in DBR lasers by strong optical injection." *Lasers and Electro-Optics, 2000. (CLEO 2000). Conference on. IEEE, 2000.*
- [138] Chang, Chih-Hao, Lukas Chrostowski, and Connie J. Chang-Hasnain. "Injection locking of VCSELs." *IEEE Journal of Selected Topics in Quantum Electronics*, vol. 9, no.5, p. 13861393, 2003.:
- [139] Chrostowski, Lukas, "Optical injection locking of vertical cavity surface emitting lasers (Doctoral)." University of California Barkley, 2004.
- [140] Jin, X., & Chuang, S.-L, "Bandwidth enhancement of Fabry-Perot quantum-well lasers by injection-locking." *Solid-State Electronics*, vol. 50, no.6, 1141–1149, 2006.
- [141] N. B. Terry, N. A. Naderi, M. Pochet, A. J. Moscho, L. F. Lester and V. Kovanis, "Bandwidth enhancement of injection-locked 1.3  $\mu\text{m}$  quantum-dot DFB laser," in *Electronics Letters*, vol. 44, no. 15, pp. 904-905, July 17 2008.
- [142] R. Rosales *et al.*, "InAs/InP Quantum-Dot Passively Mode-Locked Lasers for 1.55- $\mu\text{m}$  Applications," in *IEEE Journal of Selected Topics in Quantum Electronics*, vol. 17, no. 5, pp. 1292-1301,2011.
- [143] E. Sooudi *et al.*, "Injection-Locking Properties of InAs/InP-Based Mode-Locked Quantum-Dash Lasers at 21 GHz," in *IEEE Photonics Technology Letters*, vol. 23, no. 20, pp. 1544-1546, 2011.
- [144] E. Sooudi *et al.*, "Optical Frequency Comb Generation Using Dual-Mode Injection-Locking of Quantum-Dash Mode-Locked Lasers: Properties and Applications," in *IEEE Journal of Quantum Electronics*, vol. 48, no. 10, pp. 1327-1338, 2012.
- [145] M. Cheng, T. Cheng-Ting, C. Yu-Chieh, and L. Gong-Ru, "Direct QAM-OFDM encoding of an L-Band master-to-slave injection-locked WRC-FPLD Pair for  $28 \times 20$  Gb/s DWDM-PON transmission." *Journal of Lightwave Technology*, vol. 32, no. 17, pp. 2981–88, 2014.
- [146] C. H. Yeh, C. W. Chow, Y. F. Wu, S. P. Huang, Y. L. Liu, and C. L. Pan. "Performance of long-reach passive access networks using injection-locked Fabry-Perot laser diodes with finite front-facet reflectivities." *Journal of Lightwave Technology*, vol. 31, no. 12, pp. 1929–34, 2013.

- [147] L. G. Kazovsky, W. T. Shaw, D. Gutierrez, N. Cheng, and S. W. Wong, "Next-generation optical access networks," *Journal of Lightwave Technology*, vol.25, no. 11, pp. 3428–42, 2007.
- [148] Saliou, F., Simon, G., Chanclou, P., Pizzinat, A., Lin, H., Zhou, E., & Xu, Z, "WDM PONs based on colorless technology. *Optical Fiber Technology*", Vol. 26, p. 126–134, 2015.
- [149] K. Y. Cho, U. H. Hong, Y. Takushima, A. Agata, T. Sano, M. Suzuki, and Y. C. Chung, "103-Gb/s long-reach WDM PON implemented by using directly modulated RSOAs," *IEEE Photonics Technology Letters* vol. 24, no. 3, pp. 209–11, 2012.
- [150] J. Kani, "Enabling Technologies for Future Scalable and Flexible WDM-PON and WDM/TDM-PON Systems," *IEEE Journal of Selected Topics in Quantum Electronics*, vol. 16, no. 5, pp. 1290-1297, Sept.-Oct. 2010.
- [151] C. W. Chow *et al.*, "13 Gbit/s WDM-OFDM PON using RSOA-based colourless ONU with seeding light source in local exchange," in *Electronics Letters*, vol. 47, no. 22, pp. 1235-1236, 2011.
- [152] Lee, H.-K., Cho, H.-S., Kim, J.-Y., & Lee, C.-H, "A WDM-PON with an 80 Gb/s capacity based on wavelength-locked Fabry-Perot laser diode," *Opt. Express*, vol. 18, no. 17, pp. 18077–18085, 2010.
- [153] Chi, Y.-C., Li, Y.-C., Wang, H.-Y., Peng, P.-C., Lu, H.-H., & Lin, G.-R, "Optical 16-QAM-52-OFDM transmission at 4 Gbit/s by directly modulating a coherently injection-locked colorless laser diode," *Opt. Express*, vol. 20 no. 18, pp. 20071–20077, 2012.
- [154] C. H. Yeh, C. W. Chow, Y. F. Wu, S. P. Huang, Y. L. Liu, and C. L. Pan. "Performance of long-reach passive access networks using injection-locked Fabry-Perot laser diodes with finite front-facet reflectivities." *Journal of Lightwave Technology*, vol. 31, no. 12, pp. 1929–34, 2013.
- [155] Lin, G. R., Liao, Y. S., Chi, Y. C., Kuo, H. C., Lin, G. C., Wang, H. L., & Chen, Y. J, "Long-Cavity Fabry Perot Laser Amplifier Transmitter with Enhanced Injection-Locking Bandwidth for WDM-PON Application," *Journal of Lightwave Technology*, vol. 28, no. 20, pp. 2925–2932, 2010.
- [156] M. Z. M. Khan, T. K. Ng, C. S. Lee, P. Bhattacharya and B. S. Ooi, "Investigation of Chirped InAs/InGaAlAs/InP Quantum Dash Lasers as Broadband Emitters," in *IEEE Journal of Quantum Electronics*, vol. 50, no. 2, pp. 51-61, Feb. 2014.

- [157] Telecommunications Standardization Sector of the ITU (ITU-T), ITU-T Recommendation G.975.1—Forward Error Correction for High Bit-Rate DWDM Submarine Systems, International Telecommunications Union (ITU), Geneva, Switzerland, 2004.
- [158] Kaushal, Hemani, and Georges Kaddoum. “Free Space Optical Communication: Challenges and Mitigation Techniques.” arXiv preprint. arXiv: 1506.04836 (2015).
- [159] Parca, Giorgia, Ali Shahpari, Valeria Carrozzo, Giorgio Maria Tosi Belleffi, and Antonio L. J. Teixeira. “Optical wireless transmission at 1.6-Tbit/s (16×100 Gbit/s) for next-generation convergent urban infrastructures.” *Optical Engineering*, vol. 52, no. 11, pp.116102–116102, 2013.
- [160] Hamza, Abdelbaset S., Jitender S. Deogun, and Dennis R. Alexander. "Free space optical data center architecture design with fully connected racks" in *IEEE Global Communications Conference*, pp. 2192-2197, 2014.
- [161] Bohata, J., S. Zvanovec, P. Pesek, T. Korinek, M. Mansour Abadi, and Z. Ghassemlooy. “Experimental verification of long-term evolution radio transmissions over dual-polarization combined fiber and free-space optics opticalinfrastructures.” *Applied Optics*, vol. 55, no. 8, pp. 2109–2116, 2016.
- [162] Cvijetic, Neda, Dayou Qian, Jianjun Yu, Yue-Kai Huang, and Ting Wang. "100 Gb/s per-channel free-space optical transmission with coherent detection and MIMO processing" in *European Conference on Optical Communication (ECOC)*, 2009.
- [163] E. Ciaramella et al., "1.28 terabits/s (32x40 Gbit/s) WDM transmission system for free space optical communications," *IEEE Journal on Selected Areas in Communications*, vol. 27, no. 9, pp. 1639-1645, 2009.
- [164] Ren, Yongxiong, Zhe Wang, Peicheng Liao, Long Li, Guodong Xie, Hao Huang, Zhe Zhao et al. "400-Gbit/s free space optical communications link over 120-meter using multiplexing of 4 collocated orbital-angular-momentum beams" in *Optical Fiber Communication Conference (OFC)*, pp. M2F-1, 2015.
- [165] Maged A. Esmail, Amr Ragheb, H. Fathallah, and M-S Alouini. "Experimental demonstration of outdoor 2.2 Tbps super-channel FSO transmission system." in *IEEE International Conference on Communications Workshops (ICC)*, pp. 169-174, 2016.
- [166] Janjua, Bilal, Hassan M. Oubei, Jose R. Durán Retamal, Tien Khee Ng, Cheng-Ting Tsai, Huai-Yung Wang, Yu-Chieh Chi et al. "Going beyond 4 Gbps data rate by employing RGB laser diodes for visible light communication." *Optics Express*, vol. 23, no. 14, pp. 18746-18753, 2015.

- [167] Lu, Hai-Han, Chung-Yi Li, Chien-An Chu, Ting-Chien Lu, Bo-Rui Chen, Chang-Jen Wu, and Dai-Hua Lin. "10 m/25 Gbps LiFi transmission system based on a two-stage injection-locked 680 nm VCSEL transmitter." *Optics Letters*, vol. 40, no. 19, pp. 4563-4566, 2015.
- [168] W. S. Tsai et al., "A 50-m/40 Gb/s 680-nm VCSEL-Based FSO Communication," *IEEE Photonics Journal*, vol. 8, no. 2, pp. 1-8, 2016.
- [169] Lu, Hai-Han, Chun-Yu Lin, Ting-Chien Lu, Chien-An Chu, Hung-Hsien Lin, Bo-Rui Chen, Chang-Jen Wu, and Wen-Shing Tsai. "150 m/280 Gbps WDM/SDM FSO link based on OEO-based BLS and afocal telescopes." *Optics Letters*, vol. 41, no. 12, pp. 2835-2838, 2016.
- [170] Tsai, Wen-Shing, Hai-Han Lu, Chung-Yi Li, Ting-Chieh Lu, Chen-Hong Liao, Chien-An Chu, and Peng-Chun Peng. "A 20-m/40-Gb/s 1550-nm DFB LD-based FSO link." *IEEE Photonics Journal*, vol. 7, no. 6, pp. 1-7, 2015.
- [171] Hamedazimi, Navid, Zafar Qazi, Himanshu Gupta, Vyas Sekar, Samir R. Das, Jon P. Longtin, Himanshu Shah, and Ashish Tanwer. "FireFly: a reconfigurable wireless data center fabric using free-space optics." *ACM SIGCOMM Computer Communication Review*, vol. 44, no. 4, pp. 319-330, 2015.
- [172] Huang, Hao, Guodong Xie, Yan Yan, Nisar Ahmed, Yongxiong Ren, Yang Yue, Dvora Rogawski et al. "100 Tbit/s free-space data link enabled by three-dimensional multiplexing of orbital angular momentum, polarization, and wavelength." *Optics Letters*, vol. 39, no. 2, pp. 197-200, 2014.
- [173] Oh, Chin Wan, Zizheng Cao, Eduward Tangdiongga, and Ton Koonen. "Free-space transmission with passive 2D beam steering for multi-gigabit-per-second per-beam indoor optical wireless networks." *Optics Express*, vol. 24, no. 17, pp. 19211-19227, 2016.
- [174] Shahpari, Ali, Artur N. Sousa, Ricardo Ferreira, Mário Lima, and António Teixeira. "Free space optical communications for ultrahigh-capacity PON system," in *Second International Conference on Applications of Optics and Photonics*, pp. 92861Y-92861Y, 2014.
- [175] Wang, Ke, Ampalavanapillai Nirmalathas, Christina Lim, Efstratios Skafidas, and Kamal Alameh. "Experimental demonstration of free-space based 120 Gb/s reconfigurable card-to-card optical interconnects." *Optics Letters*, vol. 39, no. 19, pp. 5717-5720, 2014.
- [176] International Standard IEC 60825-1 © IEC: 1993 + A1:1997 + A2:2001: Safety of Laser Products – Part 1: Equipment Classification and Requirements. International Electrotechnical Commissions, Geneva (2001).

## Appendix

### Quantum Confinement

In this section, we present a breakthrough in the development of semiconductor laser which is introduction of quantum confinement of carriers with lessened dimensionality in structures. Quantum confinement effects appear when the geometrical dimensions of the device are in the same order of magnitude as the DeBroglie wavelength of the electrons (few 10s of nm). Density of states (DOS) is the number of available states at each energy level that electrons and holes can occupy and it is given, for bulk as,

$$g(E) \propto E^{1/2}$$

where  $g(E)$  is the density of quantum state and  $E$  is the energy. Equation 2.1 indicates that density of quantum states is a function of energy  $E$ . Fig. 2.4 shows different quantum confinement structures alongside their density of states (DOS). The potential felt by electron and holes can be approximated by the basic quantum-wall problem in one dimension, i.e. when reducing the dimensionality from 3D to 2D [92]. This can be modeled by time-independent one-dimensional form of Schrödinger's wave equation shown below:

$$\frac{\partial^2}{\partial x^2} \psi(x) + \frac{2m}{\hbar} [E_0 - U(x)] \psi(x)$$

where  $\hbar$  is the reduced planks constant,  $\psi$  is the time-independent wave function,  $U$  is potential function experienced by the particle,  $E$  is the total energy of the particle.  $m$  is the effective mass of the particle. The solutions of above equation in the form of Eigen energies is given by,

$$E_n = n^2 \left( \frac{\pi^2 \hbar^2}{2mL^2} \right)$$

Eigen energy and  $L$  is the width or thickness of the quantum-well. Note that  $L$  in the above solution can be used to control how far these energies (states) are from each other. Quantum well are one dimensional confined nanostructures, as shown in Fig. 2.4 (c) and (d). Two-dimensional confined structures are called quantum wires whereas three-dimensional confinement results in quantum dots in which the size has been reduced in all three dimensions, as illustrated in Fig. 2.4 (e) and (g), respectively. Quantum dots have density of state in the form of delta function which represents a single state for all the carriers to occupy (see Fig 2.4 (h)). These features of quantum confinement, significantly improves the number of electron-hole pair recombination that results in photons of more discretized wavelengths [93].

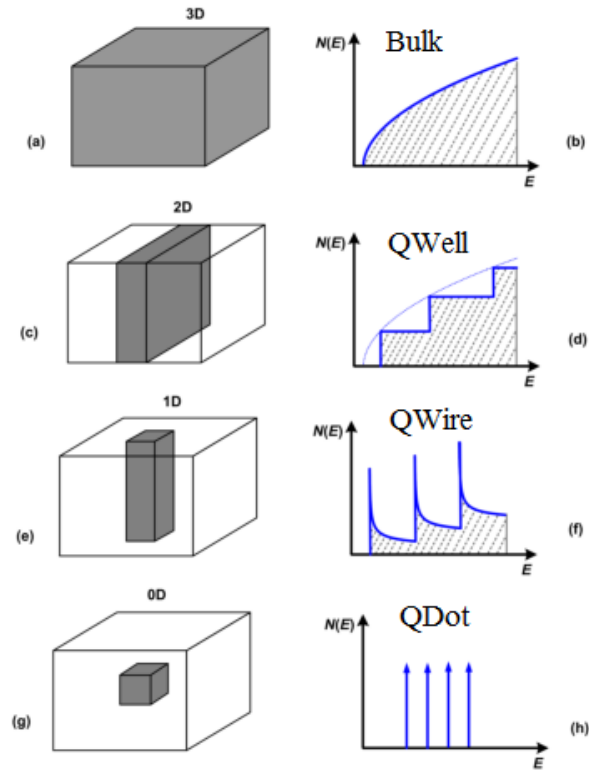


Figure: Quantum confinements along with their respective density of states. (a), (b). Zero-dimensional confinement (bulk material). (c), (d). One-dimensional confinement (quantum well). (e), (f). Two-dimensional confinement (quantum wire). (g), (h). Three dimensional confinement (quantum dot) [1].

## VITAE

Name : Muhammad Talal Ali khan.

Nationality : Pakistan.

Date of Birth : September 1<sup>st</sup>, 1992.

Email : engrtalalkamran@gmail.com, g201409540@kfupm.edu.sa

Address : C-15 Mills Officer Colony Near Ali Hospital, Bhakkar.

Academic Background :

- Master of Science (M.Sc.) in Electrical Engineering, King Fahd University of Petroleum and Minerals, January 2017.
- Bachelor of Science (B.Sc.) in Electrical Engineering, COMSATS Institute of Information Technology, June 2013.

Publication:

- **[J1] M. Talal A. Khan**, E. Alkhazraji A. Ragheb, H. Fathallah, M.Z.M. Khan (2016). “100 Gb/s single channel transmission using injection-locked 1621 nm quantum-dash laser for WDM-based optical access network” (not yet published, In review IEEE-PTL, 2016).
- **[J2] M. Talal A. Khan**, M.A. Shemis, A. Ragheb, H. Fathallah, M.Z.M. Khan (2016). “4 m/100 Gb/s Optical Wireless Communication Based on Far L-band Injection Locked Quantum-dash Laser”. (not yet published, In review IEEE-PJ, 2016).
- **[C1] M. Talal A. Khan**, E. Alkhazraji, A. Ragheb, H. Fathallah, M.Z.M. Khan (2016). “Far L-band Single Channel High Speed Downstream Transmission Using Injection-Locked Quantum-Dash Laser for WDM-PON” (Not yet published, accepted in 5<sup>th</sup> International Conference on Photonics, Optics and Laser Technology, PHOTOPTICS 2017).



- [C2] E. Alkhazraji, **M. Talal A. Khan**, M.Z.M. Khan (2016). “Broadband Lasing Characteristics of a Chirped InAs/InP Quantum-dash Laser (Not yet published, accepted in 5<sup>th</sup> International Conference on Photonics, Optics and Laser Technology (PHOTOPTICS 2017)).
- [C3] **M. Talal A. Khan**, A. Ragheb, H. Fathallah, M.Z.M. Khan (2016). “64 Gb/s Quantum-dash Laser based Indoor Free Space Optical Communication”. (Submitted in 26<sup>th</sup> Wireless and Optical Communications Conference (WOCC 2017)).
- [C4] **M. Talal A. Khan**, M.A. Shemis A. Ragheb, H. Fathallah, M.Z.M. Khan (2016). “Optical Wireless Communication at 100 Gb/s Using L-Band Quantum dash-laser” (Submitted in 26<sup>th</sup> Wireless and Optical Communications Conference (WOCC 2017)).
- [C5] M.A. Shemis, **M. Talal A. Khan**, M.Z.M. Khan (2016). “Self-injection Locked InAs/InP Quantum-dash Laser for High Capacity Optical Communication System”. (Submitted to the 12<sup>th</sup> Conference on Lasers and Electro-Optics Pacific Rim (CLEO-PR 2017)).